

Electronic Thesis and Dissertation Repository

---

10-29-2010 12:00 AM

## Surface Modifications of Poly(dimethylsiloxane) for Biological Application of Microfluidic Devices

Jessica M. Dechene, *The University of Western Ontario*

Supervisor: Dr. Peter R. Norton, *The University of Western Ontario*

A thesis submitted in partial fulfillment of the requirements for the Doctor of Philosophy degree in Chemistry

© Jessica M. Dechene 2010

Follow this and additional works at: <https://ir.lib.uwo.ca/etd>

 Part of the [Materials Chemistry Commons](#)

---

### Recommended Citation

Dechene, Jessica M., "Surface Modifications of Poly(dimethylsiloxane) for Biological Application of Microfluidic Devices" (2010). *Electronic Thesis and Dissertation Repository*. 24.  
<https://ir.lib.uwo.ca/etd/24>

This Dissertation/Thesis is brought to you for free and open access by Scholarship@Western. It has been accepted for inclusion in Electronic Thesis and Dissertation Repository by an authorized administrator of Scholarship@Western. For more information, please contact [wlsadmin@uwo.ca](mailto:wlsadmin@uwo.ca).

Surface Modifications of  
Poly(dimethylsiloxane) for Biological  
Applications of Microfluidic Devices

(Spine title: Surface Modifications of Poly(dimethylsiloxane))

(Thesis format: Monograph)

by

Jessica Mary Dechene

Graduate Program  
in  
Chemistry

A thesis submitted in partial fulfillment  
of the requirements for the degree of  
Doctor of Philosophy

School of Graduate and Postdoctoral Studies  
The University of Western Ontario  
London, Ontario, Canada

© Jessica M. Dechene 2010

# Certificate of Examination

THE UNIVERSITY OF WESTERN ONTARIO  
SCHOOL OF GRADUATE AND POSTDOCTORAL STUDIES  
CERTIFICATE OF EXAMINATION

**Chief Advisor:**

\_\_\_\_\_  
Dr. Peter R. Norton

**Examining Board:**

\_\_\_\_\_  
Dr. Yang Song

**Advisory Committee:**

\_\_\_\_\_  
Dr. Oleg Semenikhin

\_\_\_\_\_  
Dr. Paul Charpentier

\_\_\_\_\_  
Dr. Molly Shoichet

The thesis by

**Jessica Mary Dechene**

entitled:

**Surface Modifications of Poly(dimethylsiloxane) for Biological  
Applications of Microfluidic Devices**

is accepted in partial fulfillment of the  
requirements for the degree of

**Doctor of Philosophy**

Date: \_\_\_\_\_

\_\_\_\_\_  
Chair of Examining Board  
Dr. Calin Mihăilescu

# Abstract

The spatial control of cellular adhesion is fundamental to the development of studies of cell interaction, cellular microarrays, and cell based biosensors. The ability to pattern cell adhesion on flat substrates and in microfluidic channels is important for locating cell near microdetectors in cell based biosensor devices. Cell adhesion can be controlled by patterning a material's wettability, as many cells prefer to adhere to a hydrophilic surface over hydrophobic materials, due to differences in protein adsorption and conformation on these materials.

This thesis focuses on patterning the surface wettability of poly(dimethylsiloxane) (PDMS) in order to spatially control cell adhesion. The polymer is selectively modified by the deposition of aluminum through a stencil mask in a magnetron sputtering system. After etching away the aluminum layer, a hydrophilic oxygen rich silica-like layer is exposed. This technique permits the creation of hydrophilic dots which are surrounded by the hydrophobic native PDMS. A second technique involving the use of photolithography results in a surface that can undergo hydrophobic recovery. By contrast, the selected areas covered by aluminum are protected against hydrophobic recovery. Finally, photolithography is used to selectively react a methyl terminated alkyl silane with the modified surface.

Each surface modification was characterized by X-ray photoelectron spectroscopy, atomic force microscopy, contact angle measurements, force distance curves, cell attachment and viability tests; the effectiveness of the techniques to pattern wettability and cell adhesion was assessed. The relative adsorption of fibronectin and fibrinogen was visualized on the patterned surface. Further, the relative availability of the cell binding sites were also visualized on the surface through immunofluorescent labeling.

While all patterning methods were effective at controlling surface wettability, cells did not show any selectivity on the surfaces patterned for hydrophobic recovery. The use of an alkyl silane proved more effective, as cell attachment did show some selectivity. However, cells were able to adhere and grow on the hydrophobic silanized

regions. The stencil mask patterned surfaces showed cell selectivity, with cells almost completely avoiding the native hydrophobic PDMS background.

Overall, the stencil mask patterning technique proved to be the most effective at controlling cell adhesion. Thus this surface patterning technique was integrated into reversibly and irreversibly sealed microfluidic channels.

**Keywords:** cell adhesion, hydrophobic recovery, magnetron sputtering, microfluidic, micropatterning, photolithography, plasma modification, protein adsorption, protein conformation, silanization, surface modification

# Acknowledgements

It would be impossible to finish a graduate degree without the support and friendship of the people you meet along the way. I would like to take this opportunity to first and foremost thank my thesis supervisor Dr. Peter Norton for his invaluable insights and guidance while pursuing this work. Without his mentoring and experience I would not be where I am today. He has helped make my graduate experience an enjoyable one and helped me develop into an independent researcher. I look forward to attending many BBQ and Christmas parties in the future.

Thank you also to everyone in my lab for all your help and experience. I found our frequent discussions both beneficial and interesting. Your company during long sputtering sections, help keep me sane. Particularly, I would like to thank Natasha Patrito and Clair McCague for their guidance and support when I first arrived, and Jayna Chan for her constant "motivation". I can't forget the many friends I made in the department and across the university. Miss Amanda Leclair, your friendship and many scientific discussions are greatly appreciated. Although we did not share a supervisor, you were as much my lab mate as anyone else. And Trissa Pontes, I don't know how I'll ever handle lunch time without you. Thank you for your friendship and being in my wedding party.

A great thank you to all the staff and faculty here in the Chemistry department. A special thanks to Nancy Bell, Todd Simpson, Rick Glue, Tim Goldhawk, Mark Beisingner and Mary Jane Walzak from the Nanofab and Surface Science labs. I would like to acknowledge the Developmental Studies Hybridoma Bank where the HFN 7.1 developed by Klebe, R.J. was obtained, and developed under the auspices of the NICHD and maintained by The University of Iowa, Department of Biology, Iowa City, IA 52242.

I would also like to thank my family. My Mom for supporting me no matter what I wanted to do, for being patient with me when I could find my pencil. My father, although your many history and science lessons would occasionally make me late for school, you activated my curiosity and inspired me to learn. My sisters and brother, you guys are my best friends, I'm so lucky to have such close siblings.

I would like to thank my husband Dan. You are the love of my life, my best friend, my cheering squad, prime motivator and my rock. Your support and encouragement keep me going, you make me laugh and you make me smile. I love you so much. You are the only person I know willing to BBQ in the middle of winter in flip flops.

I would like to acknowledge the financial support I received through the University of Western Ontario, the Natural Sciences and Engineering Research Council

*Acknowledgements*

---

(NSERC), Ontario Graduate Scholarship (OGS) which was vital in giving me the opportunity to pursue my degree.

And lastly thank you to all my friends who have been there for me throughout my studies. The many wing nights, hockey games, GWBBQs, GSBBQs, and Settler of Catan games have been the highlights the last five years.

# Table of Contents

Certificate of Examination . . . . .	ii
Abstract . . . . .	iii
Acknowledgements . . . . .	v
Table of Contents . . . . .	vii
List of Tables . . . . .	xi
List of Figures . . . . .	xii
Acronyms . . . . .	xv
<b>1 Introduction . . . . .</b>	<b>1</b>
1.1 Cell Patterning for Cell Based Microsystems and Microfluidics . . . . .	1
1.2 Cell Adhesion and Proliferation on Surfaces <i>In Vitro</i> . . . . .	3
1.2.1 Surface Wettability Effect on Cell Adhesion . . . . .	3
1.2.2 Surface Charge Effects on Cell Adhesion . . . . .	6
1.2.3 Surface Roughness Effects on Cell Adhesion . . . . .	7
1.2.4 Surface Stiffness Effects on Cell Adhesion . . . . .	8
1.3 Patterning Cell Adhesion . . . . .	8
1.3.1 Photolithography . . . . .	8
1.3.2 Microcontact Printing . . . . .	11
1.3.3 Microfluidic Patterning . . . . .	13
1.3.4 Stencil Patterning . . . . .	15
1.3.5 Ink-jet printing . . . . .	16
1.4 PDMS as a Component for Cell Based Microsystems and Microfluidics	16
1.5 Chemical Modification of PDMS Surfaces . . . . .	19
1.5.1 Plasma and High Energy Modification of the PDMS Surface .	20
1.6 Scope of Thesis . . . . .	22



<b>2</b>	<b>Patterning the Wettability of PDMS for Spatial Control of Cellular Adhesion</b>	<b>25</b>
2.1	Introduction	25
2.2	Materials and Methods	28
2.2.1	Reagents	28
2.2.2	Preparation and Modification of PDMS	29
2.2.2.1	Preparation of Bulk PDMS	29
2.2.2.2	Preparation of Micrometer- and Nanometer-Thick PDMS Films	29
2.2.2.3	Magnetron Surface Modification of PDMS	31
2.2.2.4	Preparation of Hydrophobically Recovered PDMS	31
2.2.2.5	Preparation of ODTMS Treated PDMS	31
2.2.3	Hydrophobic/Hydrophilic Patterning of PDMS	32
2.2.3.1	Stencil Mask Patterned Surfaces	32
2.2.3.2	Photolithographic Patterning of Hydrophobically Recovered PDMS	34
2.2.3.3	Octadecyltrimethoxysilane Patterning of PDMS	35
2.2.4	Characterization of Modified and Patterned PDMS	35
2.2.4.1	Sessile Drop Water Contact Angle Measurement	35
2.2.4.2	X-ray Photoelectron Spectroscopy	38
2.2.4.3	Water Localization Test	39
2.2.5	Cell Culture and Patterning	39
2.2.5.1	Imaging	40
2.2.5.2	Live Cell Imaging	40
2.3	Results and Discussion	42
2.3.1	Stencil Mask Patterning of PDMS	42
2.3.1.1	Live Cell Imaging	45
2.3.2	Patterning of Hydrophobically Recovered PDMS by Photolithography	47
2.3.3	Patterning of ODTMS on Modified PDMS by Photolithography	57
2.4	Conclusions	62

<b>3</b>	<b>Cell and Protein Interactions with PDMS and Surface Modified PDMS . . . . .</b>	<b>64</b>
3.1	Introduction . . . . .	64
3.2	Materials and Methods . . . . .	65
3.2.1	Reagents . . . . .	65
3.2.2	Preparation of PDMS and modified PDMS surfaces . . . . .	66
3.2.3	Preparation of Patterned PDMS Surfaces . . . . .	66
3.2.4	Cell Proliferation and Viability Testing . . . . .	66
3.2.5	Cell Imaging . . . . .	69
3.2.6	Fibronectin Conjugated with Oregon Green Dye . . . . .	71
3.2.7	Fibronectin and Fibrinogen Adsorption Studies . . . . .	72
3.2.8	Fibronectin Conformation Study . . . . .	72
3.2.9	Confocal Imaging . . . . .	75
3.3	Results and Discussion . . . . .	75
3.3.1	Cell Proliferation and Viability Studies . . . . .	75
3.3.2	Protein Adsorption on Patterned PDMS . . . . .	80
3.3.3	Fibrinogen Adsorption on Patterned PDMS . . . . .	80
3.3.3.1	Fibronectin Adsorption . . . . .	83
3.3.4	Conformational Studies of Adsorbed Fibronectin on Patterned PDMS . . . . .	88
3.4	Conclusions . . . . .	93
<b>4</b>	<b>Atomic Force Studies of PDMS and Surface Modified PDMS . . . . .</b>	<b>95</b>
4.1	Introduction . . . . .	95
4.2	Materials and Methods . . . . .	97
4.2.1	Reagents . . . . .	97
4.2.2	Preparation of PDMS and Modified PDMS surfaces . . . . .	98
4.2.3	Preparation of Patterned PDMS Surfaces . . . . .	98
4.2.4	Cell Culture and Patterning . . . . .	98
4.2.4.1	Optical Imaging . . . . .	99
4.2.5	Atomic Force Microscopy . . . . .	99
4.2.6	Force Distance Curves . . . . .	101
4.2.7	Interactions Between a Tip-less Cantilever and Modified PDMS . . . . .	104
4.3	Results and Discussion . . . . .	104
4.3.1	Topographical Analysis of PDMS and Modified PDMS . . . . .	104
4.3.2	Surface Stiffness of PDMS and Magnetron Modified PDMS . . . . .	113
4.4	Interactions of Cells and a Tip-less Cantilever with Magnetron Modified PDMS . . . . .	115
4.5	Conclusions . . . . .	124

<b>5</b>	<b>Fabrication of Patterned Microfluidic Channels . . . . .</b>	<b>127</b>
5.1	Introduction . . . . .	127
5.2	Materials and Methods . . . . .	130
5.2.1	Reagents . . . . .	130
5.2.2	Preparation of PDMS Substrates . . . . .	130
5.2.2.1	Bulk PDMS . . . . .	130
5.2.2.2	Molded PDMS by Soft Lithography . . . . .	131
5.2.2.3	Preparation of Thin PDMS Films . . . . .	133
5.2.2.4	Magnetron Surface Modification of PDMS . . . . .	133
5.2.3	PDMS Bonding . . . . .	133
5.2.3.1	PDMS-Glass Bonding . . . . .	133
5.2.3.2	PDMS-PDMS Bonding . . . . .	134
5.2.3.3	Tensile Testing . . . . .	134
5.2.3.4	Leakage Testing . . . . .	136
5.2.4	Stencil Mask Fabrication . . . . .	137
5.2.5	Fabrication and Testing of Patterned Microfluidic Channels . . . . .	139
5.2.5.1	Reversible Bonded Patterned Channels . . . . .	139
5.2.5.2	Chromium Protection of Aluminum Coated PDMS . . . . .	140
5.2.5.3	Irreversible Bonded Channels . . . . .	141
5.2.5.4	Fibrinogen Patterned Microfluidic Channels . . . . .	144
5.2.6	Imaging . . . . .	145
5.3	Results and Discussion . . . . .	145
5.3.1	Reversibly Bonded Patterned Channels . . . . .	145
5.3.2	Irreversibly Bonded Patterned Channels . . . . .	147
5.3.2.1	PDMS-PDMS and PDMS-Glass bonding . . . . .	147
5.3.2.2	Physical Mask Fabrication . . . . .	149
5.3.2.3	Chromium Masking . . . . .	151
5.3.2.4	Channel Fabrication . . . . .	151
5.4	Conclusion . . . . .	155
<b>6</b>	<b>Thesis Summary and Future Work . . . . .</b>	<b>157</b>
	<b>References . . . . .</b>	<b>161</b>
	<b>Curriculum Vitae . . . . .</b>	<b>177</b>

## List of Tables

2.1	XPS atomic composition analysis of native and modified PDMS . . .	28
2.2	Contact angles of PDMS, modified PDMS, glass and modified glass .	58
2.3	XPS atomic composition analysis of ODTMS modified PDMS . . . .	59
3.1	The size of squares found on a hemocytometer and their corresponding surface area and volume . . . . .	67
3.2	Cell viability after 24, and 48 hrs on PDMS and modified PDMS . . .	79
3.3	Summary of cell patterning, protein adsorption, and protein concentration on patterned PDMS. (+) indicates an increase inside of the dots, (-) indicates an increase outside of the dots, and (=) indicates uniformity across the surface. . . . .	93
4.1	Surface topography of PDMS and modified PDMS . . . . .	110
5.1	Bonding efficiency, pull-off strength, maximum flow rate and channel pressure for PDMS-glass and PDMS-PDMS sealed devices . . . . .	148

# List of Figures

1.1	Cell attachment on hydrophobic and hydrophilic surfaces . . . . .	5
1.2	Positive and negative photolithography . . . . .	9
1.3	Photolithographic patterning of alkyl silanes on a glass surface . . . . .	10
1.4	Microcontact printing . . . . .	12
1.5	Patterning using microfluidic channels . . . . .	14
1.6	Patterning using a stencil mask . . . . .	15
1.7	Chemical structure of poly(dimethylsiloxane) . . . . .	17
1.8	Reaction scheme for platinum catalyzed PDMS curing . . . . .	18
1.9	Layered structure of plasma treated PDMS . . . . .	21
2.1	Schematic representation of the magnetron sputtering deposition process	26
2.2	Reaction between ODTMS and magnetron treated PDMS . . . . .	32
2.3	Stencil mask patterning method . . . . .	33
2.4	Photolithographic patterning of hydrophobically recovered and mag- netron Treated PDMS . . . . .	34
2.5	Photolithographic patterning of ODTMS on magnetron treated PDMS	36
2.6	Water droplet on surfaces of different wettabilities . . . . .	38
2.7	Reaction mechanism of formaldehyde fixation . . . . .	41
2.8	Bright field reflection-mode optical images of the stainless steel screens used as stencil masks . . . . .	43
2.9	Optical images of aluminum arrays patterned on PDMS . . . . .	44
2.10	Optical images of water droplets localized on stencil masked patterned PDMS . . . . .	45
2.11	Optical images of cells incubated on stencil mask patterned PDMS . . . . .	46
2.12	Optical images of live cells on stencil mask patterned PDMS . . . . .	48
2.13	Optical images of photomasks used to photolithographically pattern aluminum on PDMS . . . . .	49
2.14	Optical images of photomasks and corresponding aluminum patterned surfaces . . . . .	51
2.15	Optical images of water droplets localized on PDMS surfaces pho- tolithographically patterned with hydrophobically recovered areas . . . . .	51
2.16	Optical images of cells incubated on PDMS surface photolithographi- cally patterned with hydrophobically recovered areas . . . . .	52
2.17	Static contact angle of thin PDMS samples . . . . .	54
2.18	Advancing contact angle of thin PDMS samples . . . . .	55
2.19	Receding contact angle of thin PDMS samples . . . . .	56

2.20	Contact angle hysteresis of thin PDMS samples . . . . .	56
2.21	XPS survey spectrum of ODTMS modified PDMS . . . . .	59
2.22	C1S XPS spectrum of PDMS and ODTMS modified PDMS . . . . .	60
2.23	Optical images of water droplets localized on a modified PDMS surface photolithographically patterned with ODTMS . . . . .	60
2.24	Optical images of cells incubated on the ODTMS patterned surface . . . . .	61
3.1	Grid structure of a hemocytometer . . . . .	68
3.2	Structure of trypan blue . . . . .	68
3.3	Wide field fluorescent microscope . . . . .	70
3.4	Structure of DAPI . . . . .	71
3.5	Illustration of immunofluorescent labeling . . . . .	73
3.6	Schematic representation of a confocal microscope . . . . .	74
3.7	Cell growth on PDMS and modified PDMS . . . . .	76
3.8	Cell growth on PDMS-Al and PDMS-R, stained with DAPI . . . . .	78
3.9	Cell growth on PDMS-Al and PDMS-R . . . . .	78
3.10	Confocal images of Alexa Fluor 488 conjugated fibrinogen adsorption on stencil masked patterned samples . . . . .	81
3.11	Confocal images of Alexa Fluor 488 conjugated fibrinogen adsorption on patterned hydrophobic recovered PDMS samples . . . . .	82
3.12	Confocal images of Alexa Fluor 488 conjugated fibrinogen adsorption on ODTMS patterned samples . . . . .	82
3.13	Fibronectin adsorption on stencil masked patterned samples . . . . .	83
3.14	Fibronectin adsorption on patterned hydrophobic recovered PDMS samples . . . . .	84
3.15	Fibronectin adsorption on ODTMS photolithographically patterned samples . . . . .	85
3.16	Fn adsorbed onto stencil masked patterned samples . . . . .	85
3.17	Fn-OG adsorbed onto patterned hydrophobic recovered PDMS . . . . .	86
3.18	Fn-OG adsorbed onto ODTMS patterned PDMS . . . . .	87
3.19	Fn Conformation on patterned PDMS samples . . . . .	90
3.20	Fn conformation of stencil masked patterned PDMS . . . . .	91
3.21	Fn conformation on ODTMS patterned PDMS . . . . .	92
4.1	Typical AFM setup . . . . .	100
4.2	Typical force curve . . . . .	103
4.3	AFM of aluminum coated PDMS . . . . .	106
4.4	AFM of photolithographically patterned PDMS . . . . .	108
4.5	AFM of ODTMS functionalized PDMS . . . . .	109
4.6	AFM of stencil masked patterned PDMS . . . . .	111
4.7	AFM of ODTMS functionalized PDMS . . . . .	112
4.8	Force curves of PDMS and magnetron treated PDMS . . . . .	113
4.9	AFM of C2C12 and COS-7 cells on PDMS . . . . .	116

4.10	Optical and AFM images of C2C12 cells on stencil masked PDMS . . .	117
4.11	AFM of C2C12 cells on stencil masked patterned PDMS . . . . .	118
4.12	AFM of C2C12 cells on wet and dry stencil masked patterned PDMS	119
4.13	Cross-sectional analysis of surface wrinkles formed on wet and dry stencil masked patterned PDMS . . . . .	120
4.14	Topographical cross-sectional analysis of C2C12 cells fixed on wet and dry stencil masked patterned PDMS . . . . .	120
4.15	Tip-less cantilever interacting with modified PDMS . . . . .	122
4.16	Tip-less cantilever pushing on dry and wet modified PDMS . . . . .	123
4.17	Tip-less cantilever pushing a glass bead into modified PDMS . . . . .	124
5.1	Section of a microfluidic channel . . . . .	128
5.2	Fabrication microfluidic channels in PDMS by soft lithography . . . . .	132
5.3	Schematic illustration of the bonding procedures of PDMS-glass and PDMS-PDMS . . . . .	135
5.4	Experimental set-up of the tensile bonding pull-off test . . . . .	136
5.5	Fabrication procedure used to form stencil masks . . . . .	138
5.6	Stencil masked used to pattern microfluidic channels . . . . .	142
5.7	Fabrication procedure used to create the patterned bottom of the mi- crofluidic device . . . . .	143
5.8	Fabrication procedure used to create irreversibly bonded patterned mi- crofluidic channels . . . . .	144
5.9	Reversibly bonded patterned microfluidic channels . . . . .	146
5.10	Straight channel used for leakage test . . . . .	149
5.11	Custom stencil masks . . . . .	150
5.12	Chromium dots over aluminum . . . . .	152
5.13	Cells grown on patterned PDMS, patterned with aluminum dots which were then coated with chromium . . . . .	153
5.14	Images of the half channel mask . . . . .	154
5.15	Straight channel used for leakage test . . . . .	155

## Acronyms

<b>3-APTMS</b>	<i>2-Aminopropyltrimethoxy Silane</i>
<b>3-MPTMS</b>	<i>3-Mercaptopropyl-Trimethoxy Silane</i>
<b>AFM</b>	<i>Atomic Force Microscopy</i>
<b>ATR-FTIR</b>	<i>Attenuated total reflection Fourier transform infrared spectroscopy</i>
<b>BSA</b>	<i>Bovine serum albumin</i>
<b>DAPI</b>	<i>"4',6-Diamidino-2-phenylindole"</i>
<b>DMEM</b>	<i>Dulbecco's Modified Eagle Medium</i>
<b>DMSO</b>	<i>Dimethyl sulfoxide</i>
<b>DNA</b>	<i>Deoxyribonucleic Acid</i>
<b>ECM</b>	<i>Extra Cellular Matrix</i>
<b>EDTA</b>	<i>Ethylenediaminetetraacetic acid</i>
<b>ELISA</b>	<i>Enzyme-Linked Immunosorbent Assays</i>
<b>FBS</b>	<i>Fetal Bovine Serum</i>
<b>Fg</b>	<i>Fibrinogen</i>
<b>Fg-488</b>	<i>Fibrinogen conjugated to Alexa Fluor 488</i>
<b>FITC</b>	<i>Fluorescein Isothiocyanate</i>
<b>Fn</b>	<i>Fibronectin</i>
<b>Fn-OG</b>	<i>Fibronectin conjugated to Oregon Green</i>
<b>FRET</b>	<i>Fluorescence Resonance Energy Transfer</i>
<b>HMDS</b>	<i>Hexamethyldisilazane</i>
<b>IgG</b>	<i>Immunoglobulin G</i>
<b>ODTMS</b>	<i>Octadecyltrimethoxysilane</i>
<b>OG</b>	<i>Oregon Green</i>
<b>PATTI</b>	<i>Pneumatic adhesion tensile testing instrument</i>
<b>PBS</b>	<i>Phosphate Buffered Saline</i>
<b>PDMS</b>	<i>Polydimethylsiloxane</i>



<b>PDMS-AI</b>	<i>Magnetron treated poly(dimethylsiloxane) after aluminum etch</i>
<b>PDMS-ODTMS</b>	<i>Octadecyltrimethoxysilane treated poly(dimethylsiloxane)</i>
<b>PDMS-R</b>	<i>Hydrophobically recovered poly(dimethylsiloxane)</i>
<b>PEG</b>	<i>Poly(ethylene) glycol</i>
<b>PSD</b>	<i>Power Spectral Density</i>
<b>QCM</b>	<i>Quartz crystal microbalance</i>
<b>RGD</b>	<i>Arginine-Glycine-Aspartic Acid</i>
<b>RIE</b>	<i>Reactive Ion Etching</i>
<b>SAMs</b>	<i>Self Assembled Monolayers</i>
<b>SSIMS</b>	<i>Static secondary ion mass spectrometry</i>
<b>UV</b>	<i>Ultraviolet</i>
<b>Vn</b>	<i>Vitronectin</i>
<b>XPS</b>	<i>X-Ray Photoelectron Spectroscopy</i>

# Chapter 1

## Introduction

### 1.1 Cell Patterning for Cell Based Microsystems and Microfluidics

*In vitro* cell culturing techniques involve growing cells outside of the body in cell culture flasks or petri dishes. Outside of their natural environment cells are kept alive in a cell media containing antibiotics, glucose, growth factors and other nutrients [1]. The growth factors generally come in the form of calf or fetal bovine serum (FBS). While cell culture lacks the three-dimensional architecture of an organism's tissue it still provides many advantages, as *in vivo* methods require the use of live animals, are expensive, cumbersome and ethically questionable [1, 2]. Also, it is not feasible to perform *in vivo* testing in humans due to potential toxicity, thus, testing *in vitro* on human cells can give insight lacking in animal models. Despite its advantages, cell culture requires large fluid volumes, bulky incubators and other expensive equipment as large sample numbers are required to obtain statistically relevant data. To overcome this, microfabrication and microfluidics technologies have been used to miniaturize components and create new devices which reduce the cost and time of cell culture studies [1].

Some advantages in using microfabrication and microfluidics technologies include the small size, the ability to perform multiple assays on a single array, multiple processes integrated on one chip, as well as small reagent and sample sizes [2]. These

advantages make microfabrication and microfluidic techniques ideal for cell culture as they will allow for both controlled cellular micropatterning and control over the cell's environment [2]. Micropatterning cell cultures can allow for fundamental studies of cell interactions and can help integrate cells into cell based biosensors. Micropatterning for cell cultures is typically achieved by selectively modifying a surface to create islands of materials which promote cell adhesion, while providing a background which is non-adhesive and inhibits cell adhesion [2–4].

Controlling the size of cell adhesive regions may limit the ability of a cell to spread and thus control the cell's size and shape. Doing so has been shown to affect cell growth, proliferation, cell function and cell death [5–8]. Cell patterns can also be used to create co-cultures and study the interactions between different cell types [9]. Other cellular interactions, such as cell-cell and cell-surface interactions have also been studied [4].

Cell patterning is also an important component for cell based biosensors and bioarrays, as it is necessary to spatially position cell(s) directly on top of detectors in these devices [10, 11]. In a cell-based biosensor the cell acts as a transducer which responds to environmental changes in a way that is measurable by a secondary transducer [12–14]. The secondary transducer is a device such as a microelectrode or optical sensor which then converts the cell's response into an electrical signal which is processed and analyzed [12]. Typical cell signals include fluorescence, metabolism, impedance, intracellular and extracellular potentials [14]. Cell based sensors can be used for drug discovery, clinical diagnostics and for the detection of toxic agents [2].

## 1.2 Cell Adhesion and Proliferation on Surfaces

### *In Vitro*

Many cells grow as adherent monolayers *in vivo*, and thus must attach and spread out on a substrate before they are able to proliferate [1]. In order to adhere to a surface a cell must bind to extra cellular matrix (ECM) proteins on the surface *via* specific receptors. The surface properties can greatly affect the ability for cells to adhere and spread. Properties such as surface wettability, charge, chemistry, roughness and stiffness have all been shown to play an essential role in determining whether cells are able to adhere [15, 16].

Before a cell approaches a surface, proteins found in the serum begin to adsorb to the surface. The ability of a protein not only to adsorb but to do so in an appropriate conformation, will determine whether or not cells are able to attach. Cells bind to the serum proteins, such as vitronectin (Vn) or fibronectin (Fn), through integrins in the cell membrane. The integrins attached to binding domains, such as the arginine-glycine-aspartic acid (RGD) peptide sequence, found on serum proteins.

While many scientists have tried to establish criteria for a good biologically active surface, it has not been easy or definitive since different cell lines may react differently to the same surface. Also it is difficult, if not impossible, to completely separate surface properties that affect cell growth. None-the-less general trends have been established and are discussed below.

#### 1.2.1 Surface Wettability Effect on Cell Adhesion

When proteins are in solution they interact with water molecules and attempt to lower the the entropic penalty caused by the interaction between hydrophobic side chains

with water by creating a folded protein structure [17, 18]. Generally the interior of the structure is occupied by the non polar or hydrophobic amino acid side chains, while the exterior is occupied with the polar, acidic and basic side chains. Even so, the exterior or accessible area of the protein structure is 40 to 50 % non polar groups. On a hydrophobic surface it is thermodynamically favorable for the proteins to adsorb due to the large number of non polar groups on the protein [16–18]. On hydrophilic surface there is a large energy barrier to protein adsorption caused by the tightly bound water molecules on the surface. While there are some exceptions [19], more often than not, hydrophobic surfaces adsorb more protein than hydrophilic surfaces [20, 21].

In order to overcome the energy barrier associated with adsorbing to a surface, proteins can undergo conformational changes. The changes can increase the entropy of the system, by affecting the secondary structure and by increasing the contact between the protein and the surface. Most adsorbed proteins undergo some type of structural change; generally this change is more stable than in a dissolved state and is affected by the wettability of the surface [16, 22–24]. These conformational changes can affect the protein’s activity by either exposing or hiding different functionalities such as the RGD binding sequence, which directly affect cell adhesion (Figure 1.1).

Self assembled monolayers (SAMs) of alkyl thiols on gold surfaces are used to vary surface wettability when studying protein adsorption and cell adhesion. Terminating groups such as  $\text{CH}_3$ ,  $\text{OH}$ ,  $\text{COOH}$ , and  $\text{NH}_2$  are often used to obtain a series of surfaces with changing chemistry and wettability. Important ECM proteins, Fn and Vn were found to adsorb the least on the OH terminated SAMs, however, the OH terminated SAMs showed the higher availability of the binding domains for both proteins [25, 26]. Similarly, Fn and Vn adsorption increased on more hydrophobic SAMs created by mixing OH and  $\text{CH}_3$  thiols [27]. As the amount of OH terminated

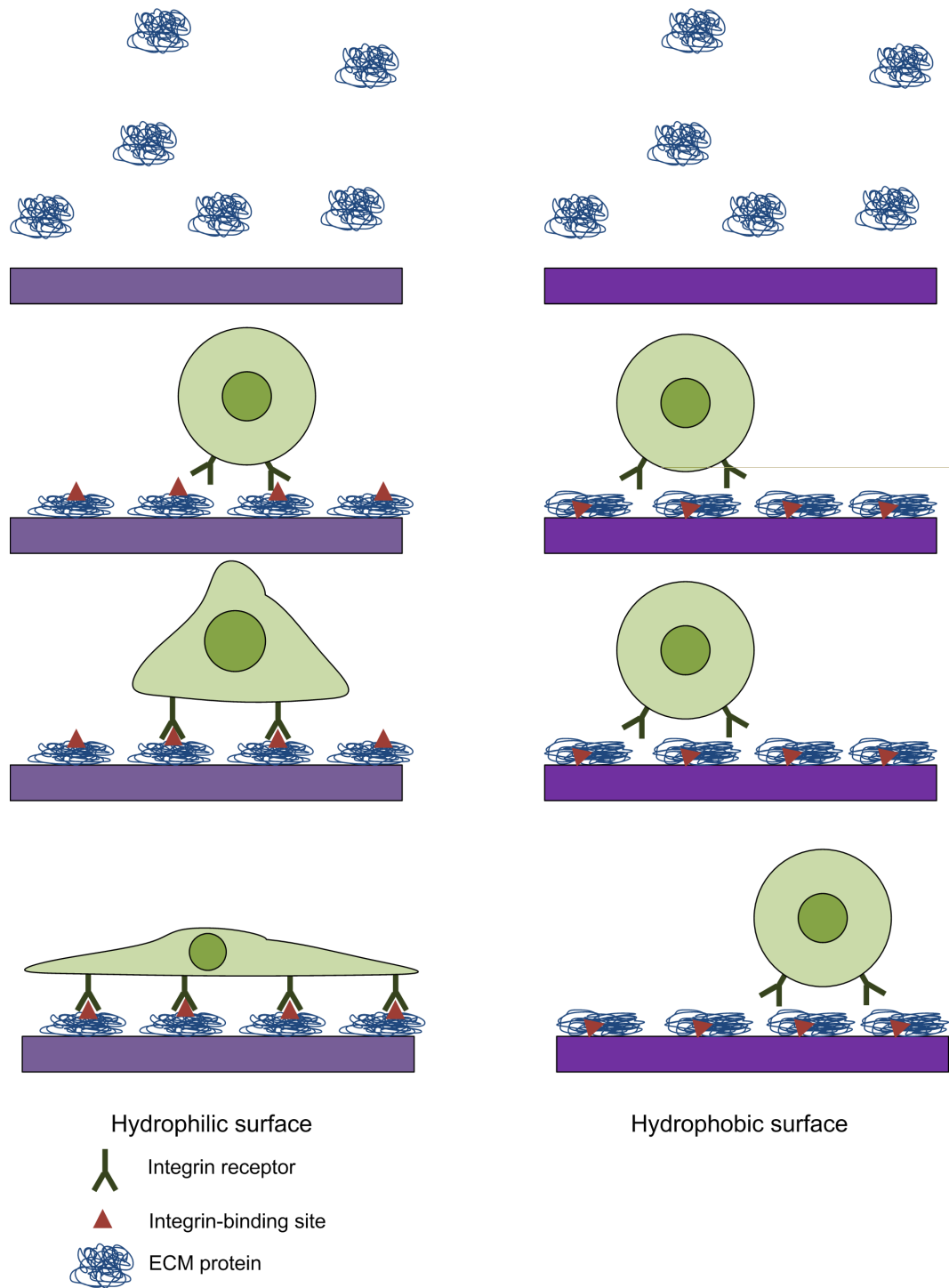


Figure 1.1: Protein conformation and its affects on cell attachment on hydrophilic (left) and hydrophobic (right) surfaces

thiols increased relative to the CH<sub>3</sub> terminating thiols, protein adsorption decreased but the availability of the binding sites increased significantly.

The differences in protein conformation on hydrophobic and hydrophilic SAMs have been directly linked to increased cell spreading and adhesion on hydrophilic surfaces [27,28]. The increase in cell adhesion is not limited to SAMs but also to other materials [15,29–33]. An important example is that of polystyrene. Polystyrene is used to manufacture cell culture plates and petri dishes. Due to polystyrene's hydrophobic surface, many cells are unable to spread and adhere, limiting its use. Surface treatments, including acid treatments and exposure to high energy ionizing radiation are known to decrease polystyrene's contact angle and thus increase cell adhesion [29]. These high energy radiation treatments are used to manufacture standard tissue culture plates [1].

While cells often prefer hydrophilic materials, there are some exceptions. Polyethylene glycol (PEG) is a hydrophilic material which shows little bioactivity. PEG's hydrophilicity reduces the amount of protein adsorption to its surface, such that, it can no longer promote cell adhesion [34]. When PEG is mixed with other more hydrophobic materials, it can be used to lower the surface's hydrophobicity and increase cell adhesion [35]

### 1.2.2 Surface Charge Effects on Cell Adhesion

Due to electrostatic interactions between charged molecules, surface charge plays a vital role in protein adsorption and cell adhesion [16,36–38]. Often surfaces with amine functionality show an increase in cell adhesion even over surfaces with lower contact angles [30,31,39]. At a biological pH of 7.4, amine groups are positively charged, which provides an attractive interaction with the negative cell membrane

[16]. Other functional groups such as OH and COOH groups, provide a lower contact angle but are neutral and negatively charged respectively. Cells have been observed only making contact with positively charged surfaces when adhering to mixed surfaces. These cells formed a bridge over the negatively charged areas in order to make contact with the positive surface [36,37]. The effects of a charged surface is often mitigated by the ions in solution, as these ions will act as counter ions and reduce the interaction between the surface charge and the cell membrane.

### 1.2.3 Surface Roughness Effects on Cell Adhesion

In their natural environment cells may encounter many different surfaces, some of which will be smooth while others maybe significantly rougher. Often an increase in surface roughness is assumed to be responsible for better cellular adhesion [40–43]. Rougher surfaces will provide larger surface areas for adhesion and have been linked to increased protein adsorption [40]. Some reports have even suggested that increased surface roughness can lead to higher availability of protein binding sites [44]. This increase in cell adhesion occurs despite the increase in hydrophobicity associated with increased roughness [45].

The type of surface topography can greatly affect the biological processes of cells. Cells will orientate in the direction of ridges or groves in a surface [46, 47]. Cells have also been shown not to proliferate well on surfaces with sharp edges, as this topography does not mimic physiological conditions and leads to cellular rejection [47, 48]. Some cell types have also been reported to prefer smooth surfaces, others intermediate roughness [42, 49]. Overall the effects of surface roughness is cell-type dependent as cells will respond best to surfaces which mimic their physiological environment.



### 1.2.4 Surface Stiffness Effects on Cell Adhesion

Another important physical property of a surface that affects cell growth is the surface stiffness or elastic modulus [50–52]. To study surface stiffness without affecting chemistry or roughness, polymeric materials with varying degrees of crosslinking are used, typically polyacrylamide gels.

Typically, cells have been reported to proliferate and spread better on stiffer surfaces, that is ones with larger moduli [51–55]. On materials with a modulus less than 16 to 30 kPa, cells are unable to spread, remaining balled up, and thus do not adhere to the surface [53–55]. Cells begin to spread out when the modulus of the surface nears that of the cell, indicating that the ideal surface would be stiffer than the cell [55]. Further, cells which are plated on polymers with a stiffness gradient tend to migrate towards the stiffer areas after initial plating [53].

## 1.3 Patterning Cell Adhesion

Cell patterning is performed by creating cell adhesive regions and surrounding them with non adhesive backgrounds. The microelectrical and semi-conducting industries have provided many approaches for micropatterning surface chemistry. These approaches have been adapted for use in cell patterning and are discussed below.

### 1.3.1 Photolithography

Photolithography involves the use a photoactive polymer, a photoresist, to create a pattern on the surface of a substrate [3, 4, 56]. There are two standard types of photolithography: positive and negative (Figure 1.2). In both cases a thin layer of photoresist is exposed to light through an optical mask containing the desired pattern.

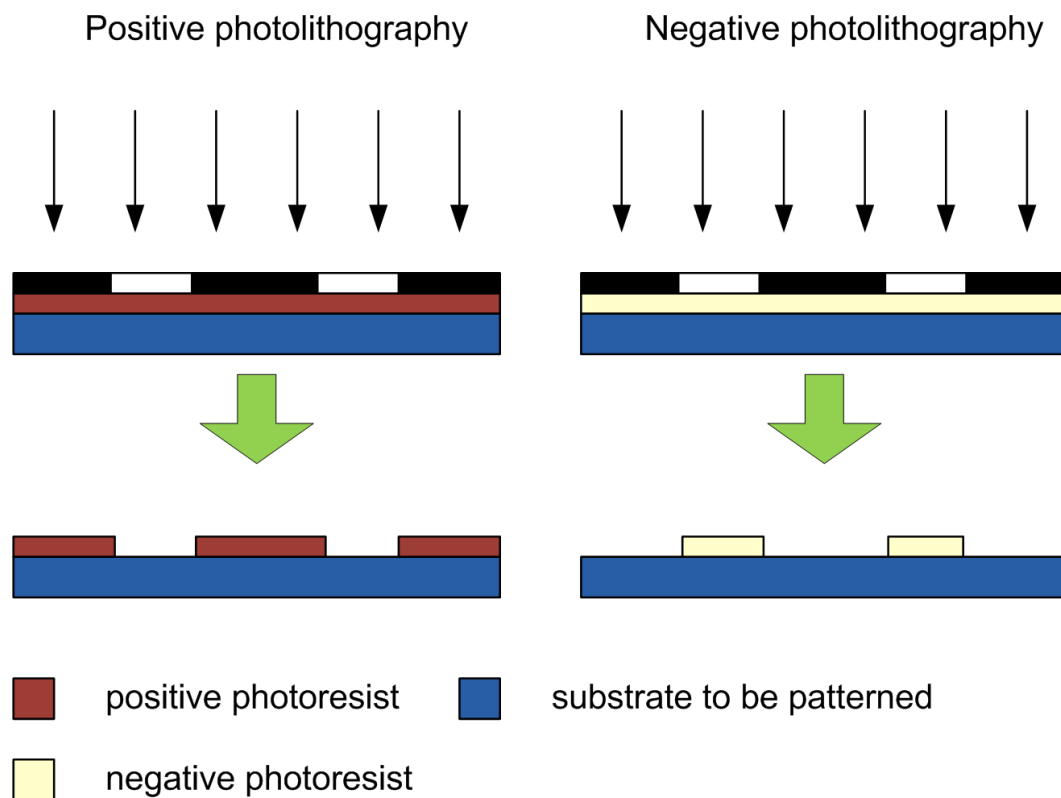


Figure 1.2: Photolithography using positive and negative photoresists

For a positive resist, the area exposed to light will break down and be washed away. A negative resist will be further cross linked and thus be more resistant to solvent. After developing, the desired pattern remains on the surface and the photoresist can be used as a protective mask for further processing.

In order to pattern cell adhesion, photolithography has been used to selectively deposit molecules onto glass, quartz, pyrex, silicon and gold [3, 4]. After creating a photolithographic pattern, the exposed surface can react with molecules containing particular functionality. Amine terminated alkyl silanes are often used to react with glass surfaces through a photoresist mask [57–62]. Once the remaining photoresist is removed, the non-amine coated surface can be backfilled with a cell repelling material such as methyl terminated alkyl silanes (Figure 1.3). Proteins have also been

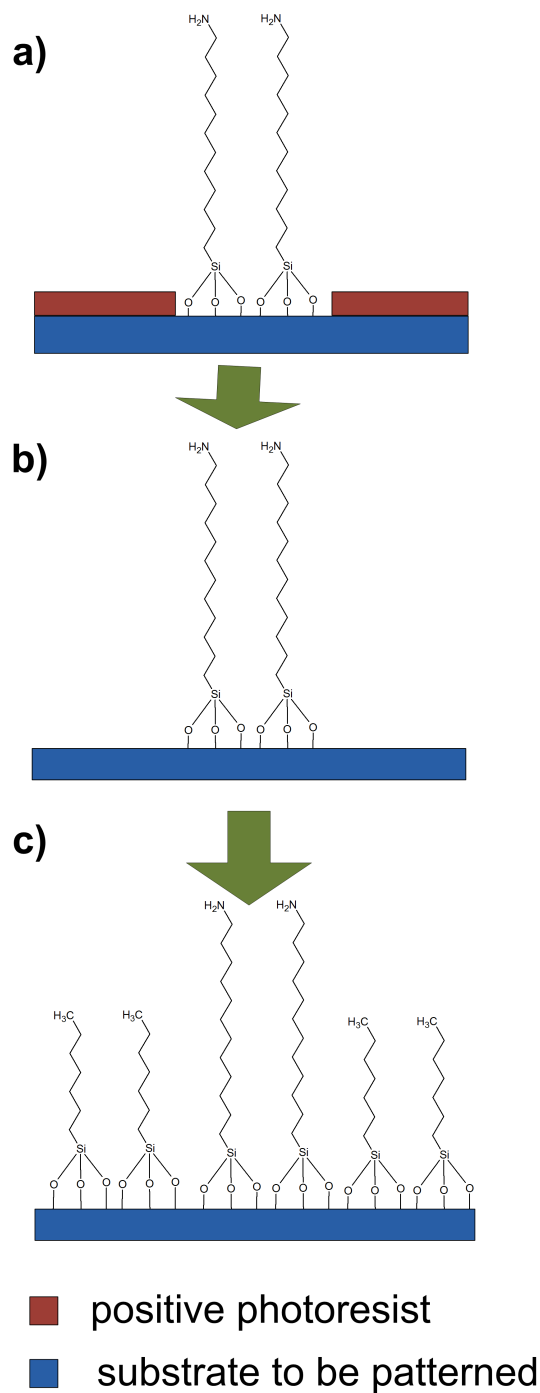


Figure 1.3: Photolithographic patterning of alkyl silanes on a glass surface. a) an amine terminated alkyl silane reacts with the exposed glass surface, b) the remaining photoresist is washed away, c) the surface is backfilled with a methyl terminated alkyl silane

immobilized on the surface using similar techniques [9]. Cells have been shown to prefer certain metal oxides, and thus cell adhesion can be spatially controlled by photolithographically patterning metal oxide deposition [63]. Further, thin gold layers have been photolithographically patterned onto glass surfaces [64]. The gold patterns were then reacted with amine terminated alkyl thiols, and the glass background with PEG-silanes.

Photolithography has become the dominate technique for cell and protein patterning [4]. Photolithography creates accurate patterns with submicron resolution, and can be used to pattern a significant number of different molecules. As it requires a cleanroom facility and expensive equipment, photolithography is often inaccessible to many biologists [4,5]. Further, the use of harsh chemicals can denature biological molecules of interest and thus care must be taken when patterning these molecules. Often, the high resolution of photolithography is not necessary, which has led to the development of other techniques for cell patterning.

### 1.3.2 Microcontact Printing

Microcontact printing using a elastomeric stamp to transfer molecules of interest to another surface. Poly(dimethylsiloxane) (PDMS) is most commonly used to form a stamp, as it is durable, biocompatible, and can make conformal contact with non flat surfaces, and its surface can be modified to work with a large number of molecules. A stamp is formed by casting liquid polymer against a mold. While molds are normally created using photolithography, they can be reused many times. Further, stamps have been used hundreds of time without degradation to the pattern [5].

Once the stamp has been created it is inked with the material to be patterned onto the surface. The stamp is then brought into conformal contact with the sub-

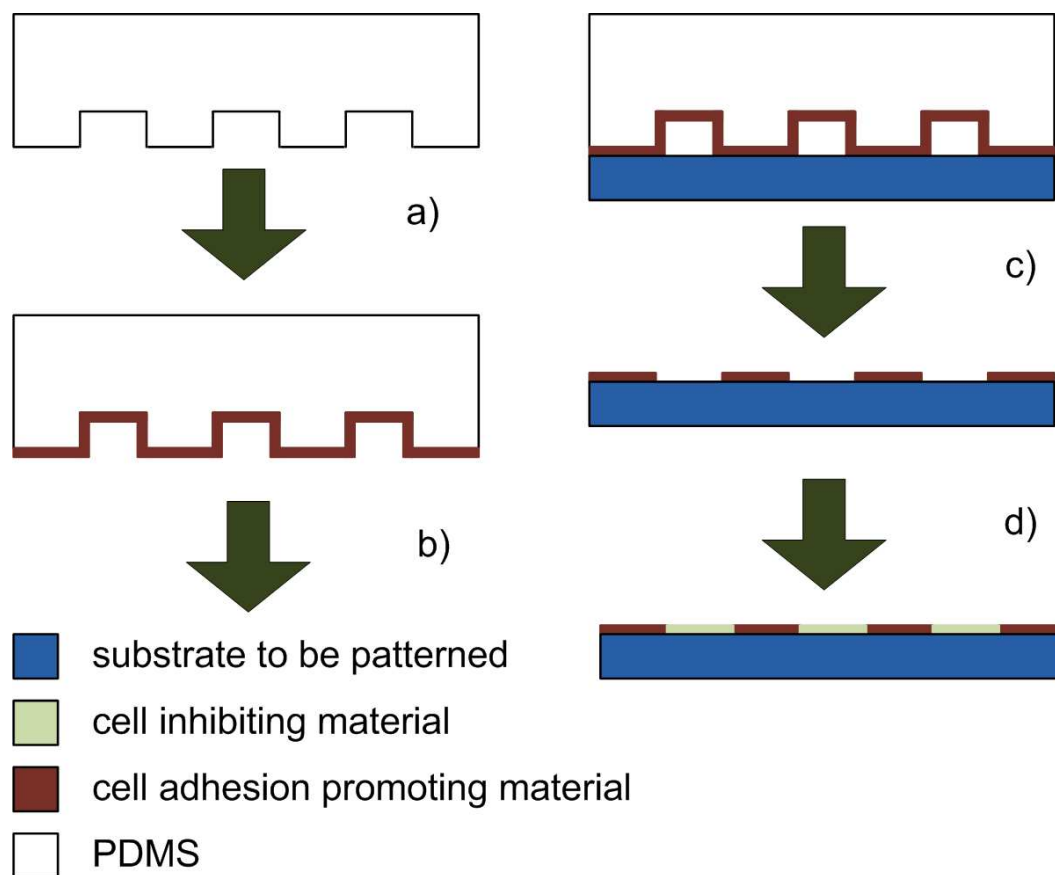


Figure 1.4: Microcontact printing used to pattern cell adherent and cell inhibiting materials. a) a PDMS stamp is inked with cell adhesion promoting material, b) the material is then stamped onto the substrate, c) the surface is backfilled with a cell inhibiting material

strate, transferring the ink (Figure 1.4). Often the non-coated regions of the substrate are backfilled with another molecule. Microcontact printing is often used to pattern gold substrates with SAMs of alkyl thiols [65].

Microcontact printing has been used to create islands of ECM proteins in order to direct cell adhesion [10, 65]. A methyl terminated thiol was stamped onto a gold surface and back filled with tris(ethylene glycol terminated alkenethiol). Fn was then adsorbed onto the surface only over the methyl terminated surface, while avoiding the ethylene glycol surface. Methyl terminated thiols have also been used

as cell adhesion inhibiting layers and backfilled using hydroxyl terminated thiols [6]. Cells then preferentially grew on the hydroxyl terminated regions, as they were more hydrophilic.

While microcontact printing is most often performed to create SAMs on gold surfaces, it has also been used to pattern alkylsiloxanes on glass [66] and to directly transfer dried proteins [67]. Microcontact printing is a versatile method which patterns a variety of molecules onto a large number of surfaces [4]. Due to the nature of the elastomeric stamp, resolution beyond a few micrometers is difficult and areas of only a few  $\text{cm}^2$  can be patterned at a time. The selection of substrate-ink combinations can be limited as the ink must show a stronger affinity to the substrate than the stamp, but must still be able to wet the stamp [4, 5, 56].

### 1.3.3 Microfluidic Patterning

Molded PDMS can also be used to create patterns using microfluidics. The PDMS mold is placed into contact with the substrate forming a network of microchannels which define the desired pattern. The material of interest is injected into the microchannels such that only select areas of the substrate come into contact with the material (Figure 1.5). The material is brought through the channels by capillary force, pressure from a pump, or electro-osmotically driven flow [68]. Microfluidics can be used to directly pattern cells [69–71], proteins [72, 73] and other biomolecules [74–76] onto a substrate without the need for drying. Microfluidics allows for the parallel patterning of many different molecules, which is not possible with other patterning methods [74, 75]. A big drawback of microfluidic patterning is its limited geometries as all channels must be interconnected.

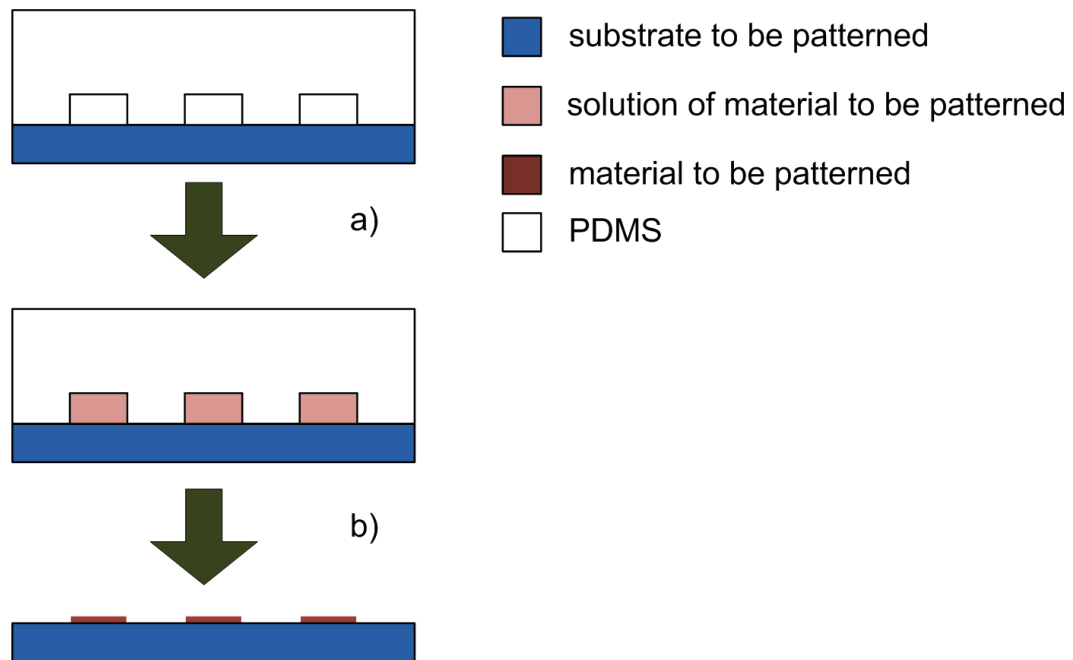


Figure 1.5: Patterning using microfluidic channels. a) molded PDMS is brought into contact with a substrate and a solution of the material of interest is pumped through the channels, depositing the material, b) the PDMS mold is removed from the surface and a thin layer of the desired material is left behind

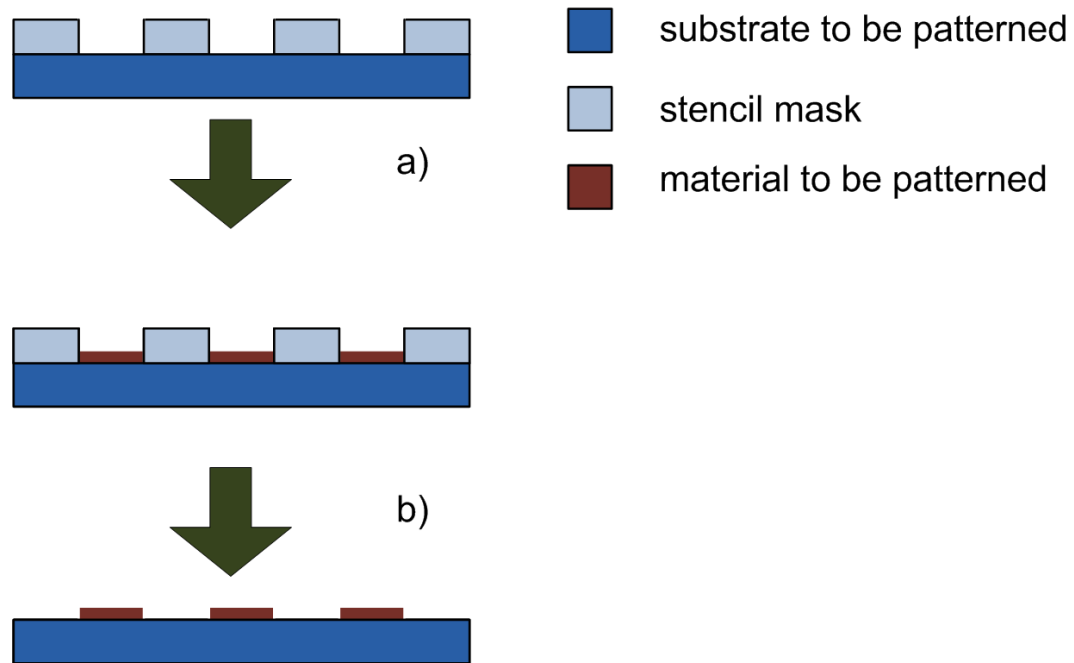


Figure 1.6: Patterning using a stencil mask. a) a stencil mask is brought into contact with a surface and the material of interest is deposited through the mask, b) the mask is removed, leaving the material behind only in the desired regions

### 1.3.4 Stencil Patterning

Thin materials which contain holes can act as a stencil mask for patterning. These materials are placed into contact with a surface and act as a barrier, protecting the substrate from further modification (Figure 1.6). Stencil masks have been used for direct patterning of cells [77], proteins [78] and other materials [79,80]. They have also been used to protect pre-deposited materials from ablation [81,82]. After initial deposition, the mask can be realigned which allows for patterning multiple materials on a single substrate [80]. Stencil patterning is compatible with almost any substrate type, but is limited in its geometries.



### 1.3.5 Ink-jet printing

A standard ink-jet printer can be modified to deposit a variety of molecules onto a substrate. The pattern can be controlled with conventional graphic software using a desktop computer. Ink-jet printing has been used to print alkyl thiols onto a gold surface and has provided patterns similar to those obtained by microcontact printing [83]. ECM proteins have been printed and these patterns further used to control cell attachment [84–86]. Live cells have also been patterned directly using inkjet printing with a survival rate over 75% [87]. The use of multiply feed nozzles can lead to mixing of feed molecules during printing, similar to colour printing, and can allow for chemical gradients [83]. Ink-jet printing is limited to the resolution of office printers, the smallest reported feature size has been on the order of 100  $\mu\text{m}$ ; still inkjet printing can allow for large scale patterning of a variety of molecules.

## 1.4 PDMS as a Component for Cell Based Microsystems and Microfluidics

Microfluidic technology was developed in silicon and glass, utilizing well developed techniques borrowed from the microelectronics industry [88, 89]. These techniques require the use of a clean room environment, as they involve photolithography and etching of silicon and glass, making them inaccessible for many researchers. Aside from being relatively expensive, silicon is opaque in the visible and ultraviolet (UV) regions, making it unsuitable for techniques involving optical detection, for example optical microscopy. While glass is less expensive and transparent, its amorphous structure makes it difficult to etch vertical walls. After etching, the channels are open on one side, making it necessary to seal the glass or silicon to another substrate. As

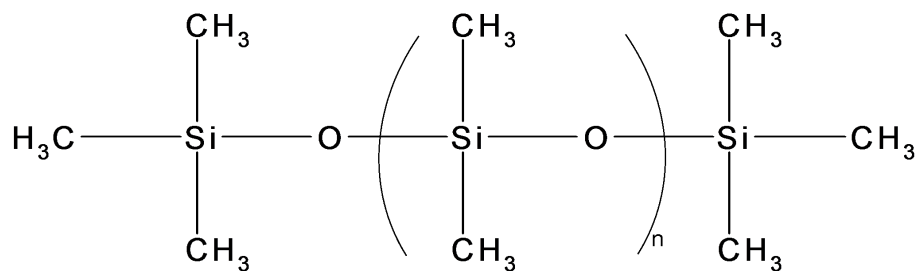


Figure 1.7: Chemical structure of poly(dimethylsiloxane)

the sealing process for both silicon and glass requires high temperatures and voltages, it makes this step difficult.

A less expensive and more robust alternative to silicon and glass is the use of polymers, in particular PDMS, to build microfluidic devices [90]. Polymers, unlike glass and silicon, can form channels by embossing or molding, and can easily be sealed thermally, or with adhesives [91]. However, polymers can be incompatible with organic solvents, low molecular weight organic solutes and high temperatures, making them unsuitable for some processes.

For biological applications, PDMS microfluidic devices are becoming the standard. PDMS is inexpensive, easily molded to form micron scale shapes, optically transparent at wavelengths greater than 280 nm, is produced by low temperature polymerization, is nontoxic, and can be readily sealed to many other materials by making molecular (van der Waals) contacts with the surface [91,92]. PDMS is a flexible polymer composed of repeating siloxane,  $\text{SiO}(\text{CH}_3)_2$ , units (Figure 1.7). PDMS is available commercially from Dow Corning as a two-part base/cure kit forming an elastomeric material when the base is further crosslinked using a platinum catalyst and siloxane crosslinking units found in the cure (Figure 1.8).

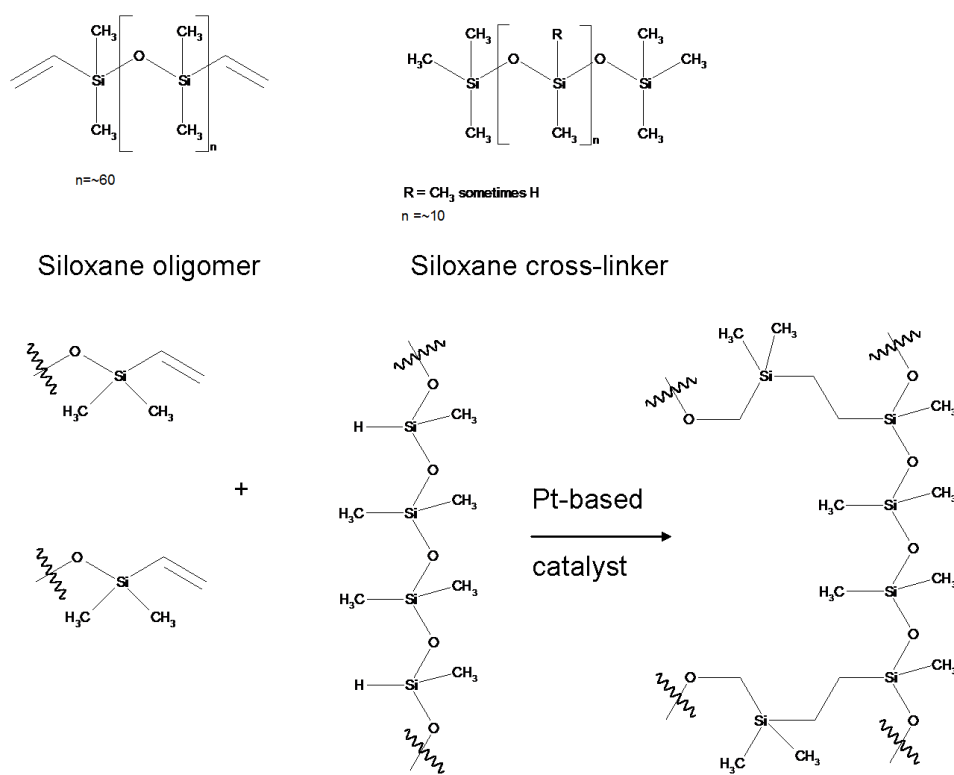


Figure 1.8: Reaction scheme for platinum catalyzed PDMS curing

## 1.5 Chemical Modification of PDMS Surfaces

Despite its many advantages, PDMS is extremely hydrophobic and chemically inert, due to the closely packed methyl groups on the material's surfaces. As many biological assays are performed in aqueous media, PDMS's extreme hydrophobicity limits its use in biological devices. PDMS microfluidic devices are difficult to fill with aqueous solutions, adsorb hydrophobic analytes and generate unstable electroosmotic flows [93]. Further, cell adhesion is inhibited on hydrophobic materials limiting its use in devices which are dependent on adherent cells [89, 90, 93]. Biologically active PDMS surfaces have been obtained previously through chemical vapor deposition of bioactive molecules [94], surface adsorption of surfactant or proteins [95], radiation induced graft polymerization [93, 96], and plasma treatments [89–91, 97, 98].

The surface of PDMS can be modified with passive coating techniques. Materials such as lipid bilayers, proteins, polyelectrolytes and surfactants can be deposited on the polymer surface using a number of methods including chemical vapor deposition, Langmuir-Blodgett film formation and diffusion from solutions [94, 99–101]. Passive coating methods rely on weak physical interactions to adhere the material of interest to the PDMS surface, making the coating unstable. These coatings can be easily damaged or eroded in microfluidic or physiological conditions where they are exposed to intermittent or continuous flows.

Covalent linkages can be used to increase the stability of the coatings. Radiation induced grafting and cerium (IV) catalyzed polymerization have both been used to covalently modify the siloxane surface [93, 96, 102–104]. Both rely on a radical-initiated reaction at the PDMS surface. Silanization has also been used to create covalently linked coatings, by first oxidizing the siloxane surface then exposing it to a chemical silanizing agent [89, 105, 106].

### 1.5.1 Plasma and High Energy Modification of the PDMS Surface

The most direct method to increase the biocompatibility of PDMS is to expose its surface to high energy sources such as UV-radiation and gaseous plasmas [98,107–109]. In fact, the use of high energy sources is commonly an intermediate step in covalent modification. The most common high energy source is that involving an oxygen plasma. Energetic photons, electrons or ions found in a plasma break bonds within the polymer backbone. Carbon-containing fragments leave the surface in the form of volatile organic species, while low-molecular weight polymer chains and stable radicals remain on the polymer's surface. Silicon and oxygen radicals recombine through bridging Si-O-Si bonds creating an oxygen enriched silica-like layer on the surface [110–112]. The formation of a silica-like layer results in a decrease in the polymers's hydrophobicity, increasing its ability to maintain electroosmotic flows and cellular adhesion [89]. Unfortunately this hydrophilic surface is transient, as the elastomer undergoes hydrophobic recovery within several minutes following modification [110, 113–115].

Different analytical techniques have been used to evaluate the chemical composition of the plasma-modified PDMS surface and have confirmed the increase in oxygen content. The techniques include: static secondary ion mass spectrometry (SSIMS), X-ray photoelectron spectroscopy (XPS), attenuated total reflection Fourier transform infrared spectroscopy (ATR-FTIR), and neutron refractometry [112, 113, 116, 117]. ATR-FTIR spectra showed strong O-H stretching modes at  $3400\text{ cm}^{-1}$  and Si-OH stretching modes at  $908\text{ cm}^{-1}$ , indicating that the modified polymer is terminated by silanol (Si-OH) moieties [117]. Further, hydroxyl-sensitive silanating agents react readily with plasma treated siloxanes, once again indicating Si-OH group termina-

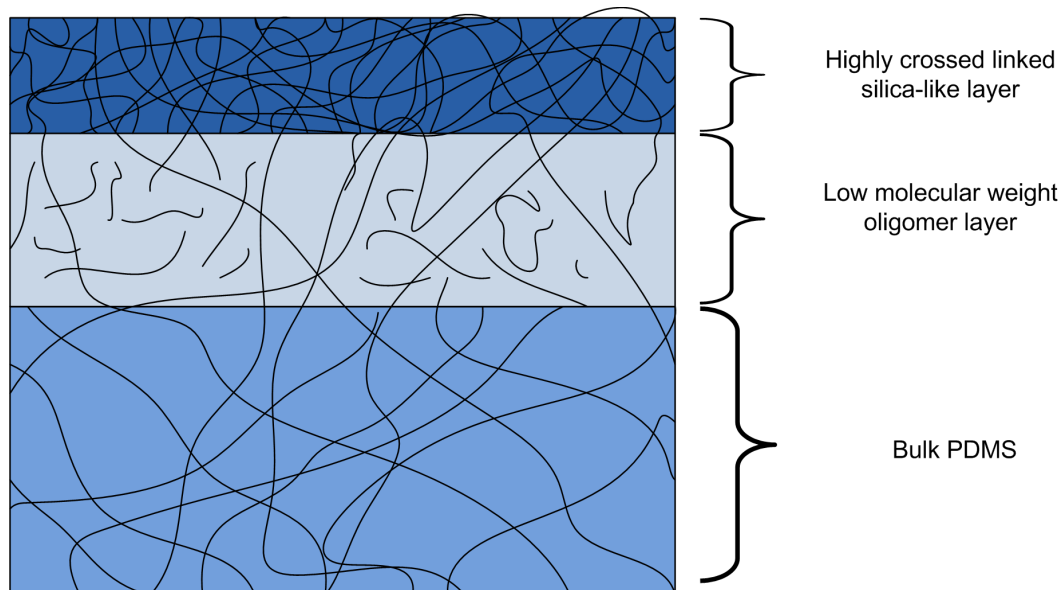


Figure 1.9: Layered structure of plasma treated PDMS

tion [105]. Tapping-mode atomic force microscopy (AFM) has shown that the stiffness of the polymer surface increases significantly after plasma treatment giving additional evidence of a heavily crosslinked surface [116].

After plasma treatment, the uppermost surface of the polymer contains the silica-like layer. Beneath this layer, low molecular weight PDMS fragments created during plasma exposure remain uncrosslinked [110]. Figure 1.9 shows the three layer structure of plasma treated PDMS. The third layer consist of the bulk elastomer which is unaffected by the high energy plasma. The low molecular weight fragments move through cracks in the silica-like layer coating the surface which leads to the recovery of the polymer's hydrophobicity. Other theories have been reported to explain hydrophobic recovery, including reorientation of the silanol groups, condensation of silanol groups at the surface, and changes in the surface roughness [98]. There has been a general consensus that the migration of low molecular weight fragments to the modified surface is the most likely mechanism [89].

Even though it suffers from hydrophobic recovery, plasma treatment of PDMS

is the fastest and most used method to increase the bioactivity and hydrophilicity of the polymer. Plasma treatment of PDMS can also be used to bond the polymer irreversibly to itself glass, silicon, silicon oxide, and oxidized polystyrene [90,92,118,119]. This makes it ideal for microfluidic applications where plasma treatment of PDMS not only activates the surface but can also be used as an effective method to seal the device. Attempts have been made to prevent hydrophobic recovery including submerging the treated surface in a polar solvent such as water or methanol, however these methods are messy and difficult to transport [75,90,117].

## 1.6 Scope of Thesis

Plasma treatment of PDMS leads to a biocompatible and hydrophilic surface. This surface undergoes hydrophobic recovery within minutes after plasma exposure. Hydrophobic recovery leads to an unpredictable surface which may hinder cell adhesion and growth. Further, PDMS does not lend itself to photolithography as conventional photoresists do not wet the surface and are unable to form a thin polymer layer. Stencil mask patterning becomes the only method able to pattern plasma modification of the PDMS surface.

Our group has developed a plasma treatment of PDMS which also involves the deposition of a thin metal layer [120]. This layer preserves the modified surface as long as it remains intact, by preventing hydrophobic recovery. Chapter 2 of this thesis investigates three methods using this technique to pattern wettability and cell adhesion. In the first method a stencil mask was used to selectively treat the exposed polymer. In the second and third methods the polymer surfaces were fully modified and photolithography used to remove portions of the aluminum layer. The exposed modified surface underwent hydrophobic recovery under ambient conditions in the

second patterning method and was reacted with a methyl terminated alkyl silane in the third. Each method was characterized using the contact angle measurement, XPS, and a water droplet test. The ability of each method to pattern cell adhesion was also tested.

Chapter 3 further investigates the interactions of the surfaces developed in Chapter 2 with proteins and adherent cells. Each surface was evaluated for cell attachment and viability. Cells were counted using a hemocytometer and their viability tested by a dye exclusion technique. Protein adsorption was visualized on the patterned surfaces by adsorbing proteins which had been conjugated to a fluorescent dye. Further, the conformation of the proteins on the patterned surfaces was assessed with the use of immunofluorescence labeling and an antibody which attaches to specific binding sites, important for cellular adhesion.

In Chapter 4, the physical properties of PDMS and modified PDMS were investigated. The topography of each surface was imaged and evaluated using an AFM. Force distance curves were taken of PDMS and modified PDMS and used to establish the material's Young's modulus.

While all previous chapters have dealt with the modification, patterning and characterization of PDMS surfaces, Chapter 5 explores the fabrication and characterization of patterned microfluidic devices. Patterning was performed using the stencil mask technique, and thus custom stencil masks were fabricated. A new method, which uses the metal deposition treatment, to bond PDMS to itself and glass is also reported. Patterned surfaces were integrated into reversibly and irreversibly sealed channels, and assessed for biopatterning using a fluorescently conjugated protein.

Chapter 6 summarizes the findings in the previous chapters. It considers the benefits and limitations of each patterning method and surface modification introduced herein. It further examines the use of patterned PDMS for application in



microfluidics and cell based biosensors, and future work which is required to further advance these techniques.

## Chapter 2

# Patterning the Wettability of PDMS for Spatial Control of Cellular Adhesion

### 2.1 Introduction

Poly(dimethylsiloxane) (PDMS) has become an important polymer in the fields of biomaterials and microfluidic devices as it is inexpensive, optically transparent at wavelengths greater than 280 nm, it is produced by low temperature polymerization and it is nontoxic [90,92]. Despite its many advantages, PDMS surfaces are extremely hydrophobic, which is known to inhibit cell adhesion [89,90,93]. Consequently, the modification of PDMS surfaces to increase bioactivity is necessary to expand its use as a biomaterial. Biologically active PDMS surfaces have been obtained previously through chemical vapor deposition of bioactive molecules [94], surface adsorption of surfactant or proteins [95,121], and radiation induced graft polymerization [93,98].

Oxygen plasma treatment is perhaps the most popular method of modifying the surface properties of PDMS [88–91,98]. When PDMS is exposed to a plasma, the high energy electrons and ions remove the  $\text{CH}_3$  groups from the silicon back-bone. When studied by XPS, the surface shows a decrease in carbon content and an increase in oxygen content, the result of which is the formation of a  $\text{SiO}_x$  silica-like layer on the PDMS surface [122]. This change in chemical composition results in a decrease of the polymer's hydrophobicity [89]. Unfortunately, oxygen plasma treated PDMS

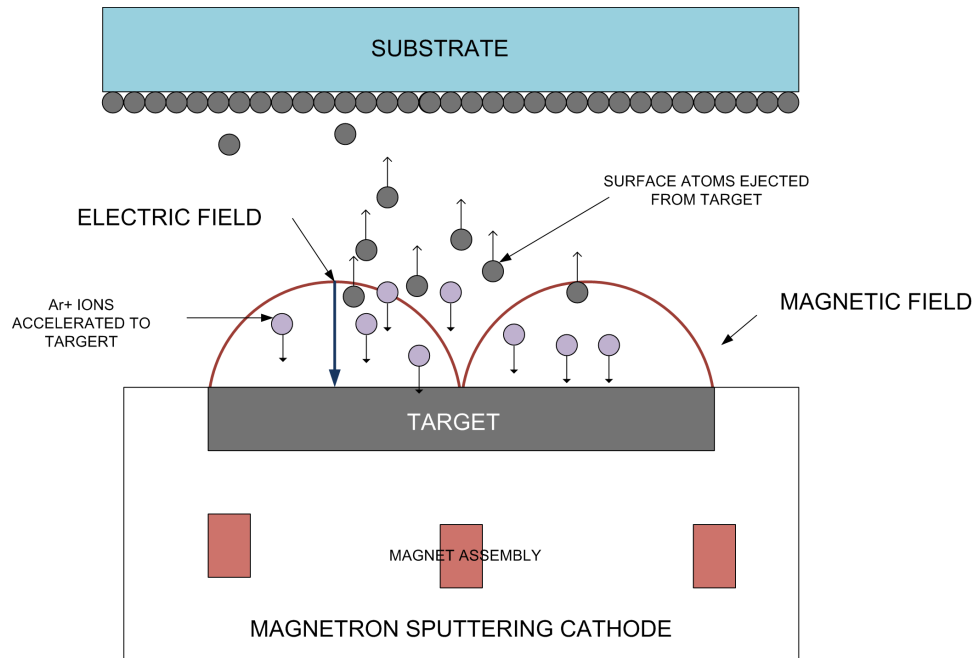


Figure 2.1: Schematic representing the deposition of a material via magnetron sputtering

recovers its hydrophobicity, within hours through the migration of PDMS chains to the surface [98]. Submerging the treated polymer in a polar liquid, such as water, immediately after plasma exposure allows the polymer to remain hydrophilic for an extended period of time [75, 90, 117].

Patterning of cells is a necessary component for cell-based biosensors [2, 69], cell culture analogues [123, 124], tissue engineering [125], microfluidic assays [69, 70, 126] and fundamental studies of cell biology [5–8]. Photolithography and microcontact printing techniques are commonly used to pattern cells onto different surfaces [3, 4]. In both methods, areas of cell-adhesive materials, such as ECM components are surrounded by areas of materials which are non-adhesive to cells, such as PEG-based surfactants and polymers, and thus block indiscriminate cell attachment [104]. Neither of these techniques creates patterns that can withstand biological conditions or microfluidic environments for an extended period of time.

Our group has recently developed a method to activate and pattern the PDMS surface that does not rely on the patterned deposition of ECM components, mediating proteins or molecules [120]. The technique produces a surface that is less fragile in physiological and microfluidic conditions and will allow for the study of ECM proteins without interference from proteins already deposited on the surface. The surface is activated by the sputter deposition of a thin aluminum layer in the presence of an argon plasma in a magnetron sputtering system (Figure 2.1). The magnetron sputter system uses assemblies to create combined magnetic and electric fields. The electric field directs the charged atoms from the plasma towards a target, such as aluminum, and upon impact, the high energy particles eject surface atoms from the target. These atoms are energetic enough to deposit on the substrate forming a thin layer.

After subsequently etching away the aluminum, the modified PDMS surface (PDMS-Al) is hydrophilic, with a contact angle of  $39^\circ$ , in comparison to  $104^\circ$  for native PDMS. Studies by XPS showed no change in silicon content, while the oxygen content increased and the carbon content decreased (Table 2.1) [120]. These results are similar to previously studies of oxygen plasma treatment, and indicates the breaking of silicon-carbon bonds and the formation of an  $\text{SiO}_x$  film. While this modification is still susceptible to hydrophobic recovery, the aluminum layer prevents this from occurring as long as it remains intact.

In order to spatially control cell adhesion, we focused on patterning the hydrophilic PDMS-Al modification within hydrophobic surroundings. We expect that the cells will prefer to grow on the PDMS-Al surface, while avoiding the hydrophobic regions as proteins, which mediate cell adhesion, are known to adsorb to hydrophilic materials with a more favourable conformation than on hydrophobic materials. In this chapter we report three methods to obtain this patterning. The first approach is to selectively magnetron modify the surface through a stencil mask. The mask

Table 2.1: XPS atomic composition analysis of native and modified PDMS

Material	Peak	Binding Energy (eV)	Atomic Composition (%)
PDMS	C 1s	284.8	51.5
PDMS	O 1s	532.6	28.8
PDMS	Si 2p	102.1	19.7
PDMS-Al	C 1s	284.8	36.9
PDMS-Al	O 1s	532.6	42.5
PDMS-Al	Si 2p	102.8	19.9

directly provides the required patterning of PDMS. An alternative approach was to use photolithography, where-in the photoresist protects the modified PDMS-Al surface while the exposed surface undergoes hydrophobic recovery. The third approach used photolithography as before, but silanization chemistry was used to treat the exposed surface, rendering it hydrophobic. The modified surfaces were characterized using contact angle and XPS. The patterned surfaces were studied using a water localization test, optical imaging, and cell culture.

## 2.2 Materials and Methods

### 2.2.1 Reagents

PDMS Sylgard 184A and B were purchased from Dow Corning. The materials used for photolithography, Microposit SC1827 positive photoresist and Microposit MF-319 developer were purchased from Rohm & Haas Electronic Materials. COS-7 and C2C12 cell lines were purchased from ATCC. Dulbecco's Modified Eagle Medium (DMEM), L-glutamine, penicillin streptomycin, FBS, trypsin/ethylenediaminetetraacetic acid (EDTA) and phosphate buffered saline (PBS) were all purchased from Invitrogen. All other chemicals were purchased from Sigma-Aldrich and used as received.

## 2.2.2 Preparation and Modification of PDMS

### 2.2.2.1 Preparation of Bulk PDMS

To allow for easy removal of PDMS, silicon wafers were exposed to hexamethyldisilazane (HMDS) vapor in a vacuum oven (YES-3TA HMDS Oven) at 150 °C and 1 torr for 5 min. To remove water vapor and oxygen from the sample and the chamber, the chamber was purged 3 times with nitrogen gas by evacuating the chamber to 10 torr and refilling the chamber with nitrogen gas to 600 torr.

PDMS precursors, Sylgard 184A and B, were combined in a 10:1 mass ratio and poured onto an HMDS primed silica wafer to a thickness between 1 and 5 mm. The polymer was kept under vacuum for 60 min to remove solvent and air bubbles produced during mixing, before baking at 70°C for 60 min.

### 2.2.2.2 Preparation of Micrometer- and Nanometer-Thick PDMS Films

Spin coating is a common method used to create thin polymers films. An excess of a polymer solution is placed in the middle of a substrate, which is then rotated at high speeds [127]. This evenly spreads the polymer solution across the substrate using centrifugal forces. The thickness of the film is controlled by the spin rate and viscosity of the polymer solution.

PDMS precursors, Sylgard 184A and B, were combined in a 10:1 mass ratio. Micrometer-thick PDMS samples were generated by casting the PDMS mixture as-is onto glass coverslips or silica wafers at 500 rpm for 5 s, then 2000 rpm for 30 s with a Solitec 5110 spin coater (Solitec Wafer Processing). Nanometer-thick PDMS samples were generated by dissolving the PDMS mixture in heptane to obtain a 5% (w/w) solution. The solution was then cast onto a silicon wafer at 500 rpm for 5 s then 3000 rpm for 30 s. All PDMS samples were cured at 70°C for 60 min.

The thickness of the micrometer-thick PDMS layer was  $33 \pm 3 \mu\text{m}$ , determined using a Dektak profilometer (Veeco Instruments Inc). A profilometer drags a diamond stylus, with a diameter of a few micrometers, laterally across a sample while maintaining a constant force [128]. The stylus moves up and down with changing topography; this movement is recorded and used to determine surface roughness and height.

The nanometer-thick PDMS films were assessed using a Gaertner L2W16D 1.3 ellipsometer. Ellipsometry is an optical technique that measures the changes that occur in polarized light when it interacts with matter [129]. When linearly polarized light interacts with a thin film on a reflective surface, the reflected light is elliptically polarized. Polarized light has two components, one parallel (p) and one perpendicular (s) to the plane of incidence. The related phase change ( $\Delta$ ) and the relative amplitude change ( $\Psi$ ) can be determined using the Fresnel equation (2.1) where  $\rho$  the complex reflection coefficient and  $r_p$  and  $r_s$  are the parallel and perpendicular Fresnel reflection coefficients. The Fresnel reflection coefficients are defined in (2.2) where  $n_1$  is the refractive index of the film,  $n_0$  the refractive index of the media,  $\phi_1$  the angle of incident between the film and the surface,  $\phi_0$  the angle of incident between the media and the film.

$$\rho = \frac{r_p}{r_s} = \tan(\Psi)e^{i\Delta} \quad (2.1)$$

$$r_p = \frac{n_1 \cos \phi_0 - n_0 \cos \phi_1}{n_1 \cos \phi_0 + n_0 \cos \phi_1}, \quad r_s = \frac{n_0 \cos \phi_0 - n_1 \cos \phi_1}{n_1 \cos \phi_0 + n_1 \cos \phi_1} \quad (2.2)$$

The thickness of the nanometer films was calculated to be  $220 \pm 3 \text{ nm}$  using the Gaertner Ellipsometer measurements Program Version 1.2 (Gaertner Scientific) with

the following optical constraints: laser wavelength = 632.8 nm; angles of incidence  $i_1 = 70^\circ$ ,  $i_2 = 50^\circ$ ; polarizer angle  $i_p = 45^\circ$ .

### **2.2.2.3 Magnetron Surface Modification of PDMS**

Aluminum was sputtered onto the PDMS substrates with a thickness of  $44 \pm 3$  nm using an Edwards Auto 500 Magnetron Sputtering System. The thickness was determined using a Dektak profilometer (Veeco Instruments Inc). The sputter system was operated at 300 W, 4.8 mTorr, with Ar gas flowing at a rate of 15 sccm. The plasma was created using a RF generator with a frequency of 13.56 MHz. Prior to metal deposition, the samples were kept in the chamber with the plasma struck and the source shutter closed for 4 min. Before use, the aluminum layer was etched away using 1.8 M orthophosphoric acid to expose the modified PDMS surface. The surface was then rinsed 3 times in deionized water and dried under a stream of air.

### **2.2.2.4 Preparation of Hydrophobically Recovered PDMS**

After magnetron surface modification, the sample was etched in 1.8 M orthophosphoric acid for 30 min, rinsed 3 times in water and dried under a stream of air. The sample then underwent hydrophobic recovery at ambient conditions for at least 72 hrs.

### **2.2.2.5 Preparation of ODTMS Treated PDMS**

After magnetron surface modification the sample was etched in 1.8 M orthophosphoric acid for 20 min, rinsed 3 times in water and dried under a stream of air. The sample was then immersed in 1% (v/v) octadecyltrimethoxysilane (ODTMS) solution in methanol with 1.5% (v/v) water, for 20 min. The sample was rinsed 3 times in



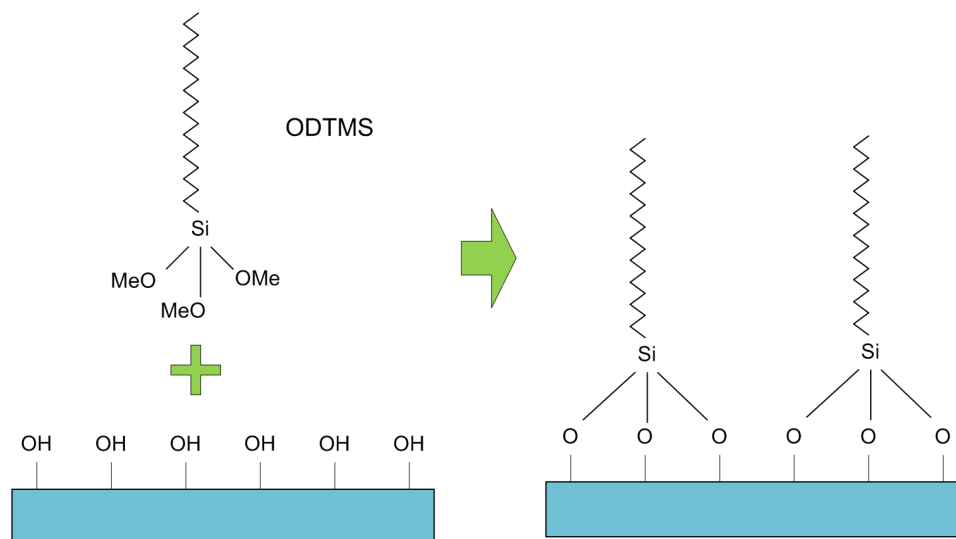


Figure 2.2: The expected reaction between ODTMS and magnetron treated PDMS methanol, and dried at 90°C for 60 min. The expected silanization reaction between ODTMS and the magnetron modified PDMS is shown in Figure 2.2

## 2.2.3 Hydrophobic/Hydrophilic Patterning of PDMS

### 2.2.3.1 Stencil Mask Patterned Surfaces

Stencil masks were commercially available steel screens with etched holes of 180 or 260  $\mu\text{m}$  diameter (InterNet Inc.). Aluminum was sputtered onto the PDMS substrates through the stencil masks to a thickness of 50 nm using an Edwards Auto 500 Magnetron Sputtering System. The sputter system was operated at 300 W, 4.8 mTorr, with Ar gas flowing at a rate of 15 sccm. Prior to metal deposition, the samples were kept in the chamber with the plasma struck and the source shutter closed for 4 min. The aluminum was etched using 1.8 M orthophosphoric acid for 30 min and rinsed 3 times in deionized water before use. This patterning sequence is illustrated in Figure 2.3.

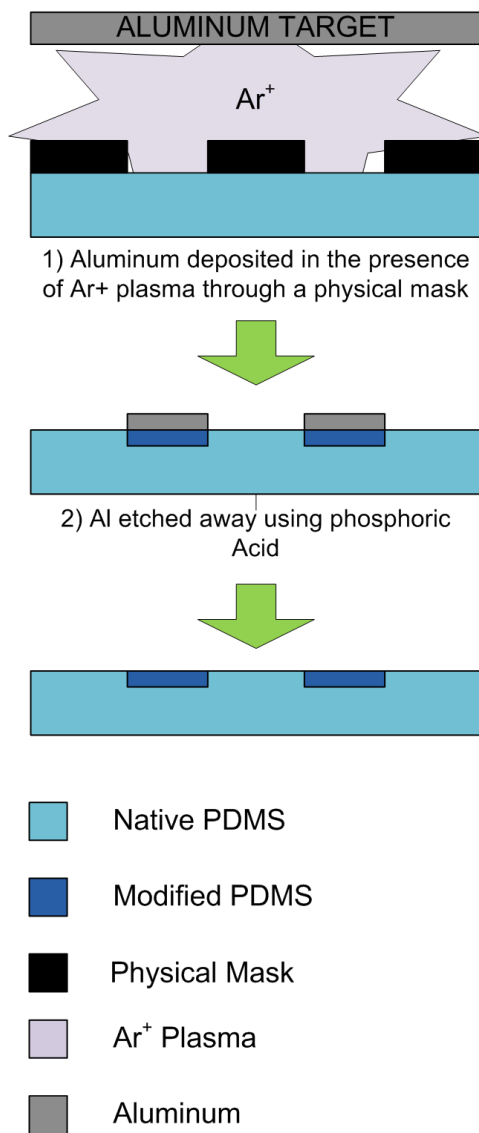


Figure 2.3: A schematic representation of the procedure for stencil mask patterning of PDMS using magnetron sputtering of aluminum

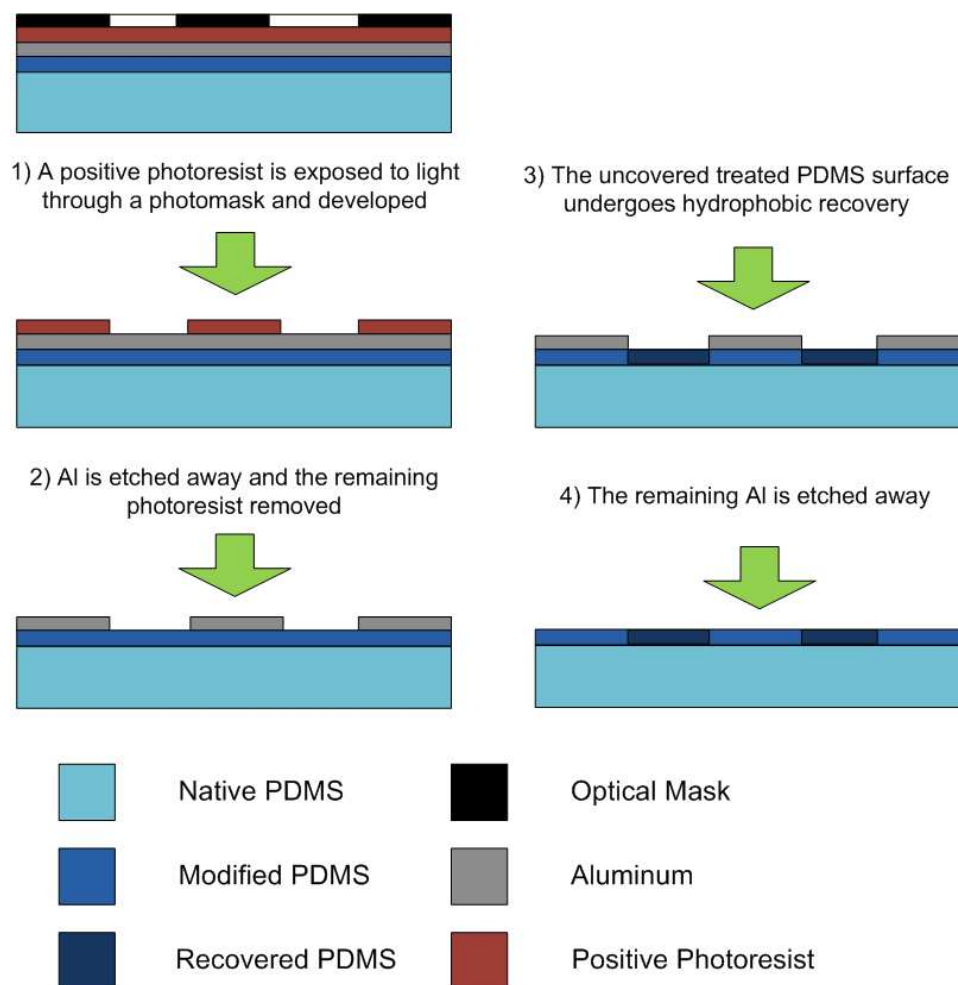


Figure 2.4: A schematic representation of the procedures for photolithographic patterning of hydrophobically recovered and magnetron treated PDMS

### 2.2.3.2 Photolithographic Patterning of Hydrophobically Recovered PDMS

A positive photoresist, Microposit S1827, was spin coated on to an unpatterned aluminum coated PDMS surface, using a Solitec 5110 spin coater, at 500 rpm for 5 s and 2000 rpm for 45 s to obtain a thickness of 4.0  $\mu\text{m}$ . The sample was soft baked at 115°C for 4 min to remove solvent. The photoresist was then exposed to 405 nm UV light through an acetate photomask for 22 s using a Karl Suss MJB3 optical lithography system (Suss MicroTec) at a power of 18  $\text{mW}/\text{cm}^2$ . The photomask was designed in L-edit (Tanner EDA) and printed onto an acetate file using a high resolution com-

mercial printer (PhotoplotStore). The photoresist was developed using Microposit MF-319 developer for 75 s, dissolving the exposed photoresist and revealing the aluminum layer below. The newly exposed aluminum was removed by immersion in 1.8 M orthophosphoric acid for 30 min and rinsed in deionized water. The remaining photoresist was removed by immersion in acetone. The patterned sample was then rinsed in deionized water and dried under a stream of air. The exposed surface was allowed to undergo hydrophobic recovery by storage in ambient conditions for at least 72 hrs. The remaining Al was etched in 1.8 M orthophosphoric acid and rinsed 3 times in deionized water prior to use. Figure 2.4, illustrates the procedures used to create the photolithographically patterned surfaces.

### **2.2.3.3 Octadecyltrimethoxysilane Patterning of PDMS**

ODTMS patterned PDMS surfaces were created using photolithography as described above. Instead of undergoing hydrophobic recovery the exposed PDMS-Al surface was treated with a 1% (v/v) solution of ODTMS (Sigma-Aldrich) in methanol (Sigma-Aldrich) with 1.5% (v/v) water for 20 min as shown in Figure 2.5. The treated surface was then rinsed in methanol 3 times and dried at 90°C for 60 min. Prior to use, the remaining aluminum was etched away in 1.8 M orthophosphoric acid for 30 min, the modified surface was then rinsed 3 times in deionized water and dried under a stream of air.

## **2.2.4 Characterization of Modified and Patterned PDMS**

### **2.2.4.1 Sessile Drop Water Contact Angle Measurement**

The angle formed when a liquid meets a solid is defined as its contact angle [130]. The contact angle can be related to the surface tension between the three interfaces

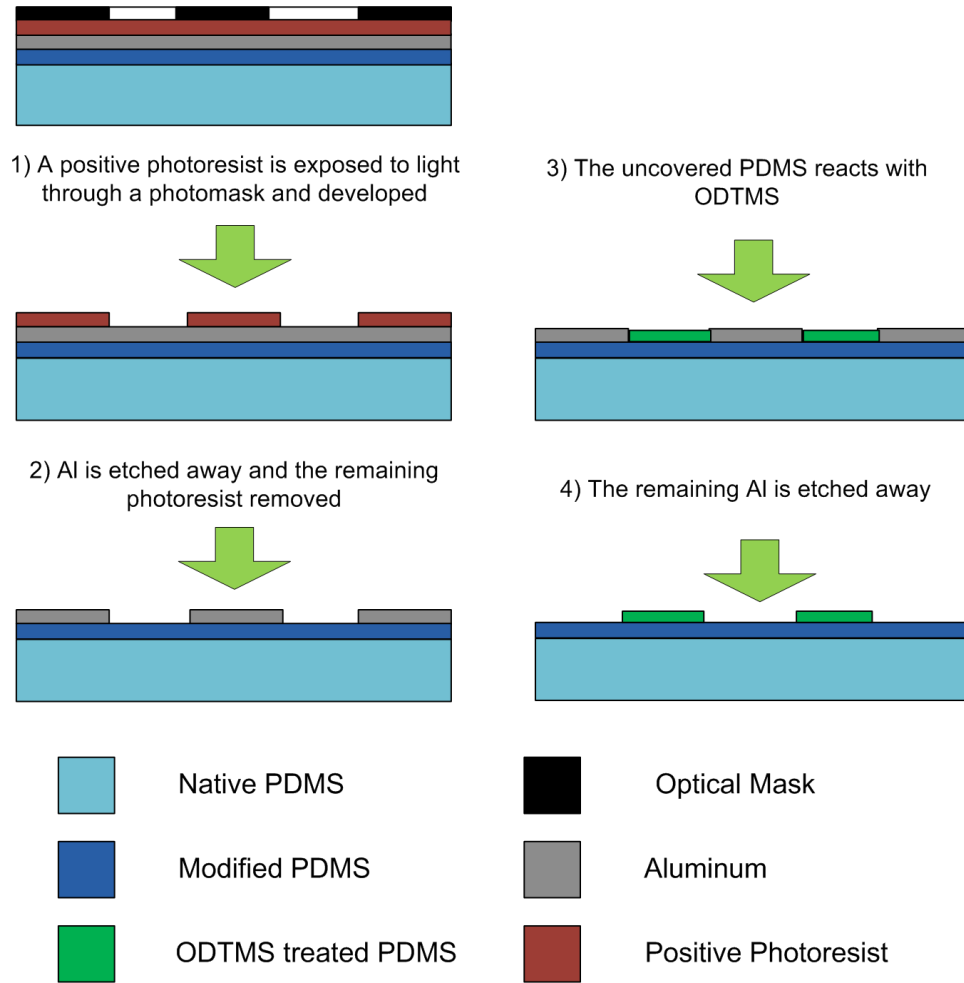


Figure 2.5: A schematic representation of the procedures for photolithographic patterning of ODTMS on magnetron treated PDMS

by the Young equation,

$$\gamma_{lv} \cos(\theta_Y) = \gamma_{sv} - \gamma_{sl} \quad (2.3)$$

where  $\gamma_{lv}$  is the liquid-vapor surface tension,  $\gamma_{sv}$  is the solid-vapor surface tension, and  $\gamma_{sl}$  is the solid-liquid surface tension. When the liquid that forms the drop is attracted to the surface it will wet the surface and form a angle close to  $0^\circ$  (Figure 2.6 a). When the liquid is not attracted to the surface, the liquid will prefer to interact with itself and minimize contact with the surface, thus forming a larger contact angle (Figure 2.6 b).

Water is often used as the liquid, and the term hydrophobic and hydrophilic is used to describe the surfaces attractiveness towards water. Surfaces that are considered hydrophobic have a contact angle with water greater than  $90^\circ$ . On the other hand, when the contact angle is less than  $90^\circ$ , the surfaces are considered hydrophilic.

Contact angle measurements were made using a model 100 manual goniometer (Rame-Hart).  $5.0 \mu\text{L}$  drops of deionized water were placed on the sample surfaces, after 10 s the data were collected to obtain the static contact angle. The advancing angle was obtained by placing the needle's tip into the water droplet and slowly adding a small amount of liquid until the base of the water droplet moved. The angle that formed just prior to the droplet moving is recorded. Similarly, the receding contact angle was measured by slowly removing water and recording the angle just before the base of the droplet moved. Each measurement was taken at least 3 times and averaged.

Micrometer-thick PDMS, magnetron treated PDMS, and hydrophobically recovered PDMS were immersed in water for up to 7 days. After each 24 hr period, 3 samples of each surface type were removed from water and dried under a stream of

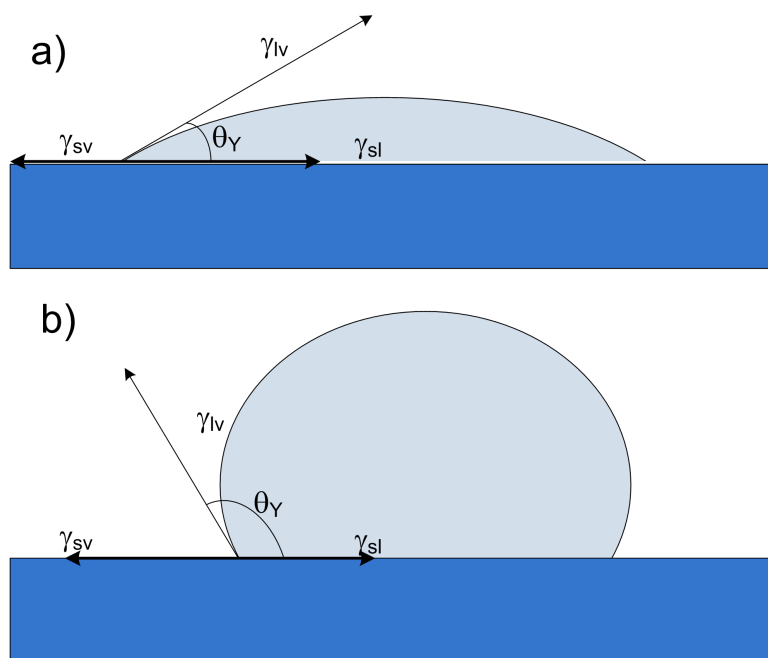


Figure 2.6: An illustration of how a water droplet might appear on (a) a hydrophilic surface, (b) a hydrophobic surface

air. The static, receding and advancing contact angles were taken 3 times on each sample.

#### 2.2.4.2 X-ray Photoelectron Spectroscopy

XPS is a surface analysis techniques that measures the elemental composition, chemical stoichiometry, chemical state, and electronic state of the elements in a material [130]. When a material is bombarded with X-rays, core electrons are ejected from the atoms that make up the material. These electrons are known as X-ray photoelectrons, and their kinetic energy can be analyzed and plotted. X-ray photoelectrons have short mean free paths (1-10 nm), making XPS a very surface-sensitive technique [130].

While the kinetic energy of the X-ray photoelectron is measured, the binding energy of the electron provides more useful information. The binding energy is char-

acteristic of each specific atom and is sensitive to the local chemical environment. The kinetic energy of an electron can be used to calculate the binding energy using the following equation:

$$E_K = h\nu - E_B - \phi \quad (2.4)$$

where  $E_K$  is the photoelectron kinetic energy,  $h\nu$  is the energy of the incoming X-ray, and  $E_B$  is the photoelectron binding energy and  $\phi$  the spectrometer work function.

The elemental composition of the ODTMS treated PDMS was analyzed by XPS using a Kratos Axis Ultra spectrometer (Kratos Analytical). The XPS spectrometer employed a Al K $\alpha$  X-ray source (1486.6 eV) operated at a source energy of 210 W, using a charge neutralizer system with a filament current of 1.6 A and a charge balance of 2.4 V. XPS survey and high-resolution spectra of the C 1s, O 1s, and Si 2p binding energy regions were collected at pass energies of 160 and 20 eV, respectively. XPS spectra were fit and the signal area was calculated using CasaXPS software. The binding energy scale was calibrated using the C 1s peak at 284.8 eV

### 2.2.4.3 Water Localization Test

To visualize the hydrophobic/hydrophilic patterning, patterned PDMS was dipped into deionized water and pulled out at a 60° angle to the water surface. The water droplets were imaged immediately after removal.

### 2.2.5 Cell Culture and Patterning

COS-7 fibroblast cells and C2C12 myoblast cells, were cultured on the PDMS substrates. DMEM supplemented with 2 mM L-glutamine, 1% penicillin-streptomycin



(Invitrogen) and 10% FBS was used for all experiments. Cell cultures were incubated at 37°C , 5% CO<sub>2</sub> and 100% humidity.

Samples of patterned PDMS were sterilized by rinsing with 70% ethanol. Prior to plating, cultured cells were washed with trypsin/EDTA to promote cell detachment from the culture flasks. The cells were mixed into media for transfer. 0.5 mL of the solution was plated onto modified PDMS samples, inside a 3 cm petri dish. An additional 2 mL of fresh media was added to each dish, the cells were then incubated for 24-36 hrs.

Prior to imaging, cells were rinsed 3 times with PBS at pH 7.4 and fixed using a solution of 4.4% paraformaldehyde in PBS for 10 min. Cells were then rinsed 3 times in PBS and water. Fixatives stabilize the structural details of cell and tissues for examination by microscopy [131]. Fixing a biological tissues preserves the sample in a state as close to its natural state as possible. Aldehyde fixation is one of the most common fixation techniques. It creates covalent chemical bonds between lysine residues found in proteins, creating a cross-linked network inside of the cell (Figure 2.7). Paraformaldehyde breaks down into formaldehyde units in the presence of heat and OH<sup>-</sup> (Figure 2.7).

### **2.2.5.1 Imaging**

All optical images were captured using a Zeiss Axioskop2 Mat Microscope with a QImaging Retiga 1300 CCD digital camera or using a Zeiss Axiovert 200M inverted microscope with a Zeiss AxioCam HRM CCD digital Camera.

### **2.2.5.2 Live Cell Imaging**

C2C12 cells were plated onto stencil masked patterned PDMS samples at a concentration of  $8.3 \times 10^3$  cells/cm<sup>2</sup>. Cells were incubated at 37°C , 5% CO<sub>2</sub> and 100%

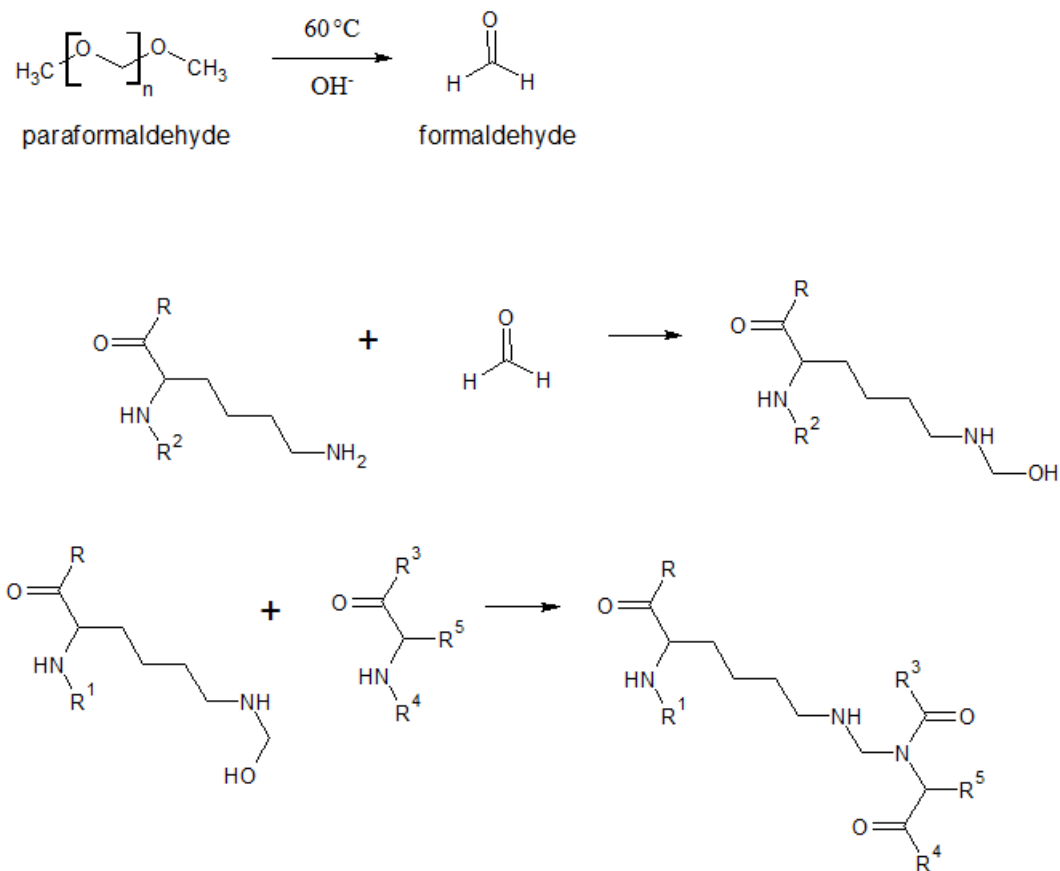


Figure 2.7: The reaction mechanism of formaldehyde fixation. Paraformaldehyde is separated into formaldehyde monomers when exposed to heat under basic conditions. Formaldehyde forms a methylene bridge between the nitrogen atom found on lysine side chains and the nitrogen atom of a peptide linkage

humidity using a Zeiss stage-Top Incubation system on a Zeiss Axiovert 200 inverted microscope. Images were recorded using a Zeiss AxioCam HRM every 15 min for a 24 hr period.

## **2.3 Results and Discussion**

### **2.3.1 Stencil Mask Patterning of PDMS**

Our group has previously reported a method that increased the wettability of PDMS through magnetron-sputter deposition of aluminum and subsequent etching of aluminum. These PDMS-Al surfaces had a lower contact angle and showed increase cell attachment compared to PDMS [120]. The decrease of the contact angle has been attributed to the formation of hydroxyl groups on the surface, which replace the hydrophobic CH<sub>3</sub> groups found in native PDMS when the surface is exposed to an argon plasma during aluminum deposition.

The first method used to pattern hydrophobic and hydrophilic regions on PDMS took advantage of the native structure of PDMS. Unmodified PDMS is naturally cytophobic due to its hydrophobicity and methoxy surface chemistry. To protect PDMS during aluminum deposition a stencil mask was used. The mesh, shown in Figure 2.8, had circular holes with diameters of 180 and 260  $\mu\text{m}$ . The related patterned aluminum deposition (Figure 2.9) appeared to be in good agreement with the size and shape of the holes found in the steel mesh. After etching, the stencil mask patterned surfaces were dipped in water. The water droplets formed only in the modified regions, while avoiding the hydrophobic PDMS (Figure 2.10). The selective water droplet formation indicates successful hydrophobic/hydrophilic patterning.

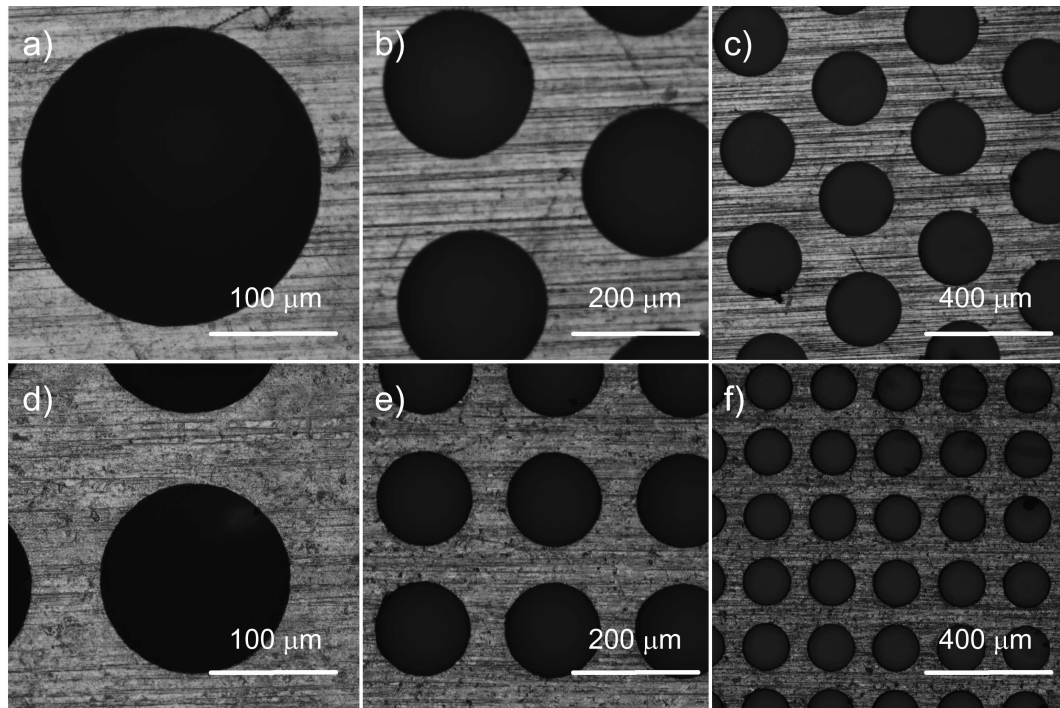


Figure 2.8: Optical images of stainless steel screens used as stencil masks composed of (a-c) a hexagonal array 260  $\mu\text{m}$  diameter circles with a centre-to-centre spacing of 360  $\mu\text{m}$ , and (d-f) a square array of 180  $\mu\text{m}$  diameter circles with a centre-to-centre spacing of 230  $\mu\text{m}$

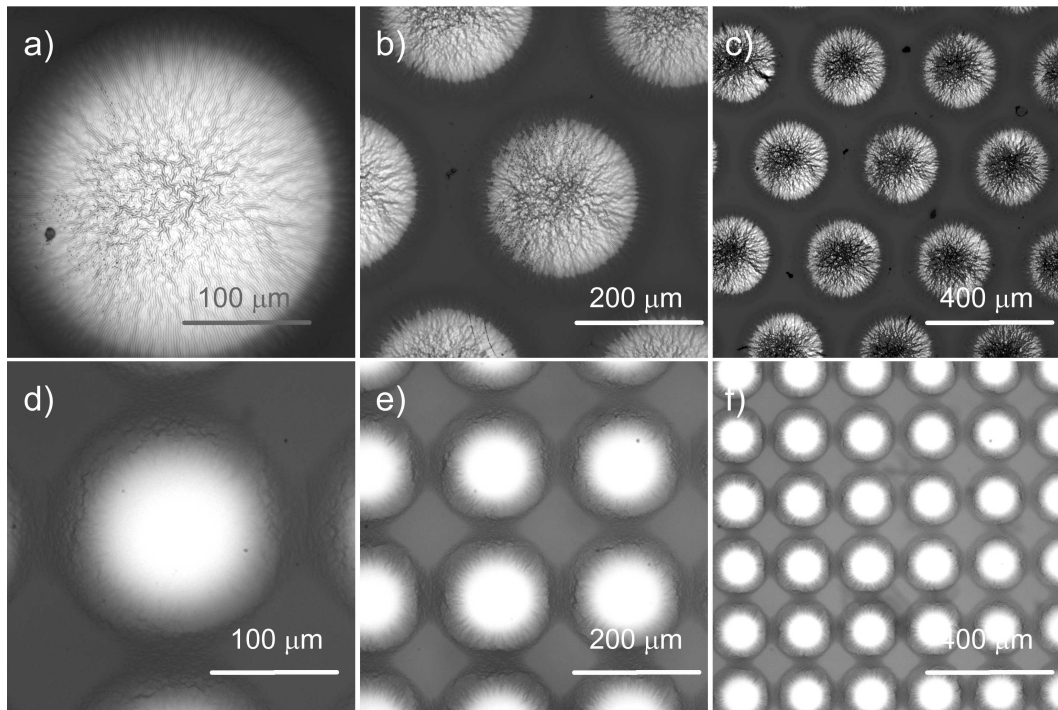


Figure 2.9: Bright field reflection-mode optical images of aluminum arrays patterned on PDMS by magnetron sputtering through a stencil mask. (a-c) hexagonal array 260  $\mu\text{m}$  diameter circles with a centre-to-centre spacing of 360  $\mu\text{m}$ , and (d-f) a square array of 180  $\mu\text{m}$  diameter circles with a centre-to-centre spacing of 230  $\mu\text{m}$

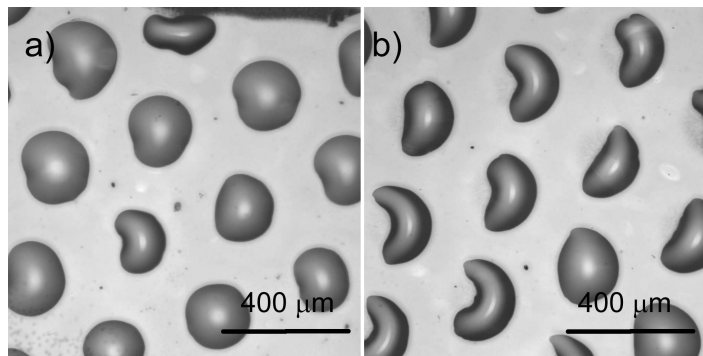


Figure 2.10: Bright field reflection-mode optical images of water droplets localized on stencil masked patterned PDMS after aluminum etching

After aluminum etching, mouse myoblast (C2C12) and African green monkey kidney (COS-7) cells were incubated on the surfaces, they appear to only grow in the areas exposed to aluminum (Figure 2.11). Outside of the modified region, few cells are observed, but long membrane protrusions span the gaps between dots. HeLa cells grown on an island of ECM proteins showed similar protrusions [132]. It was suggested that these membrane protrusions may indicate cell-to-cell communications or the secretion of ECM proteins to enhance adhesion of the cells to the non-patterned substrate. In the case of the HeLa cells, they eventually grew outside of the modified regions. It was suggested that the loss of patterned cell growth was caused by one of two effects: the cells were secreting ECM proteins so they could adhere to unmodified substrate; or the cells were degrading the non-adhesive surface. By contrast, we saw no cell growth outside of the modified regions, rather the cells preferred to grow on top of one-another. To further understand the cell behavior on our patterned substrates, live cell imaging was performed.

### 2.3.1.1 Live Cell Imaging

Live cell imaging indicated that cells were able to freely move around the modified dots. Generally, once a cell approached the edge of the dots, they would change

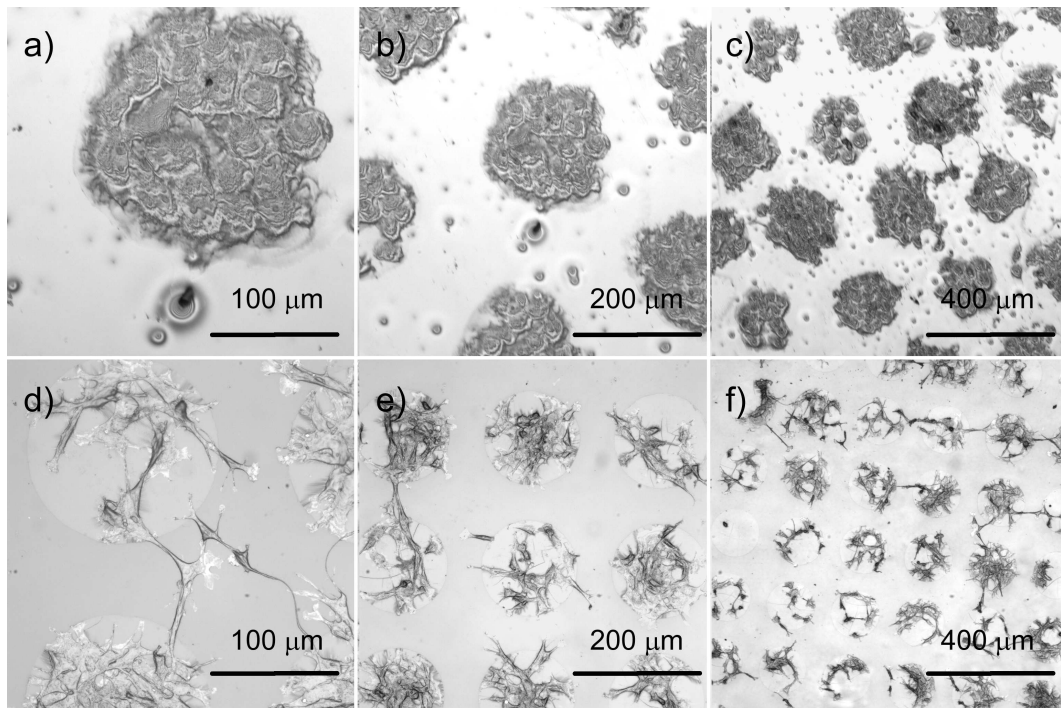


Figure 2.11: Bright field reflection-mode optical images of (a-c) COS-7 fibroblast cells, (d-f) C2C12 myoblast cells after 24 hrs incubation on stencil mask patterned PDMS

direction and remain inside the dot. On occasion a cell was observed leaving a dot. When this occurred, the cell immediately balled up, indicating that the cell was no longer able to form attachments to the surface of the polymer. These cells would float around until either they reentered the same dot or another modified region where they were able to adhere and spread out. Figure 2.12 shows a cell approaching the edge of the dot. The cell, indicated by the arrow, eventually leaves the modified region and balls up (Figure 2.12 c). After remaining over the hydrophobic area for some time the cell eventually finds the modified dot and begins to spread again (Figure 2.12 g-h).

The stencil mask patterning method has proven effective in patterning hydrophilic modified PDMS that is surrounded by hydrophobic native PDMS. Cells grew only in the modified dots, as expected. While cells are able to leave the dots and move around the surface, they do not adhere to the unmodified surface.

### **2.3.2 Patterning of Hydrophobically Recovered PDMS by Photolithography**

Stencil mask patterning has proven successful at spatially controlling cell attachment and growth. This technique is simple and stencil masks can be used multiple times. However, all stencil mask patterning has a significant drawback. Stencil masks are limited in both their feature size and geometry. To overcome these limitations, we looked to photolithography. The resolution of contact photolithography can easily reach 4 to 6  $\mu\text{m}$  feature sizes, and have been used to mass produce feature down to 1  $\mu\text{m}$  [56]. Acetate photomasks are available inexpensively and with relatively high resolution; feature sizes down to 6  $\mu\text{m}$  can be obtained. Figure 2.13 shows acetate photomasks obtained from the PhotoPlotStore. Chrome-on-glass photomasks are more durable and give better resolution; however they are significantly more



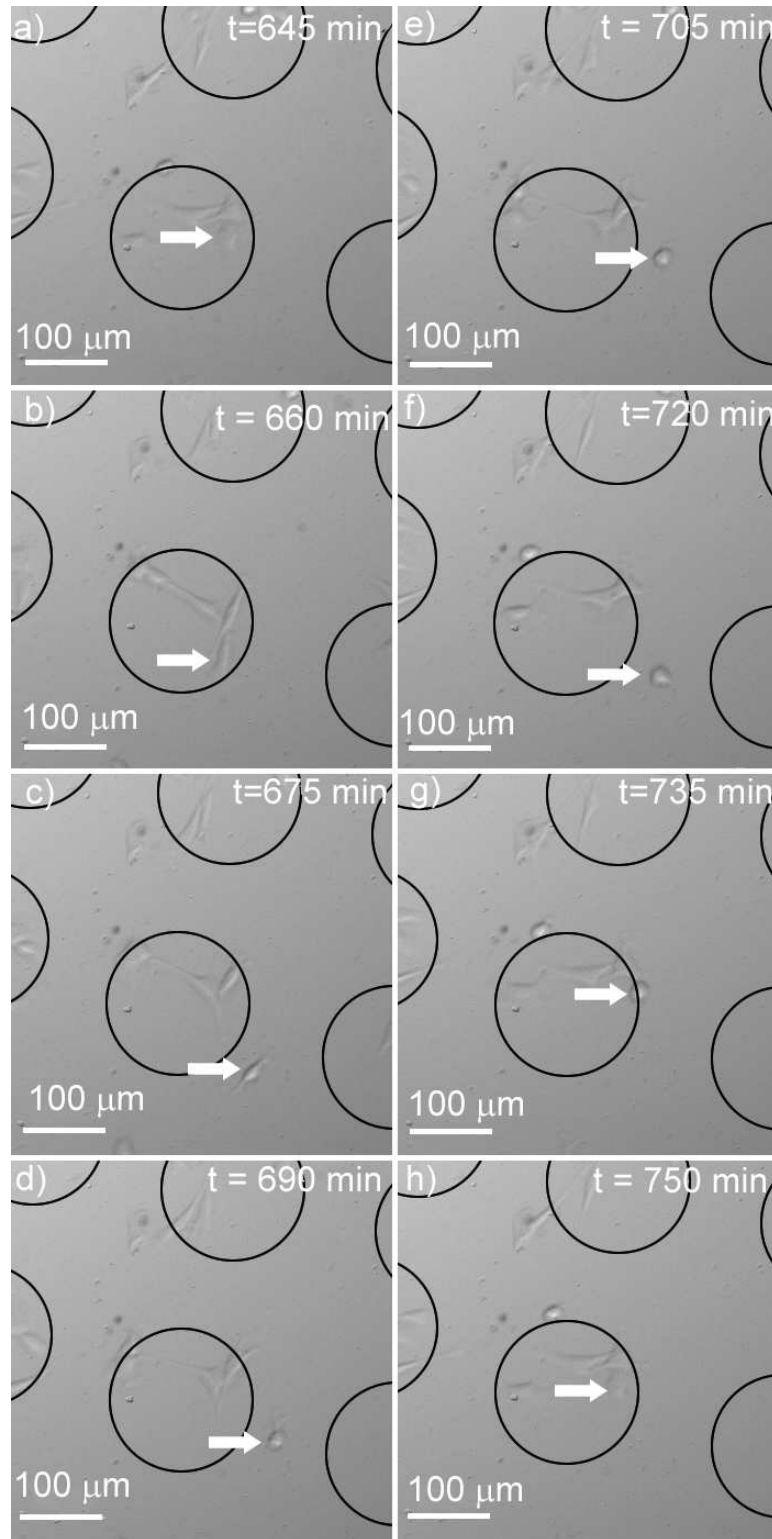


Figure 2.12: Transmission-mode optical images of live C2C12 myoblasts cells on stencil mask patterned PDMS taken after (a) 645, (b) 660, (c) 675, (d) 690, (e) 705, (f) 720, (g) 735, (h) 750 min after initial plating

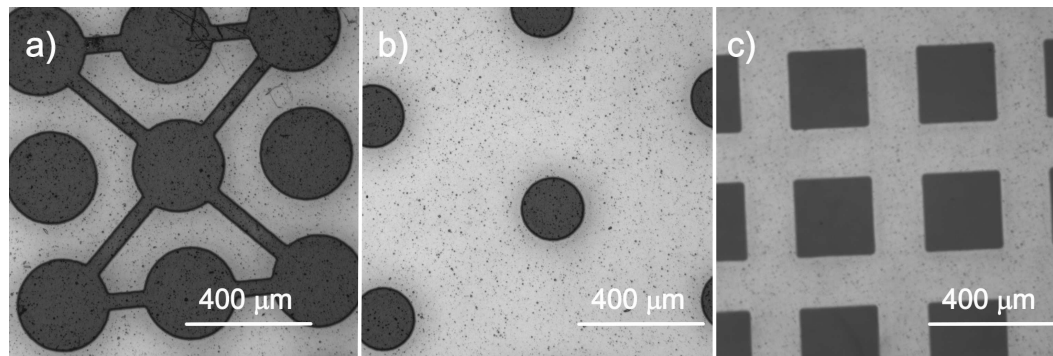


Figure 2.13: Bright field reflection-mode optical images of photomasks used to photolithographically pattern aluminum on PDMS. a) 250  $\mu\text{m}$  dots with 10  $\mu\text{m}$  interconnecting lines, b) 100  $\mu\text{m}$  dots, c) 260  $\mu\text{m}$  squares

expensive. Photolithography directly on PDMS is not possible, as photoresists are unable to spread evenly over the polymer surface. Previously, our group has used an aluminum mediating layer to overcome this problem [104]. The magnetron deposition of aluminum caused the entire polymer surface to be oxidized and thus patterned cell growth was not possible.

In order to create patterned surfaces by photolithography, the contact angle of modified PDMS has to be increased, such that it is closer to native PDMS. One method to increase the contact angle of modified PDMS is to allow the surface to undergo hydrophobic recovery (PDMS-R). PDMS-Al surfaces that have undergone hydrophobic recovery do so in a relatively short period of time. Recovery occurs through the migration of uncross-linked PDMS oligomers found under the silica-like layer. The hydrophobic oligomers work their way to the surface through cracks in the modified layer. Recovery takes place within hours of exposure to air, with the maximum contact angle occurring within 24 hrs. Hydrophobic recovery is slowed by immersion in a polar liquid such as water or methanol. The polar solvent makes migration no longer energy efficient as the solvent would prefer to interact with the hydroxyl groups found on the modified surface. After 72 hrs in air, micrometer-thick

films of treated PDMS had a contact angle of  $77 \pm 2^\circ$ , while bulk PDMS reached  $96 \pm 2^\circ$ . The micrometer-thick PDMS does not recover to the same degree as bulk PDMS. This difference can be attributed to the curing processes. While both bulk and thin PDMS are cured in the same manner, the thin PDMS will allow heat to be absorbed more evenly through the material, effectively allowing a larger percentage of the PDMS to be cross linked. Previously, it has been reported that PDMS which has been thermally aged before plasma treatment, will maintain its hydrophilicity longer and once recovered, it will have a lower contact angle than PDMS that has not undergone thermal aging [133].

A new photolithographic patterning method that takes advantage of PDMS's ability to undergo hydrophobic recovery has been developed. Figure 2.4 shows the fabrication scheme. In short, the entire PDMS surface was coated with aluminum in a magnetron sputter deposition system. Photolithography and wet chemical etching was used to generate a pattern of aluminum; exposing select areas of the polymer surface. The exposed regions were allowed at least 72 hrs to undergo hydrophobic recovery. A final etch, exposed the aluminum protected surfaces, which remained hydrophilic. These hydrophilic regions were surrounded by hydrophobically recovered PDMS. Figure 2.14 shows aluminum that has been patterned on the PDMS surface. The aluminum pattern matched closely with the photomask used. To show the success of patterning hydrophilic dots, the substrates were dipped into water and removed at a  $60^\circ$  angle after the final etch. As with the stencil mask samples, water droplets formed only in the hydrophilic dots while avoiding the recovered surroundings (Figure 2.15).

To test the ability of the photolithographic patterned samples to control cell attachment and growth, the patterned surfaces were incubated with C2C12 cells. After 24 hrs, no patterned formation is observed (Figure 2.16 a-b). As there is a low con-

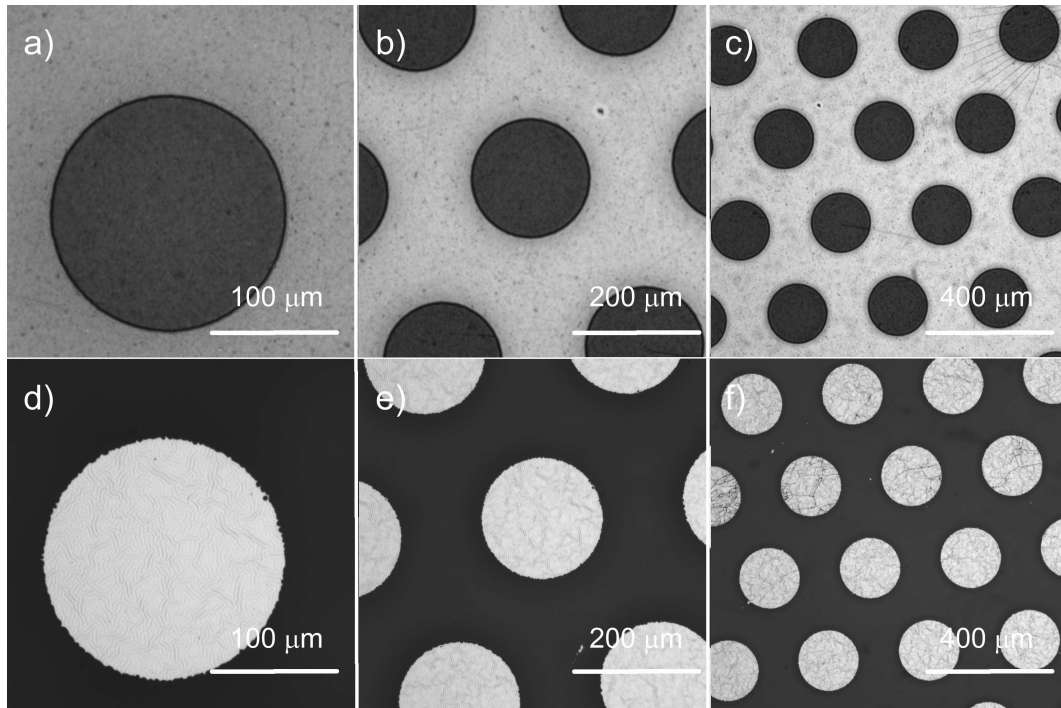


Figure 2.14: Bright field reflection mode optical images of a-c) photomasks d-f) and the corresponding aluminum patterned surfaces

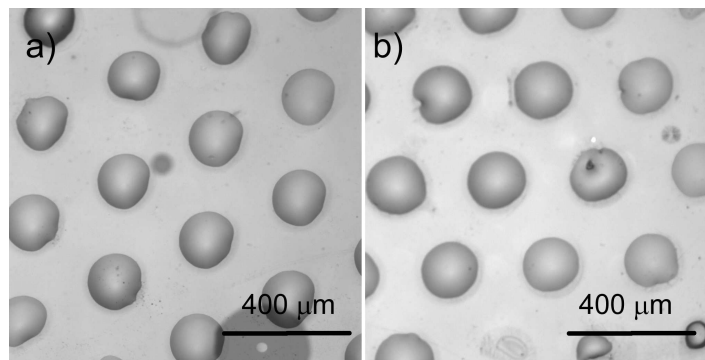


Figure 2.15: Bright field reflection-mode optical images of water droplets localized on treated PDMS surfaces patterned with hydrophobically recovered areas by photolithography

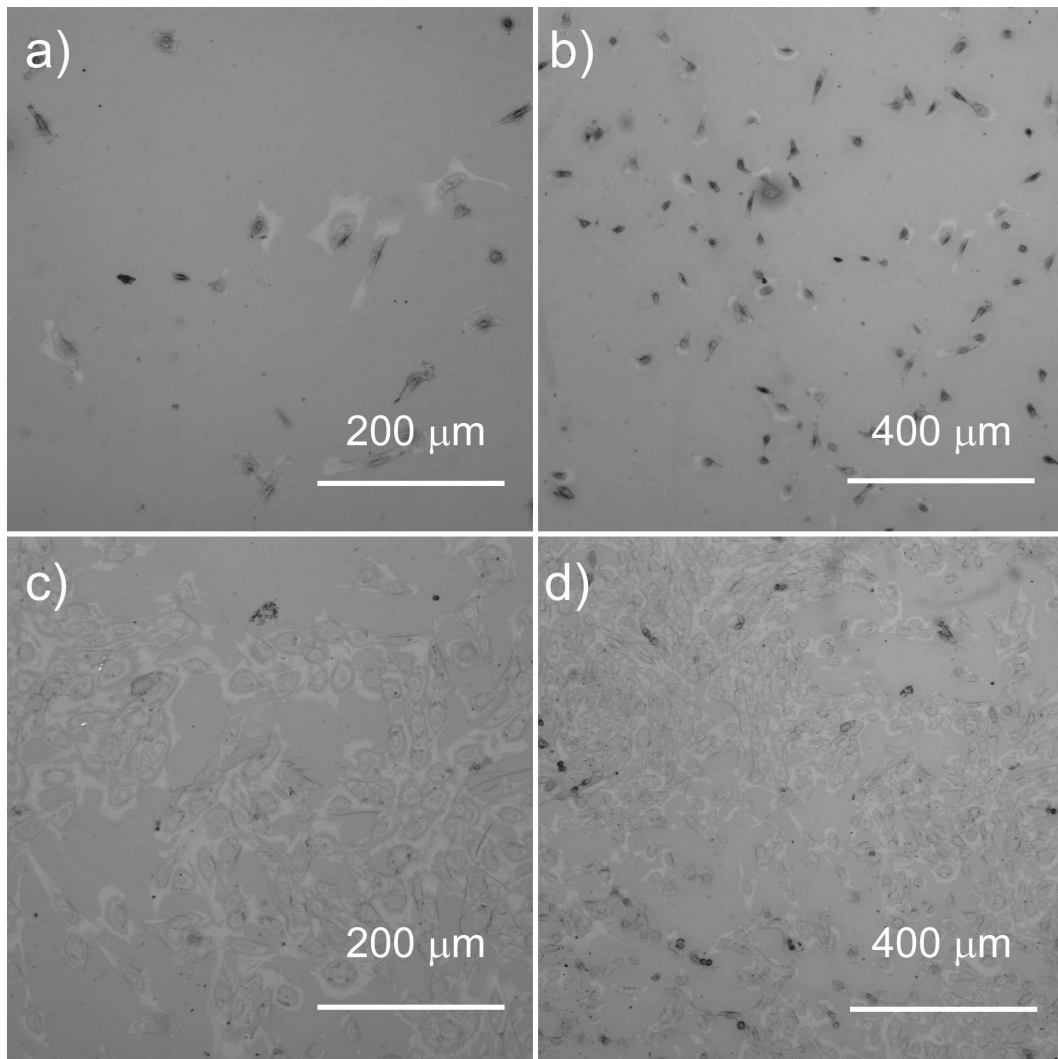


Figure 2.16: Bright field reflection-mode optical images of C2C12 myoblast cells after (a,b) 24 hrs and (c,d) 72 hrs incubated on modified PDMS surfaces patterned with hydrophobically recovered areas by photolithography

centration of cells, it is possible that they are only growing in the modified regions but patterning is not distinguishable. After 72 hrs, the cells have grown to confluency and have spread across the entire surface. It is clear, that while patterning hydrophobically recovered areas created domains of hydrophilic dots with hydrophobic surroundings, this method was not successful at spatially controlling cellular attachment.

Recovered PDMS only reaches a contact angle of  $77^\circ$ , making it significantly lower than that of native PDMS and is considered technically hydrophilic. Also, the two surfaces differ in their chemistry. The oligomers that coat the recovered PDMS only create a thin layer, under which the hydroxy groups caused by the plasma modification still exist. These hydroxy groups might still affect how the cells and serum proteins interact with the surface beyond simply its wettability. It is also possible that once in an aqueous environment, the oligomers that caused the hydrophobic recovery are either removed by the solution or move back into the bulk polymer. Aqueous solutions are used to slow or prevent hydrophobic recovery of plasma treated PDMS. This occurs because the entropic drive to coat the surface is removed, thus lowering the interaction between the air and the polymer surface. We hypothesize that not only is the contact angle of recovered PDMS lower than that of PDMS, but also that in aqueous solution, the interaction between the water molecules and the hydrophobic oligomers would cause the oligomers to move back into the bulk polymer. This would further lower the contact angle, making the recovered surface no different than that of a freshly etched surface.

The effects of immersion in water on the static contact angle were tested on PDMS, PDMS-AI and PDMS-R surfaces of micrometer thickness and displayed in Figure 2.17. PDMS showed little change over a seven day period of time, with the static contact angle remaining above  $109^\circ$ . The static angle for PDMS-AI also remained fairly consistent staying below  $30^\circ$ ; indicating, that immersion in water was

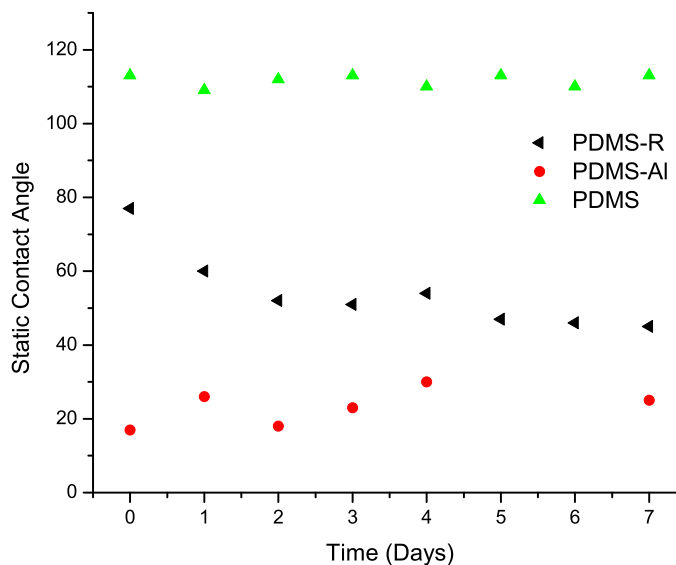


Figure 2.17: Static contact angle of  $\mu\text{m}$  thick PDMS, PDMS-R and PDMS-AI samples after immersion in water

preventing hydrophobic recovery. However, PDMS-R surfaces showed a decrease of  $32^\circ$  over seven days. After only 24 hrs, the contact angle had dipped below  $60^\circ$ ; this indicates that within 24 hrs the wettability of the surface is now favourable for cell attachment.

Advancing and receding contact angles can reveal important information on the properties of a surface [130]. The receding angle reflects the surface's ability to retain contact with the liquid, and thus the strength of the surface liquid interactions. In an ideal system, the liquid would not interact with the surface and all three contact angles would be the same. In real systems, a contact angle hysteresis normally occurs. Many factors have been reported to affect contact angle hysteresis including surface roughness, surface heterogeneity, molecular mobility and packing of the surface, surface swelling, liquid absorption and liquid retention [134, 135].

The advancing contact angle followed closely with the static contact angle and

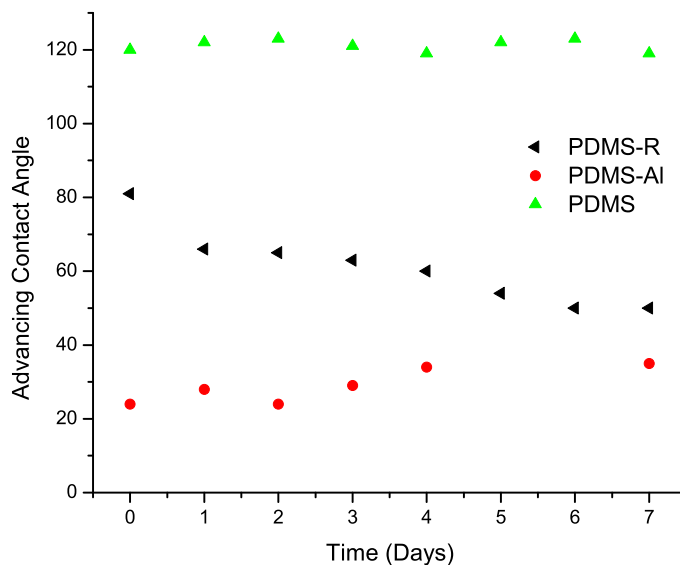


Figure 2.18: Advancing contact angle of  $\mu\text{m}$  thick PDMS, PDMS-R and PDMS-AI samples after immersion in water

can be seen in Figure 2.18. The receding angle for PDMS-AI surface approached  $0^\circ$  for all immersion times and is not shown. The receding angle for PDMS-R surfaces also followed a similar trend as the advancing and static angles (Figure 2.19) and maintained a stable contact angle hysteresis. Unmodified PDMS shows a steady decrease in its receding angle as immersion times increase. This differs significantly from the trends seen for both static and advancing angles and leads to an increase in contact angle hysteresis (Figure 2.20). As PDMS is homogenous, and has a low surface roughness [120] the hysteresis is most likely caused by either liquid absorption or molecular mobility and packing of the surface.

Photolithography has been used to create hydrophilic magnetron modified PDMS regions surrounded by hydrophobically recovered PDMS. This method was successful in creating hydrophilic islands with more hydrophobic surroundings. While these surfaces were able to direct water droplet formation, cells were able to adhere to



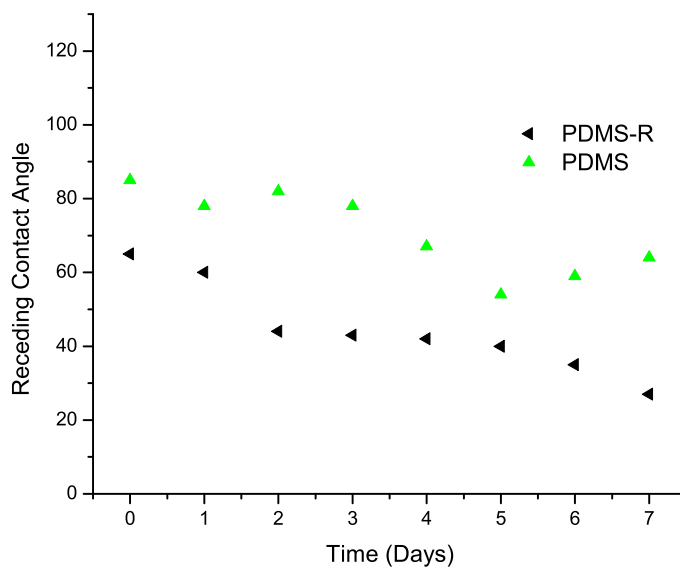


Figure 2.19: Receding contact angle of  $\mu\text{m}$  thick PDMS, and PDMS-R samples after immersion in water

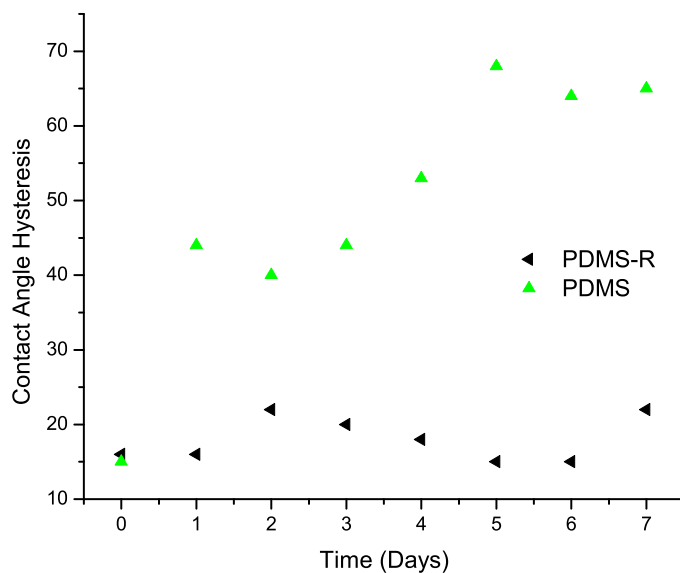


Figure 2.20: The contact angle hysteresis of  $\mu\text{m}$  thick PDMS, and PDMS-R samples after immersion in water

both surface types and showed no preference. Thus, cell patterning did not occur. Upon further examination the contact angle of the hydrophobically recovered regions showed a decrease once immersed in an aqueous environment.

### 2.3.3 Patterning of ODTMS on Modified PDMS by Photolithography

It appears that hydrophobically recovered PDMS does not retain its hydrophobic nature once in an aqueous environment. To overcome this, we modified the photolithographic patterning method. Instead of allowing modified PDMS to undergo hydrophobic recovery, we further modified the surface using silane chemistry (Figure 2.5). This modification would present functional groups which would provide similar surface chemistry as the native PDMS, while eliminating the reversible behavior of recovered PDMS.

Our group has developed a method to modify PDMS-Al surfaces with amino-terminated and mercapto-terminated silanes to provide amine and thio functionality to the surface [106]. Aminopropyltrimethoxy silane (3-APTMS) and 3-mercaptopropyltrimethoxy silane (3-MPTMS) were able to form bonds with the hydroxy groups on the PDMS-Al surface. In order to obtain a hydrophobic surface with similar chemistry as PDMS, ODTMS, a methoxy-terminated silane, was used (Figure 2.2). After treatment, the contact angle of micrometer- and nanometer-thick PDMS surfaces were  $101 \pm 3^\circ$  and  $102 \pm 2^\circ$  respectively. Similarly, glass coverslips were treated with ODTMS and found to have a contact angle of  $98 \pm 2^\circ$  indicating that the coverage of ODTMS on PDMS-Al was similar to that of ODTMS on glass.

The XPS of the ODTMS treated PDMS (PDMS-ODTMS) surface showed an increase in carbon content over the PDMS-Al surface, with a corresponding decrease

Table 2.2: Contact angles of PDMS, modified PDMS, glass and modified glass

Material	Thickness	Contact Angle ( $^{\circ}$ )
PDMS	micrometer	$113 \pm 2$
PDMS	bulk	$112 \pm 1$
PDMS-Al	micrometer	$17 \pm 5$
PDMS-Al	bulk	$37 \pm 3$
PDMS-R	micrometer	$77 \pm 2$
PDMS-R	bulk	$96 \pm 2$
Glass	n/a	$53 \pm 3$
Glass-ODTMS	n/a	$98 \pm 2$
PDMS-ODTMS	micrometer	$101 \pm 3$
PDMS-ODTMS	nanometer	$102 \pm 2$

in oxygen and silicon content. The survey spectrum of PDMS-ODTMS is shown in Figure 2.21, and the atomic composition summarized in Table 2.3. Other elements, sodium, nitrogen and calcium make up less than 1% of the total atomic composition, and are most likely impurities from the ODTMS. A high resolution carbon 1s scan was also performed. Figure 2.22 shows the carbon spectrum and peak fitting for (a) PDMS and (b) PDMS-ODTMS. PDMS shows a single carbon peak with a binding energy of 285.0 eV, whereas PDMS-ODTMS shows two carbon peaks, one with a binding energy of 285.0 eV and the second with a binding energy of 286.2 eV. The 285.0 eV peak represents the carbon atoms found in the bulk PDMS, while the second peak at 286.2 eV represents the alkyl chain from the ODTMS molecule. ODTMS only forms a thin layer on  $\text{SiO}_2$  surfaces of approximately 2.2 nm [136, 137]. Since XPS probes the first 10 nm of the surface, the chemical composition of the ODTMS layer, as well the modified PDMS layer, is determined. The increase in carbon content, as well as, the appearance of the second carbon 1s peak indicates that the surface has in fact been modified by ODTMS.

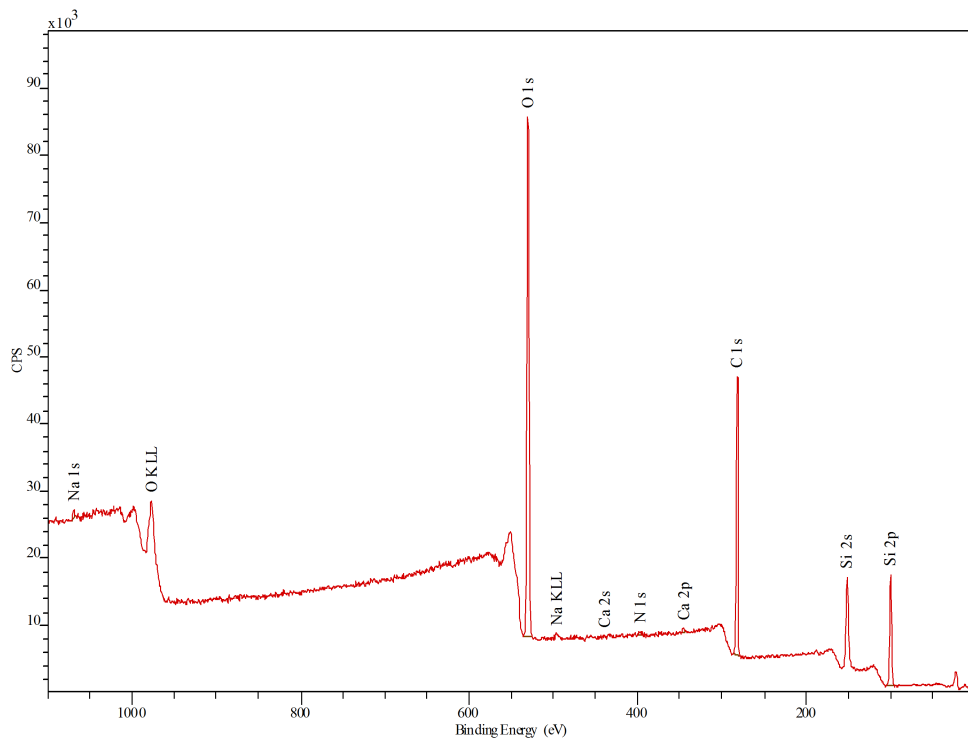


Figure 2.21: XPS survey spectrum of ODTMS modified PDMS

Table 2.3: XPS atomic composition analysis of ODTMS modified PDMS

Peak	Binding Energy (eV)	Atomic Composition (%)
C 1s	283.2	48.4
O 1s	528.0	32.6
Si 2p	100.2	18.3

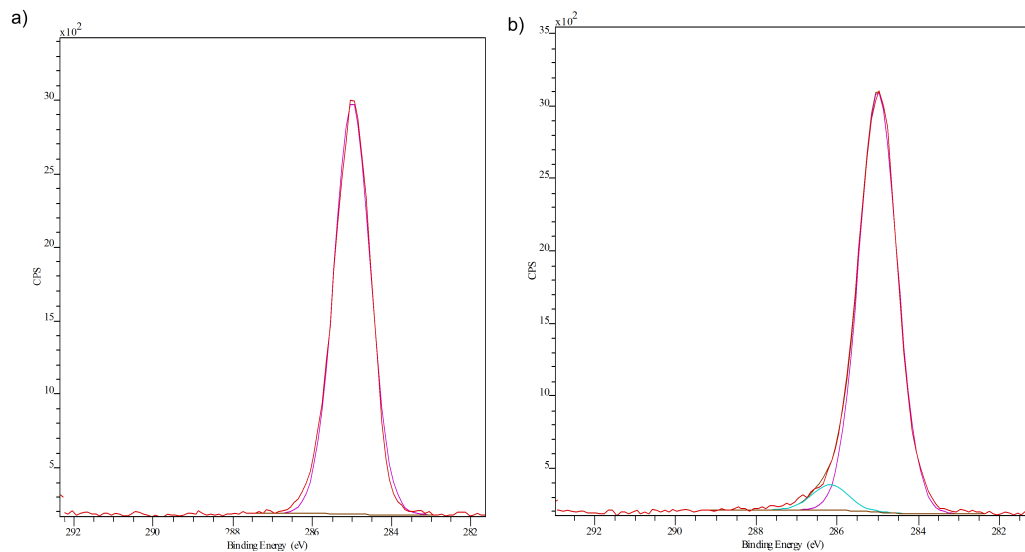


Figure 2.22: C1s XPS spectrum of a) PDMS, and b) ODTMS modified PDMS

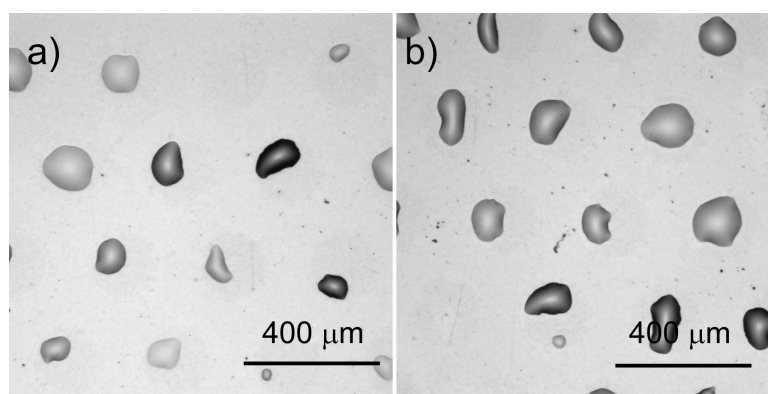


Figure 2.23: Bright field reflection-mode optical images of water droplets localized on treated PDMS surfaces patterned with ODTMS by photolithography

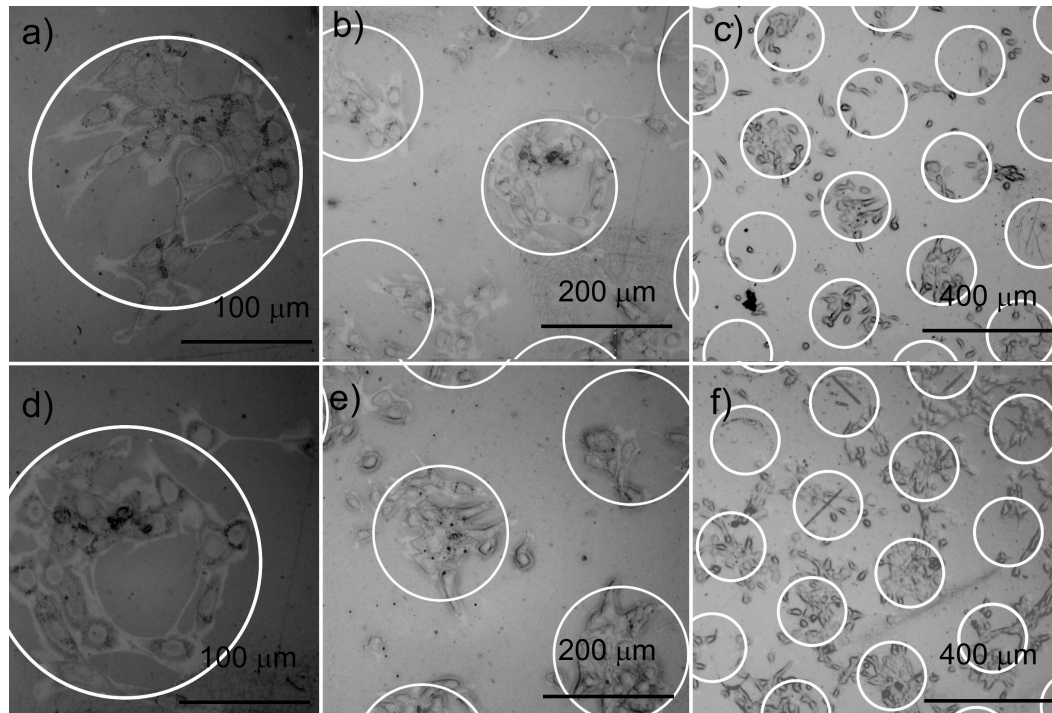


Figure 2.24: Bright field reflection-mode optical images of C2C12 myoblast cells after 24 hrs incubated on ODTMS patterned surfaces

Figure 2.23, shows water droplets that formed on the patterned surface, indicating that we have successfully patterned hydrophobicity on the hydrophilic surface. The ability of the surface to pattern cell attachment was tested using C2C12 cells. Cells preferred the hydrophilic dots over the ODTMS treated surrounded areas as seen in Figure 2.24. Unlike the stencil mask patterned surfaces, the cells were able to migrate out of the dots.

There are several differences between the ODTMS-PDMS surface and native PDMS. The contact angle of the ODTMS surface is slightly lower than that of PDMS, although the surface is very hydrophobic and similar in surface chemistry to other cytophobic surfaces [30, 39]. Aside from the contact angle, other surface properties need to be considered, such as whether the initial aluminum treatment created a rougher and stiffer surface than PDMS [120]. Thus, the physical properties of the

underlying  $\text{SiO}_x$  layer may affect how cells interact with the surface. These differences may explain why the stencil mask patterning was more successful than either of the photolithographic methods.

The ODTMS method used photolithography to protect areas of magnetron treated PDMS, while exposed regions reacted with the ODTMS molecule to create hydrophobic barrier. The reaction between ODTMS and PDMS-Al was confirmed by contact angle and XPS. This method was successful at directing cell adhesion into the hydrophilic dots, but was not as robust as the stencil mask method. Cells were able to leave the hydrophilic dots and appeared spread out when growing on the ODTMS surface.

## **2.4 Conclusions**

Three different methods of patterning PDMS were explored. We patterned hydrophilic dots and surrounded them with hydrophobic regions in order to pattern cell attachment and growth. While all methods were able to create a hydrophobic/hydrophilic pattern, the stencil mask patterning method was the most effective at patterning cells. The stencil mask patterned surface used native PDMS as the cell repellent hydrophobic surface, which was the most hydrophobic of all four surfaces. Also, the photolithographic methods relied on initial magnetron aluminum treatment of the surface. The magnetron treatment produced a surface similar to that produced through plasma treatments. Plasma treatment of PDMS is known to affect the stiffness and roughness of the surface [116,138–140] and both properties have been shown to increase cell attachment and growth [15,18,141]. The chemistry of the hydrophobic surfaces in the photolithographic patterned surfaces was not exactly the same as that of native PDMS and may interact differently with mediating proteins. We have also

shown that hydrophobically recovered PDMS can regain some of its hydrophilicity in a aqueous environment, which may explain why no patterning was seen on the surfaces that used recovered PDMS as the hydrophobic background.



# Chapter 3

## Cell and Protein Interactions with PDMS and Surface Modified PDMS

### 3.1 Introduction

The ability of a cell to attach to a surface depends on the physical and chemical properties of the surface. Surface wettability, functional groups, roughness and stiffness each play an essential role in cell adhesion [15, 18, 141]. Cells adhere to the surface through mediating proteins from the ECM. When a surface comes into a contact with culture media, before cells reach that surface, these proteins immediately adsorb and interact with the surface. When proteins adsorb to a surface, they take the most energetically favourable configuration, and this configuration depends on the wettability and chemistry of the surface [16, 141]. These conformational changes can affect the protein activity by either exposing or hiding different functionalities such as the RGD binding sequence. For cells to adhere to these surface binding sites must be accessible.

Fn has been shown to play an essential role in cellular adhesion [26, 28]. The availability of the central RGD binding sites between the 9th and 10th type II repeats on Fn can determine whether cells which express Fn binding integrin receptors, such as the  $\alpha_5\beta_1$  and the  $\alpha_v\beta_3$  integrins, will adhere to the underlying substrate the protein has adsorbed to. The ability to detect protein conformation on a surface has become

a challenge undertaken by a variety of scientists. Methods to determine Fn conformation include AFM [142], ATR-FTIR [143,144], confocal microscopy [145], quartz crystal microbalance (QCM) [146], fluorescence resonance energy transfer (FRET) [147], and enzyme-linked immunosorbent assays (ELISA) [25,26,28]. On hydrophobic surfaces, Fn is in a spherical conformation [142], demonstrates a decrease in its secondary structure, and the RGD adhesion binding site is considerably less accessible [25,26,28] than on hydrophilic surfaces.

To further investigate the efficiency of the patterning methods developed in Chapter 2, the interaction between cells and proteins with PDMS and modified PDMS were explored. First, the ability of C2C12 cells to attach and proliferate on these surfaces, as well as their viability was determined. Secondly, the relative protein adsorption and conformation on different surface and binding site availability was observed through adsorption of proteins onto patterned substrates.

## 3.2 Materials and Methods

### 3.2.1 Reagents

PDMS Sylgard 184A and B were purchased from Dow Corning. The materials used for photolithography, Microposit SC1827 positive photoresist and Microposit MF-319 developer were purchased from Rohm & Haas Electronic Materials. The C2C12 cell line was purchased from ATCC. DMEM, L-glutamine, penicillin streptomycin, FBS, Trypsin/EDTA, PBS, 4',6-diamidino-2-phenylindole (DAPI), Alexa Fluor 488 conjugated Fibrinogen (Fb-488), and fluorescein isothiocyanate (FITC) conjugated goat anti-mouse immunoglobulin G (IgG) were all purchased from Invitrogen. Mouse monoclonal antibody HFN7.1 was obtained from the Developmental Studies Hybridoma

Bank. All other chemicals were purchased from Sigma-Aldrich and used as received.

### **3.2.2 Preparation of PDMS and modified PDMS surfaces**

Micrometer thick PDMS surfaces were used and prepared through spincoating onto a glass coverslip as described in 2.2.2.2. Magnetron modified surfaces, PDMS-Al, were prepared through the deposition of aluminum in a magnetron sputtering system, followed by etching in orthophosphoric acid as described in 2.2.2.3. PDMS-Al surfaces were allowed to undergo hydrophobic recovery for at least 72 hrs to create the PDMS-R surfaces as described in 2.2.2.4. PDMS-Al was modified with ODTMS as described in 2.2.2.5,.

### **3.2.3 Preparation of Patterned PDMS Surfaces**

The creation of patterned PDMS surfaces was performed as described in 2.2.3.1, 2.2.3.2, and 2.2.3.3. In short, stencil masked patterned samples were created by aluminum deposition through a commercially available steel mesh. PDMS-R was patterned on PDMS-Al surfaces through photolithography. Exposed aluminum was etched away and the underlying modified surface allowed to undergo hydrophobic recovery for at least 72 hrs. PDMS-ODTMS was also patterned over PDMS-Al by photolithography. The exposed PDMS-Al surface reacted with ODTMS molecules. All patterned substrates were etched with orthophosphoric acid and rinsed in water before use.

### **3.2.4 Cell Proliferation and Viability Testing**

The concentration of cells in a suspension can be determined using a hemocytometer. A hemocytometer consists of a surface that has a laser inscribed grid on it, as seen

Table 3.1: The size of squares found on a hemocytometer and their corresponding surface area and volume

Size (mm)	Surface Area (mm <sup>2</sup> )	Volume (nL)
1.00 x 1.00	1.00	100
0.25 x 0.25	0.0625	6.25
0.20 x 0.25	0.050	5.0
0.20 x 0.20	0.040	4.0
0.05 x 0.05	0.0025	0.25

in Figure 3.1. The surfaces of the hemocytometer consist of several 1 x 1 mm (1 mm<sup>2</sup>) squares. Each square is further divided into 0.25 x 0.25 mm (0.0625 mm<sup>2</sup>), 0.25 x 0.20 mm (0.05 mm<sup>2</sup>) and 0.20 x 0.20 mm (0.04 mm<sup>2</sup>) sections, with the central square further divided into 0.05 x 0.05 mm (0.0025 mm<sup>2</sup>) squares. A cover slip is held 0.1 mm over the surface giving each square a defined volume as listed in Table 3.1. By counting the number of cells in the squares the concentration of cells can be determined.

To determine cell viability, a dye exclusion technique was used. Viable cells have an intact membrane that will prevent certain dyes from entering the cell, whereas dead or dying cells have membranes that are not fully functional and will allow for dye penetration. Trypan blue (Figure 3.2) is one such dye that is commonly used to distinguish between viable and non viable cells [148]. Viable cells appear clear while non viable cells are dark blue in colour under a microscope.

Samples of PDMS, PDMS-Al, PDMS-R, and PDMS-ODTMS, were sterilized by rinsing with 70% ethanol. Prior to plating, cultured cells were washed with trypsin/EDTA to promote cell detachment from the culture flasks. The cells were mixed into media for transfer and brought to a concentration of  $2.5 \times 10^4$  cells/mL. 3 mL of the cell solution was added to a 3 cm tissue culture dish (Falcon) contain-

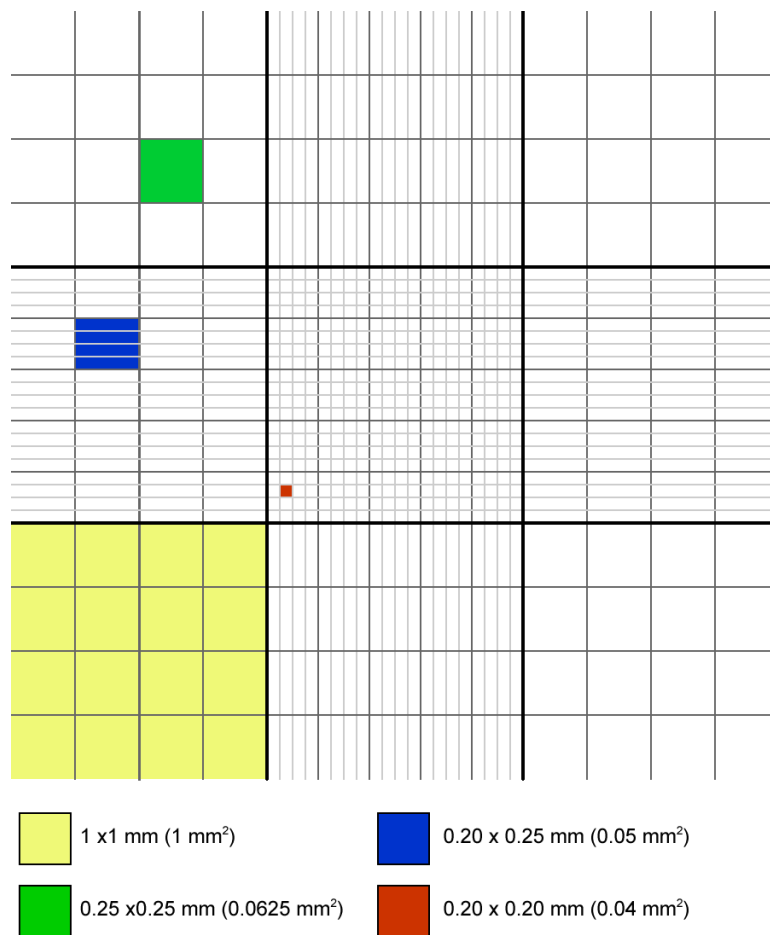


Figure 3.1: The grid structure found on a typical hemocytometer

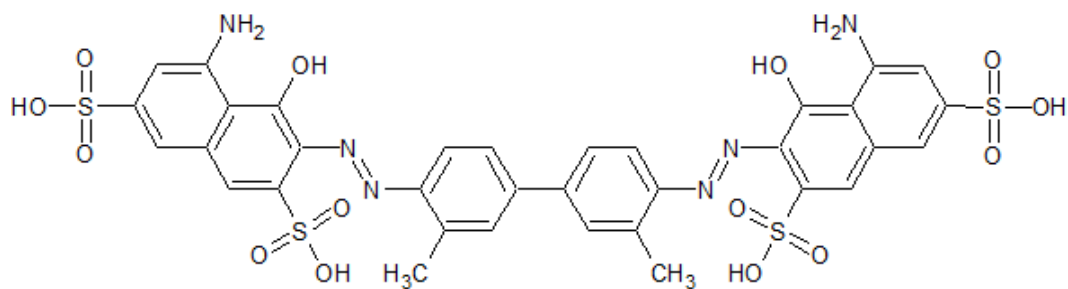


Figure 3.2: The molecular Structure of Trypan Blue, a dye used to stain non viable cells

ing a polymer sample. The cells were then incubated at 37°C , 5% CO<sub>2</sub>, and 100% humidity for 24 and 48 hrs.

To determine the degree of cell attachment, the samples were transferred to a fresh 3 cm tissue culture dish. Each sample was rinsed with trypsin/EDTA to promote cell detachment. The samples were then washed with 1 mL of cell media to remove the detached cells. The solution was then centrifuged at 1500 rpm for 10 min and the cell media removed. The cells were re-suspended in 100  $\mu$ L of PBS, and 15  $\mu$ L of that solution was mixed with 15  $\mu$ L of trypan blue for 3 min to determine cell viability. The total concentration of cells and non viable cells were found using a hemocytometer with a total cell count of at least 200. For each surface, data were collected at each time point on three samples.

### 3.2.5 Cell Imaging

Wide field fluorescent imaging is common technique used to localize fluorescent molecules on a sample [149–151]. For biological purposes, the sample is labeled with a fluorescent molecule called a fluorophore. Commonly, a wide field fluorescent microscope uses a mercury or xenon arc-discharge lamp, which emits a broad range of light. The desired excitation wavelength is selected through the use of an emission filter. The fluorophore will absorb the light and emit light of a longer wavelength. The emitted light is separated from the excitation light by a beam splitter and an emission filter. Figure 3.3, shows the typical set up for a wide field fluorescence microscope.

Optical images of cell on the surfaces were obtained using the bright field reflective mode on a Zeiss Axioskop2 Mat Microscope with a QImaging Retiga 1300 CCD digital camera. Fluorescent images of the cell nuclei were obtained using a Zeiss Axiovert 200M Microscope with a Zeiss AxioCam HRM CCD digital Camera

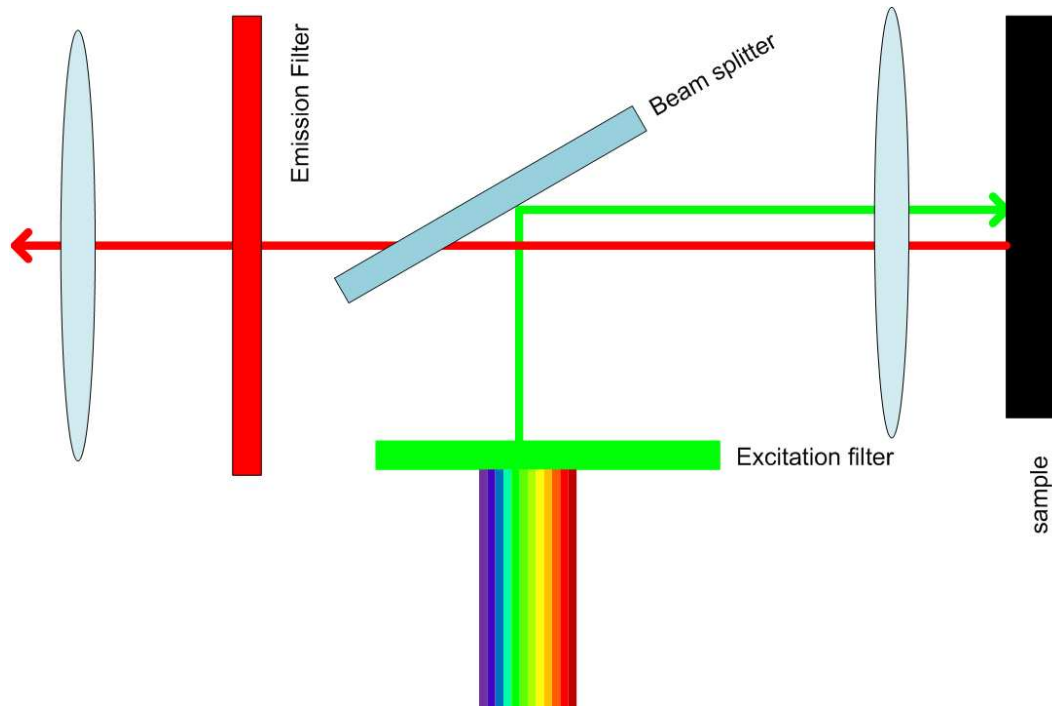


Figure 3.3: Schematic representation of the typical set up for a wide field fluorescent microscope

in wide field fluorescent mode. Before optical imaging, cells were washed 3 times in PBS and fixed in a 4% paraformaldehyde solution in PBS for 10 min. Cells were then rinsed 3 times in PBS and 3 times in water. Before fluorescent imaging cells were washed 3 times in PBS and fixed in a 4% paraformaldehyde solution in PBS for 10 min and washed 3 times in PBS. The cellular membrane was then permeabilized by immersion in acetone for 3 min at 20°C. The cell nuclei were fluorescently labeled using DAPI (Figure 3.4), which binds strongly to DNA (deoxyribonucleic acid). DAPI has a adsorption maximum at 358 nm and an emission maximum at 451 nm, when bound to DNA. UV light was used to excite DAPI and a blue filter used to obtain the fluorescent image.

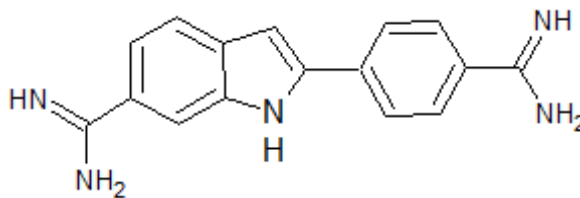


Figure 3.4: The molecular Structure of 4',6-diamidino-2-phenylindol (DAPI), a dye used to stain the DNA in the nuclei of a cell

### 3.2.6 Fibronectin Conjugated with Oregon Green Dye

In order, to visualize the adsorption of Fn on the surface of patterned PDMS, fluorescently labeled protein was required. As labeled Fn is not commercially available, an Oregon Green 488 (OG) dye was conjugated to the protein using a dialysis technique. OG can react with amine groups found on lysine residues of the protein, through its isothiocyanate functional group. This type of modification is known not to interfere with Fn's biological activity [152–154].

5 mg of human plasma fibronectin was dissolved in 5 mL PBS for a concentration of 1 mg/mL. The solution was dialyzed against 450 mL of 0.1 M sodium borate buffer, pH 9.0 for 24 hrs at 4°C, the buffer solution was changed after 12 hrs. 5 mg of OG was dissolved in 500  $\mu$ L dimethyl sulfoxide (DMSO). 250  $\mu$ L of the OG DMSO solution was added to 100 mL of 0.1 M sodium borate buffer solution, pH 9.0. The Fn solution was then dialyzed against the OG solution for 8 hrs at 4°C. To remove unreacted OG dye, the Fn solution was dialyzed against PBS (pH 7.4) for 72 hrs at 4°C with a buffer change every 12 hrs. 3.2 cm standard cellulose dialysis tubing (Spectra/Por) with a cut off molecular weight of 12 to 14 kD was used for all steps.



### 3.2.7 Fibronectin and Fibrinogen Adsorption Studies

Each patterned PDMS sample was etched in 1.8 M orthophosphoric acid for 30 min and rinsed 3 times in water immediately before adsorption studies. Fibronectin labeled with Oregon Green (Fn-OG) was diluted to a concentration of 0.1 mg/mL or 50  $\mu$ g/mL in PBS. Fibrinogen labeled with Alexa Fluor 488 was diluted to 0.1 mg/mL in PBS (Fg-488). To look at the effect of protein co-adsorption on Fn, Fn was mixed with BSA. Fn-OG was diluted to a concentration of 0.1 mg/mL in PBS and mixed at a 1:1 ratio with 4 mg/mL BSA in PBS. 1 to 2 mL of solution was poured over a patterned PDMS sample in a 30 mm tissue culture dish and allowed to adsorb for 30 min at room temperature while protected from light. Each sample was then rinsed 3 times in PBS and then 3 times in water.

### 3.2.8 Fibronectin Conformation Study

Immunofluorescent labeling is a technique that allows the location and relative amounts of an antigen to be determined [155]. Direct immunofluorescent labeling uses a fluorescently labeled antibody. The antibody will bind only to the desired antigen and can be visualized using either fluorescence microscopy or confocal microscopy. An indirect technique is used when labeling the required antibody is difficult or will adversely affect function. An indirect technique uses a primary antibody to detect the desired antigen and a secondary antibody which is fluorescently labeled and can bind to the primary antibody for detection. Direct and indirect immunofluorescent labeling are illustrated in Figure 3.5

Patterned PDMS samples were etched in 1.8 M orthophosphoric acid and rinsed 3 times in water to remove the protective aluminum coating. Immediately after etching, Fn was adsorbed to the surface for 30 min at room temperature at a concentration

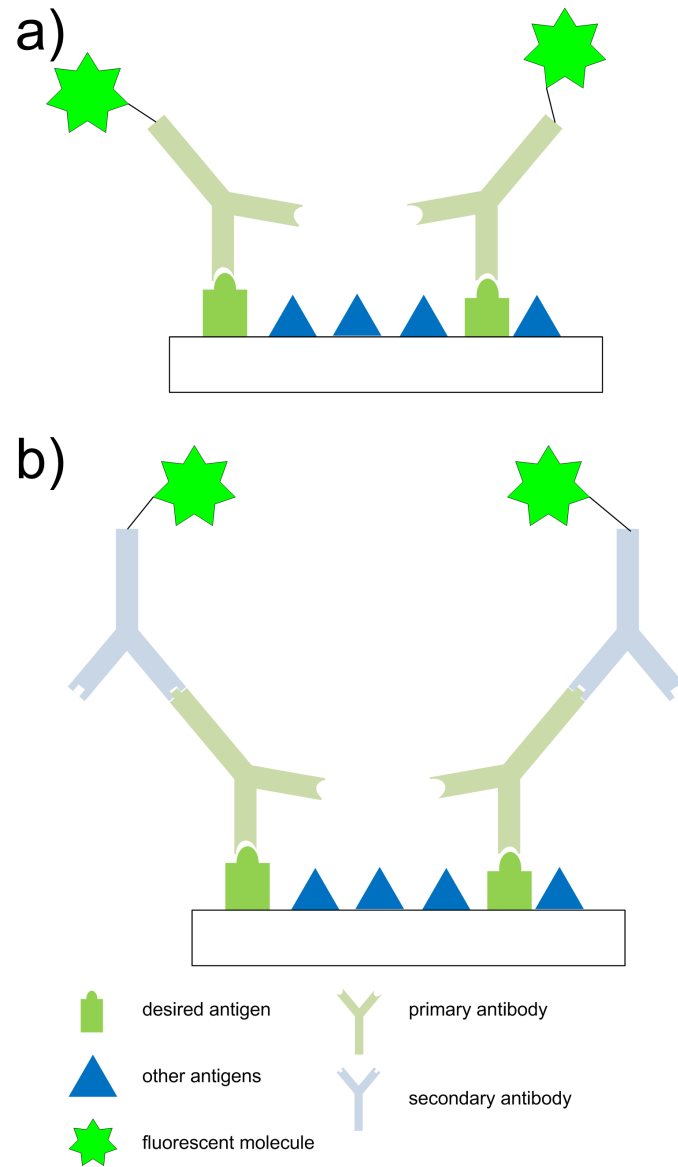


Figure 3.5: An illustration of a) direct and b) indirect immunofluorescent labeling

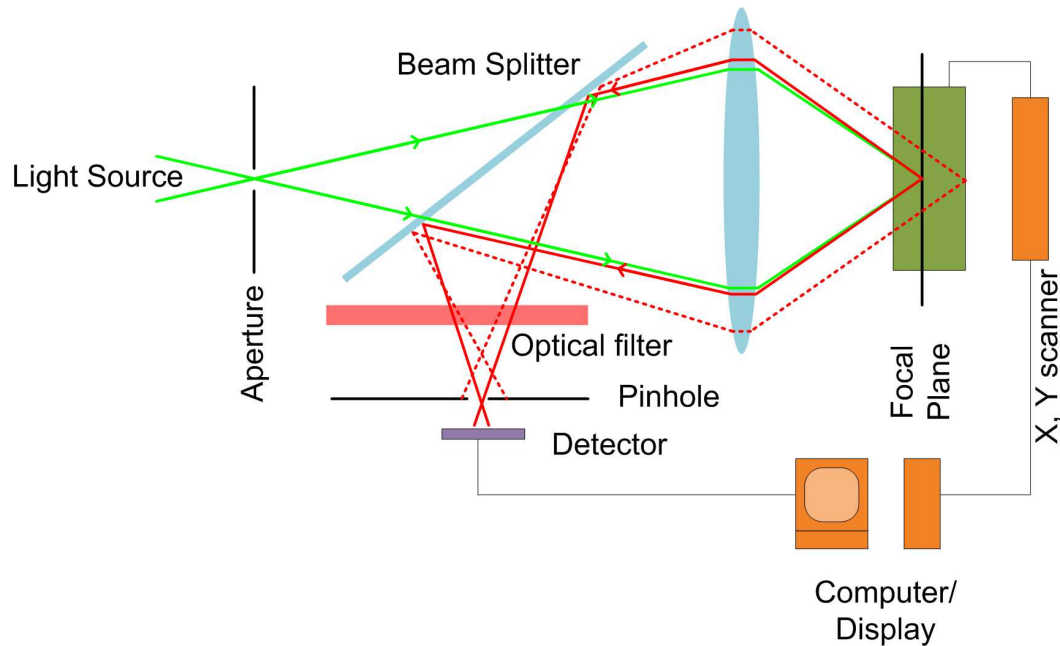


Figure 3.6: A schematic representation of a confocal microscope, the green line represents the incoming light at the excitation wavelength; the red solid line, the in-plane fluorescent light; and the red dashed line, the out of plane fluorescent light.

of 0.1 mg/mL or 50  $\mu\text{g}/\text{mL}$ . To look at the effect of BSA, 0.1 mg/mL of Fn was also mixed with 4 mg/mL BSA at a 1:1 ratio before absorption. After rinsing 3 times in PBS, the samples were immersed in blocking buffer (0.25% BSA in PBS) for 1 hr at room temperature, to eliminate unspecific binding. The samples were then incubated with a monoclonal antibody HFN7.1 at 0.240  $\mu\text{g}/\text{mL}$  for 1 hr in blocking buffer at 37°C. After rinsing 3 times in blocking buffer, the samples were then incubated with 0.25  $\mu\text{g}/\text{mL}$  FITC goat anti-mouse IgG for 1 hr at 37°C before rinsing 3 times in PBS and water. To ensure that the fluorescent signal was due to interactions between HFN7.1 and Fn and not unspecific binding of FITC goat anti-mouse IgG, each experiment was performed in the absence of the primary antibody, HFN7.1.

### 3.2.9 Confocal Imaging

Confocal microscopy is a laser scanning method used to image fluorescent molecules [151, 156]. A laser is scanned over a sample, and at each point the fluorescent signal is collected and its intensity mapped to an image. One major advantage of confocal microscopy over widefield fluorescence is that confocal uses a pinhole to remove light generated out of the focal plane. This allows for higher resolution, as well as 3D imaging. Figure 3.6 shows the set-up for a standard confocal microscope. The incoming light is focused using an objective lens to the focal plane. The fluorescent light passes back through the objective lens, and is reflected by a beam splitter towards the photo detector. The pinhole only allows light which originated in the focal plane to reach the detector. Before reaching the pinhole, light is passed through an optical filter to prevent any reflective and unwanted fluorescent light from reaching the detector. Normally a high-pass filter is used to remove light less than a specific wavelength, or a band-pass filter, which removes light outside of a specified range. To obtain an image, an x,y scanner moves the sample and intensity data are collected for each point.

Confocal images were acquired using a Zeiss 510 LSM confocal (Zeiss, Thornwood, NY) with an excitation wavelength of 488 nm corresponding to the  $\lambda_{max}$  for OG, FITC and Alexa Fluor 488.

## 3.3 Results and Discussion

### 3.3.1 Cell Proliferation and Viability Studies

Studies in Chapter 2 demonstrated that cells are able to grow on hydrophobically recovered PDMS and ODTMS treated PDMS when patterning the surface with pho-

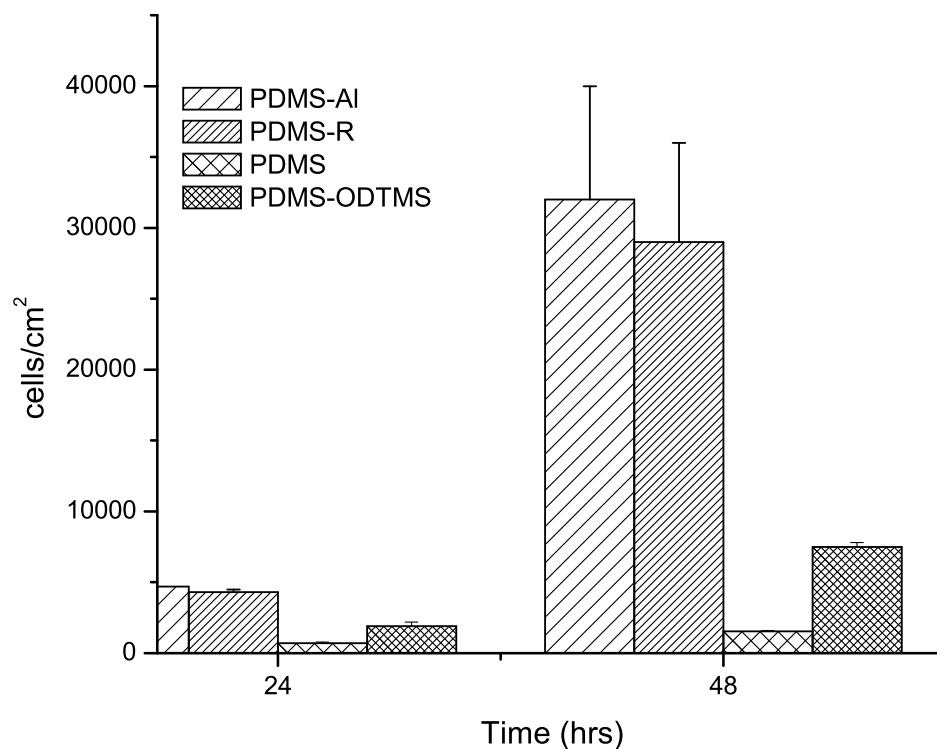


Figure 3.7: The number of cells per  $\text{cm}^2$  on PDMS, PDMS-AI, PDMS-R, PDMS-ODTMS

tolithography. Thus, patterning wettability does not necessarily lead to spatial control over cell adhesion. To better understand the interactions between cells and each surface type, we looked at the number of cells that had attached to the surface and their viability over a 48 hr period.

Figure 3.7 shows the concentration of cells attached to PDMS, PDMS-AI, PDMS-R and PDMS-ODTMS after 24 and 48 hrs. While some cells were able to attach to the PDMS surface, the number of cells was significantly lower than that observed for both PDMS-AI and PDMS-R. Since PDMS has previously been reported as cytophobic, due to its hydrophobicity and  $\text{CH}_3$  chemistry, we did not see cells growing on PDMS when we performed the stencil mask patterning, as expected. Even after

48 hrs, the number of cells attached to PDMS remained low.

The number of cells attached to PDMS-R surface did not significantly vary from the number of cells found on PDMS-Al. It appears that hydrophobic recovery has little effect on the number of cell that can attach and proliferate on the polymer surface in comparison to freshly etched magnetron treated surface. Figure 3.8 shows cells grown on both PDMS-Al and PDMS-R after 24 and 48 hrs that have been stained with DAPI. The bright spots represent the cell nuclei. We originally hypothesized that on PDMS-R patterned surfaces, cells may have begun to form patterns but were able to spread out once the hydrophobic recovered surface regained its hydrophilicity. After only 24 hrs the number of cells on both surfaces was nearly identical, indicating that the cells had no difficulty attaching to the recovered surface, thus patterning most likely never occurred. After 48 hrs the cell became confluent on both surfaces as seen in Figure 3.8 and Figure 3.9.

The ODTMS treated surface showed lower cell attachment after 24, and 48 hrs than either PDMS-Al or PDMS-R. Despite having similar surface chemistry and hydrophobicity as native PDMS, there were more cells attached to the PDMS-ODTMS surface. These results indicate that while cells would prefer the PDMS-Al surface, they are able to attach and proliferate on the PDMS-ODTMS surface. Once the cells became crowded on the PDMS-Al dots they could then simply move out from the dots, and grow on the ODTMS treated areas. This reflects what occurred on the ODTMS patterned substrates, creating merely a temporary pattern.

The percentage of viable cells was calculated from the total number of viable cells and the total number of cells, and summarized in Table 3.2. After 24 and 48 hrs all surfaces showed reasonable cell viability for the cells that had attached to their surface.

Cell growth is significantly increased on magnetron treated PDMS surfaces over

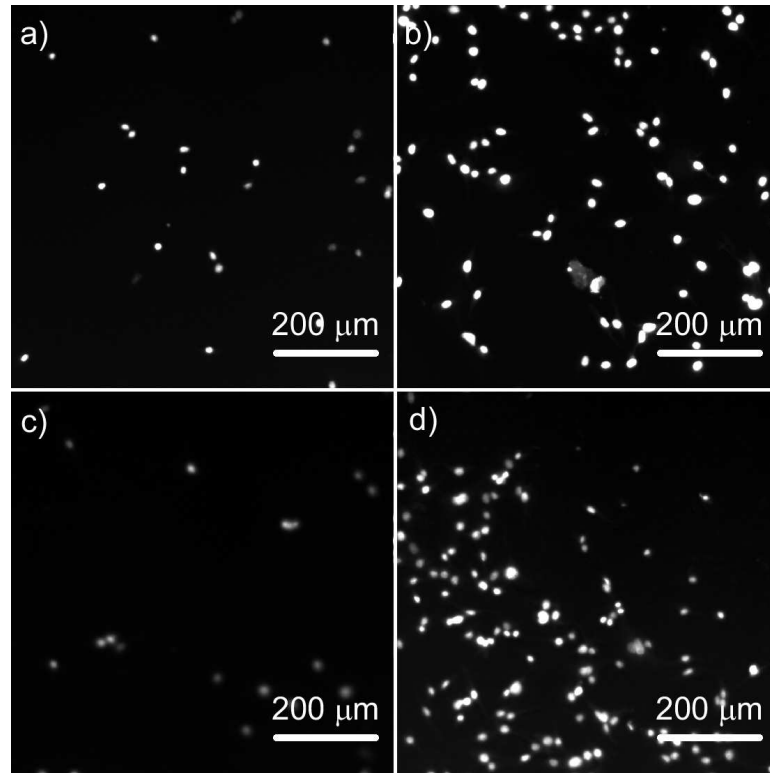


Figure 3.8: Wide field fluorescent images of DAPI stained C2C12 cells grown on PDMS-AI (a,b) and PDMS-R (c-d) for 24 hrs (a,c) and 48 hrs (b,d)

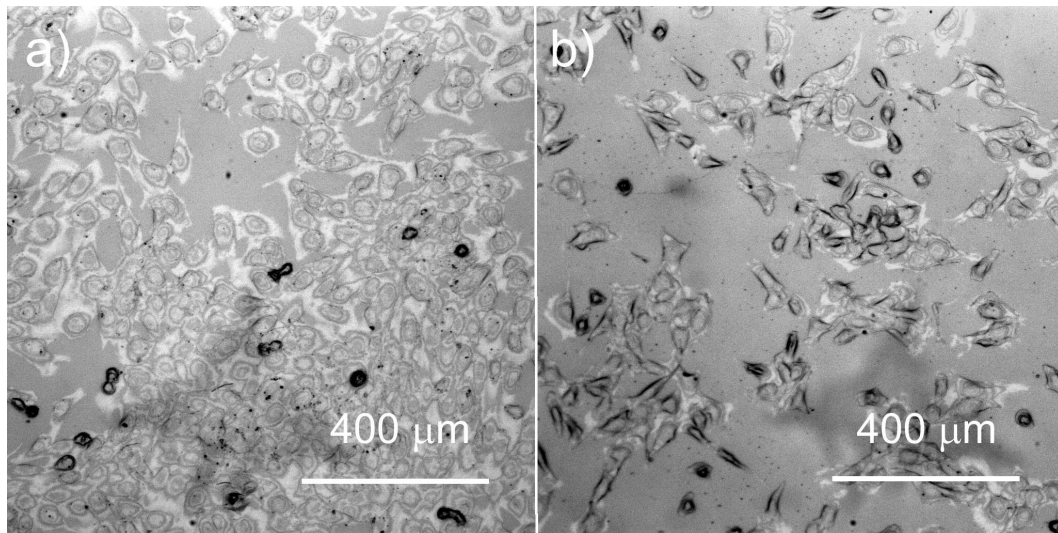


Figure 3.9: Bright field reflection mode optical images of C2C12 cells grown on (a) PDMS-AI and (b) PDMS-R for 48 hrs.

Table 3.2: Cell viability after 24, and 48 hrs on PDMS and modified PDMS

<b>Material</b>	<b>24 hrs</b>	<b>48 hrs</b>
PDMS-Al	$90 \pm 5 \%$	$99 \pm 1 \%$
PDMS-R	$83 \pm 7 \%$	$95 \pm 4 \%$
PDMS	$67 \pm 5 \%$	$81 \pm 6 \%$
PDMS-ODTMS	$92 \pm 2 \%$	$77 \pm 17 \%$

native PDMS. Hydrophobic recovery appears to have little effect over cell attachment, proliferation or viability. This indicates that cells respond to the hydrophobic recovered surface the same as they respond to freshly etched magnetron treated PDMS. The ODTMS treated surface fell between PDMS and magnetron treated PDMS in terms of cell attachment. Despite having a similar surface chemistry and wettability as PDMS, cells were able to adhere to and proliferate on the ODTMS surface. These results directly explain both the success and failure of the patterning methods explored in Chapter 2.

The modified PDMS surfaces have been plasma treated during the magnetron deposition of aluminum. Plasma treatment increases the oxygen content, roughness and stiffness of the surface [98, 110, 116, 117, 138]. Increasing these properties can lead to increased cell adhesion and proliferation. To reduce cell adhesion, the surface chemistry and the wettability of the magnetron treated surface, the surface was further modified. Hydrophobic recovery increases the contact angle by coating the surface with uncrossed-linked PDMS oligomers [110, 138]. In Chapter 2, we saw that hydrophobic recovery did not fully return to that of PDMS, and immersion in an aqueous environment further reduced the contact angle. Cells are able to adhere to the recovered surface to the same extent as the non recovered surface. Thus, it is possible that cells are still able to interact with the oxygen rich layer.



The ODTMS treatment was successful at creating a CH<sub>3</sub> rich hydrophobic layer over the magnetron treated surface. Despite having similar chemistry and wettability as native PDMS, cells adhered significantly more to the ODTMS surface than to native PDMS. The increased surface roughness and stiffness caused by the initial magnetron treatment may have played a role. It is also possible that the ODTMS layer is not uniform, and contains exposed regions of the underlying oxygen rich layer. If this is the case, cells would be able to adhere to these exposed regions.

### 3.3.2 Protein Adsorption on Patterned PDMS

Since the interaction between serum proteins and a surface directly affects the ability for cells to adhere, the adsorption of two different serum proteins on patterned PDMS substrates were considered. The first protein, fibrinogen (Fg), is found in blood serum and its adsorption is important in mediating platelet adhesion [157]. The second protein, Fn, is found in media serum used for cell culture and is directly involved with cell adhesion in cultures [15, 16].

### 3.3.3 Fibrinogen Adsorption on Patterned PDMS

In order to probe the adsorption of Fg on the surface of patterned PDMS substrates, a fluorescently labeled protein was used. Figure 3.10 shows the adsorption onto the stencil mask patterned surface. The bright areas in the image relate to an increased concentration of the protein compared to the darker areas. While it is apparent that some Fg-488 has adsorbed to hydrophobic regions, the majority of the Fg-488 is found in the hydrophilic dots.

The adsorption of Fg-488 on patterned PDMS-R surfaces was also studied (Figure 3.11). If the adsorption of Fg is related to cell growth, the Fg-488 would be

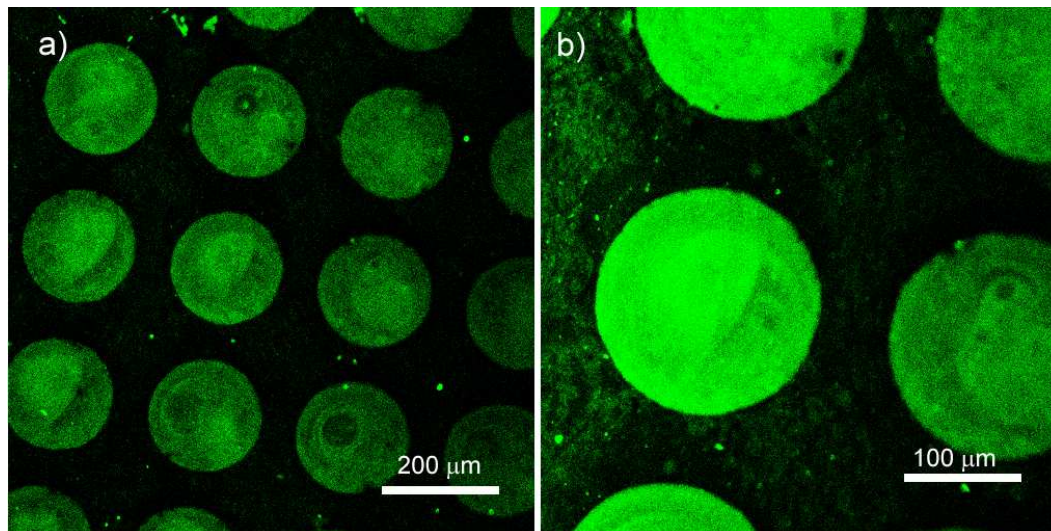


Figure 3.10: Confocal images of Alexa Fluor 488 conjugated fibrinogen adsorbed onto stencil masked patterned samples for 30 min at a concentration of 0.1 mg/mL

expected to be found evenly across the sample, as cells adhere to both surfaces. This, however, was not that case. Rather bright areas, corresponding to Fg-488 adsorption, are seen in the hydrophobic background. This is the first indication that the PDMS-R surfaces interact with biological materials differently than their non-recovered counterparts.

For patterned PDMS-ODTMS surfaces, Fg was once again seen in the hydrophobic regions. The contrast in the images between the hydrophilic and hydrophobic regions was much less pronounced than that observed for the hydrophobic recovered samples. While Fg has been linked to an increase in platelet and cell adhesion and its adsorption is important for cells grown *in vivo* [157,158], FBS, the serum used for our cell cultures has had Fg removed. Thus, Fg is not directly involved in cell adhesion on these patterned surfaces.

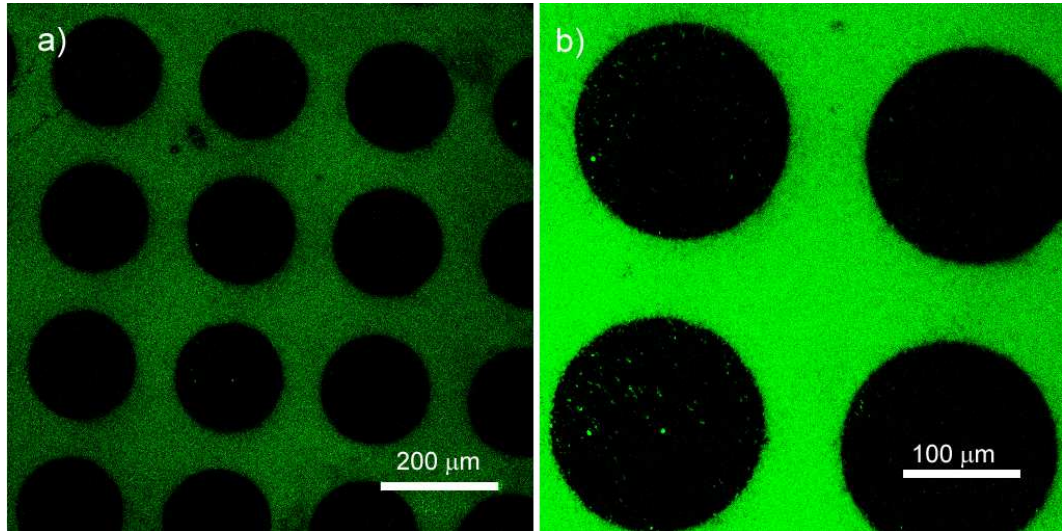


Figure 3.11: Confocal images of Alexa Fluor 488 fibrinogen adsorbed onto patterned hydrophobic recovered PDMS samples for 30 min at a concentration of 0.1 mg/mL

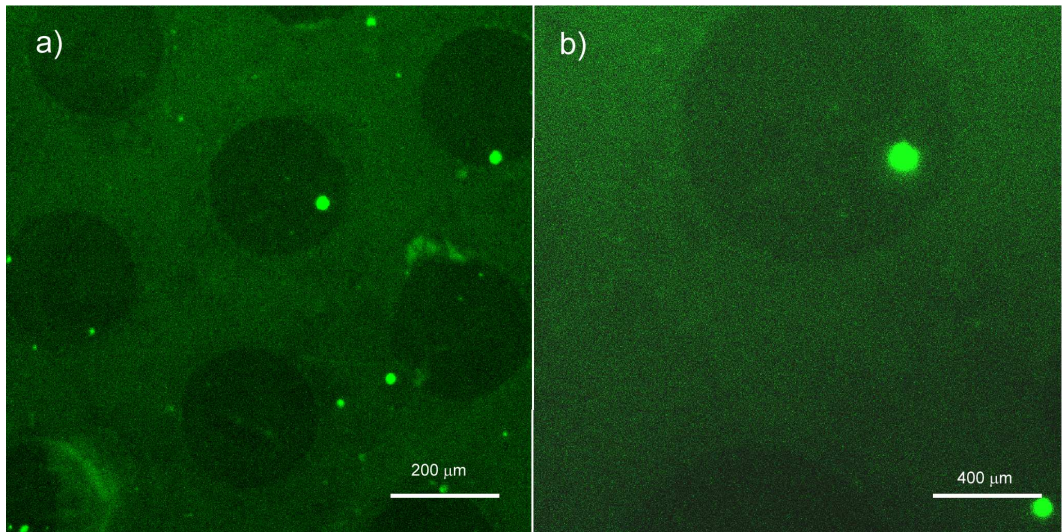


Figure 3.12: Confocal images of Alexa Fluor 488 fibrinogen adsorbed onto ODTMS patterned samples for 30 min at a concentration of 0.1 mg/mL

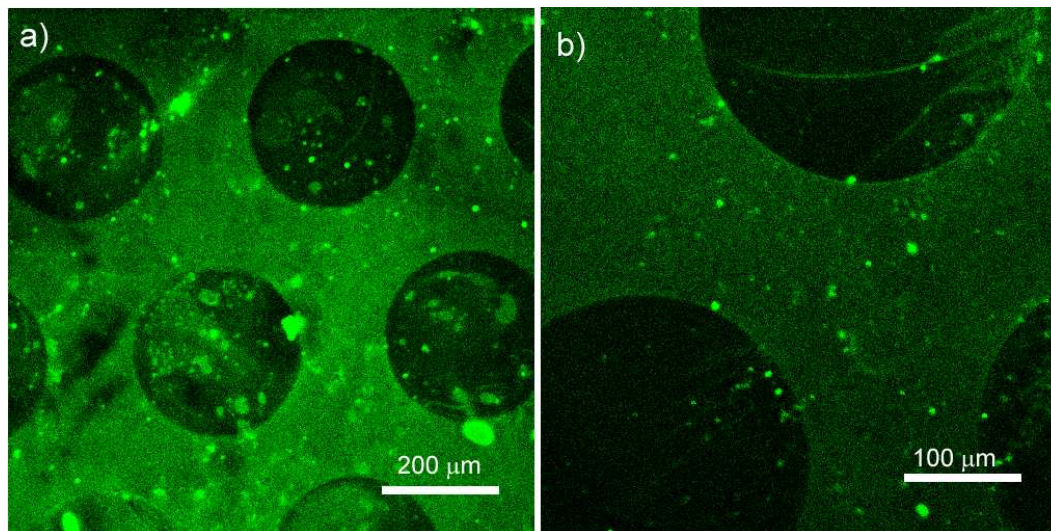


Figure 3.13: Confocal fluorescent images of Fn-OG adsorbed onto stencil masked patterned samples for 30 min at a concentration of 0.1 mg/mL

### 3.3.3.1 Fibronectin Adsorption

Fg is not involved in cell culture *in vitro*, and its adsorption pattern does not reflect the observed cell growth. Thus, the adsorption of another major adhesion promoting protein, Fn, which is present during cell culture [15, 16], was explored. In order to visualize Fn upon adsorption, Fn was conjugated with an Oregon Green dye through a dialysis technique. Figure 3.13 shows Fn-OG adsorbed to an stencil mask patterned PDMS surface. The bright areas indicate an increased concentration of Fn. Fn preferred to adsorb on the outside hydrophobic regions. It had been previously reported that Fn does adsorb more to hydrophobic surface than to hydrophilic surfaces but in a conformation not ideal for cell growth [16].

Based strictly on hydrophobic/hydrophilic effects, Fn would be expected to adsorb more on the hydrophobically recovered background on the PDMS-R patterned surface. Fn did not show a significant preference for either the hydrophilic dots or the hydrophobic recovered surroundings, as seen in Figure 3.14. This may explain the lack of patterning on the photolithographically patterned surfaces, assuming that

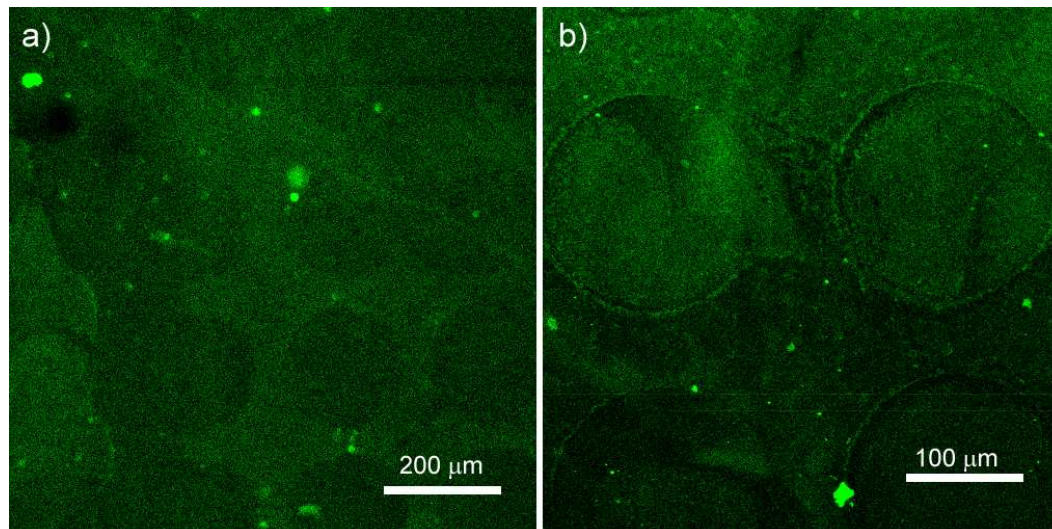


Figure 3.14: Confocal fluorescent images of Fn-OG adsorbed onto patterned hydrophobic recovered PDMS samples for 30 min at a concentration of 0.1 mg/mL

the conformation of Fn is the same across the sample. Finally the adsorption of Fn on the ODTMS surfaces was studied. Fn adsorbed more to the hydrophilic dots than the ODTMS surface (Figure 3.15). In all three cases Fn does appear to be adsorbed to both the hydrophilic and the hydrophobic regions, however the relative concentration of Fn cannot be correlated directly to cell adhesion.

Figure 3.16, shows Fn adsorption on a stencil masked patterned surface with a concentration of (a) 50  $\mu\text{g}/\text{mL}$ , and (b) 50  $\mu\text{g}/\text{mL}$  with 2 mg/mL of BSA. Lowering the concentration of Fn does not appear to affect the relative amounts of Fn found on the PDMS-Al and PDMS, with larger amounts of Fn outside of the dot on PDMS. The inclusion of a competitive protein, BSA, does affect the adsorption of Fn. Fn-OG is seen to adsorb only in the dot regions in the presence of BSA. This indicates that BSA was blocking the adsorption of Fn on the hydrophobic surface. The intensity of the fluorescence in the dot regions appear similar both with and without BSA indicating that BSA did not compete with Fn-OG for adsorption onto the PDMS-Al surface.

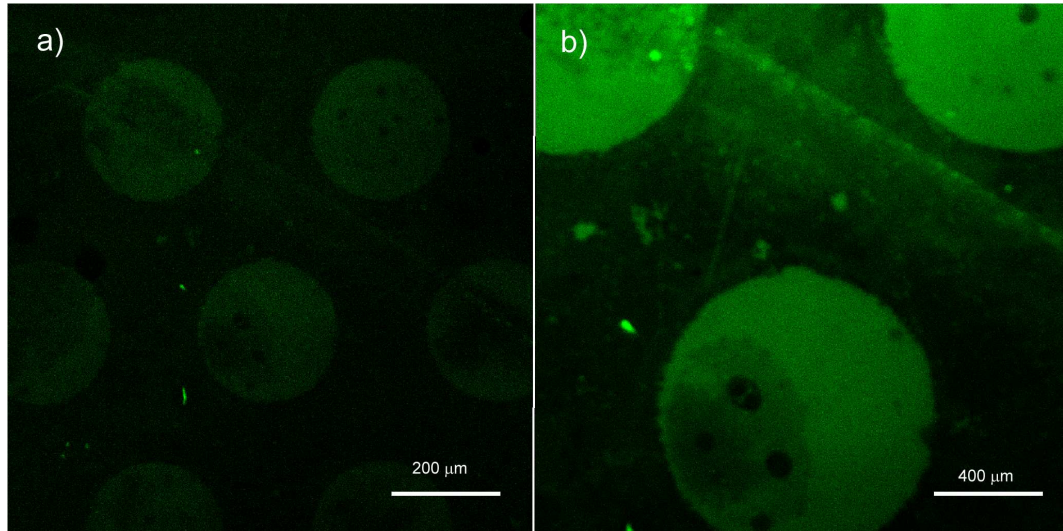


Figure 3.15: Confocal fluorescent images of Fn-OG adsorbed onto stencil ODTMS patterned samples for 30 min at a concentration of 0.1 mg/mL

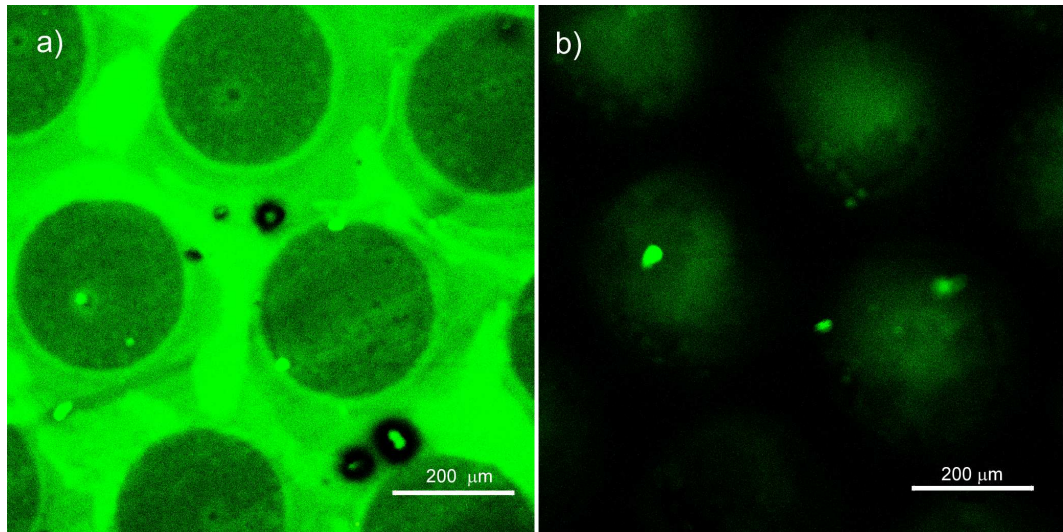


Figure 3.16: Confocal fluorescent images of Fn-OG adsorbed onto stencil masked patterned samples: a) 50 μg/mL Fn-OG, b) 50 μg/mL Fn-OG and 2 mg/mL BSA

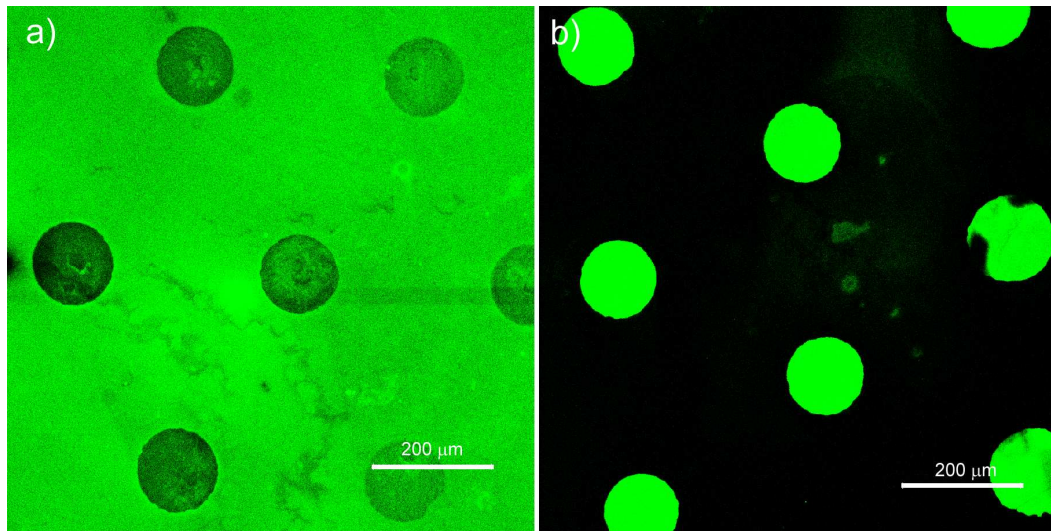


Figure 3.17: Confocal fluorescent images of Fn-OG adsorbed onto patterned hydrophobic recovered PDMS samples: a) 50  $\mu\text{g}/\text{mL}$  Fn-OG, b) 50  $\mu\text{g}/\text{mL}$  Fn-OG and 2  $\text{mg}/\text{mL}$  BSA

Fn was found in the recovered regions when Fn-OG was adsorbed onto a PDMS-R patterned sample at the lower concentration of 50  $\mu\text{g}/\text{mL}$ . This indicated that lowering the concentration had no effect on the relative amount of Fn adsorbed onto PDMS-Al and PDMS-R. The effect of BSA on the adsorption of Fn-OG on PDMS-R patterned surfaces was also explored. Similar to the stencil masked patterned samples, the BSA competed for adsorption on the more hydrophobic regions, effectively reducing the Fn-OG adsorption (Figure 3.17). In this case, the intensity of the fluorescence seen in the hydrophilic dots was greater with BSA than without, thus BSA appears to force Fn onto the PDMS-Al surface.

Figure 3.18 a shows the adsorption of Fn at a lower concentration on a PDMS-ODTMS patterned surface. Lowering the concentration of Fn has caused the adsorption of Fn to be reversed, now resembling the stencil mask patterned samples with more adsorption outside of the patterned dots. Figure 3.18b shows increased absorption of Fn in the hydrophilic dots over the ODTMS treated surroundings when

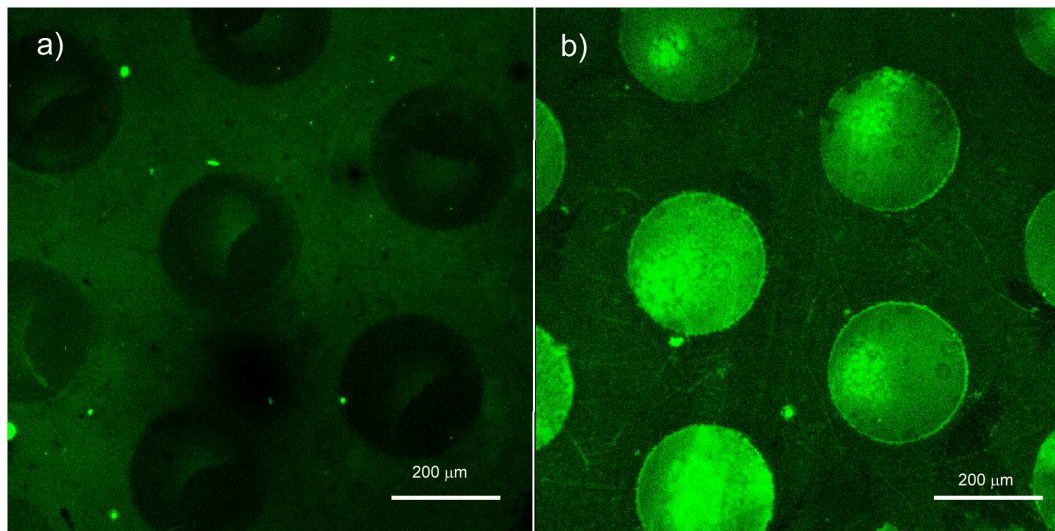


Figure 3.18: Confocal fluorescent images of Fn-OG adsorbed onto ODTMS patterned PDMS: a) 50  $\mu\text{g}/\text{mL}$  Fn-OG, b) 50  $\mu\text{g}/\text{mL}$  Fn-OG and 2  $\text{mg}/\text{mL}$  BSA

BSA is added to the system. Once again, BSA is able to block Fn adsorption on the hydrophobic surface.

Since the concentration of Fn can affect its adsorption, Fn was also adsorbed at 15  $\mu\text{g}/\text{mL}$ ; however, no fluorescence was detected using confocal microscopy. This does not indicate that no Fn was adsorbed, but that the amounts were too low to detect with the use of the conjugated protein.

The adsorption of two adhesion proteins has been explored. Since the PDMS-AI surface was present on all substrates it can be used to determine the relative trends of adsorption.

For Fg at 0.1  $\text{mg}/\text{mL}$ : PDMS-R > PDMS-ODTMS > PDMS-AI > PDMS

For Fn at 0.1  $\text{mg}/\text{mL}$ : PDMS > PDMS-R  $\approx$  PDMS-AI > PDMS-ODTMS

Both proteins showed different trends for their adsorption onto PDMS and modified PDMS. Thus, both proteins interact with the surface in very different ways. Changing the concentration also affects how the protein interacts with the surface. At a lower concentration of 50  $\mu\text{g}/\text{mL}$ , PDMS-AI showed the least adsorption on all



patterned substrates. This trend is closer to what would be expected of Fn, as it has been shown to adsorb more to CH<sub>3</sub> terminated SAMs than to OH terminated SAMs [26]. This is a result of interactions between hydrophobic side chains of the protein with the surface.

BSA has also been observed to affect the adsorption of Fn. Albumin, which is present in cell culture media at higher concentrations than Fn, will compete for positions on the surface, reducing the adsorption of Fn by up to 90% [159]. BSA appears to block Fn adsorption on the hydrophobic surfaces, while not competing for adsorption on the hydrophilic PDMS-Al surface. Thus Fn was found at higher concentrations in the hydrophilic dots for all patterned surfaces.

### 3.3.4 Conformational Studies of Adsorbed Fibronectin on Patterned PDMS

Fn is known to adsorb more to hydrophobic surfaces, but in an undesirable conformation for cell adhesion. The use of ELISA techniques to look at Fn conformation has found that while Fn adsorbs more to hydrophobic surfaces, it does so in a non-functional conformation. In this conformation, the RGD peptide sequence, which can be vital for cell attachment, is no longer accessible. Monoclonal antibodies which bind to different RGD receptors on Fn, particularly the binding sites between the 9th and 10th type II repeats, have been used to determine the availability of these sites for cell adhesion. Hydrophilic surfaces show more accessibility for the monoclonal antibodies to attach [25, 26, 28].

To fully understand the selective cell patterning seen on stencil mask and PDMS-ODTMS patterned surfaces and the lack of patterning on a PDMS-R patterned surface, it was necessary to determine the conformation of Fn on each surface

type. A monoclonal antibody known to attach Fn at the RGD peptide between the 9th and 10th type II repeats, was utilized. In order to visualize the availability of binding sites on the patterned substrates, a goat anti-mouse IgG FITC conjugate was used as a secondary antibody.

Figure 3.19, shows the adsorbed Fn fluorescently labeled for RGD sequence on the patterned surfaces. Bright regions indicate that Fn is in an optimal conformation that exposes the RGD peptide sequence and thus promotes cell adhesion. For the stencil mask surfaces, fluorescence is seen in the hydrophilic dots and not the hydrophobic surroundings (Figure 3.19a). This corresponds nicely to the known cell growth pattern on these surfaces.

As there is no discernable cell patterning on PDMS-R patterned surfaces, one would expect that protein conformation would be uniform across the surface. However, Figure 3.19b shows more fluorescence in the recovered regions of the pattern. The ODTMS surfaces also shows increased fluorescence on the hydrophobic surroundings (Figure 3.19c). To insure that the fluorescence was not caused by non-specific binding, blanks for each sample were imaged. The blanks underwent Fn adsorption and immunofluorescent labeling with the HNF7.1 step removed. Thus the fluorescently labeled secondary antibody could only attach to the surface through nonspecific binding. Figure 3.19d, shows a typical blank image. No fluorescence was detected, thus the fluorescent signal is due to the interactions between the goat anti-mouse IgG and the HNF7.1 monoclonal antibody and not non-specific binding.

The effects of lowering the concentration of Fn and the addition of BSA on the conformation of Fn were also explored. Stencil mask patterned surfaces still show increased fluorescence inside of the modified dots, even after lowering the concentration of Fn (Figure 3.20a) and adding BSA (Figure 3.20b). There was no discernable difference between the PDMS-Al dots and the PDMS-R surroundings, when the con-

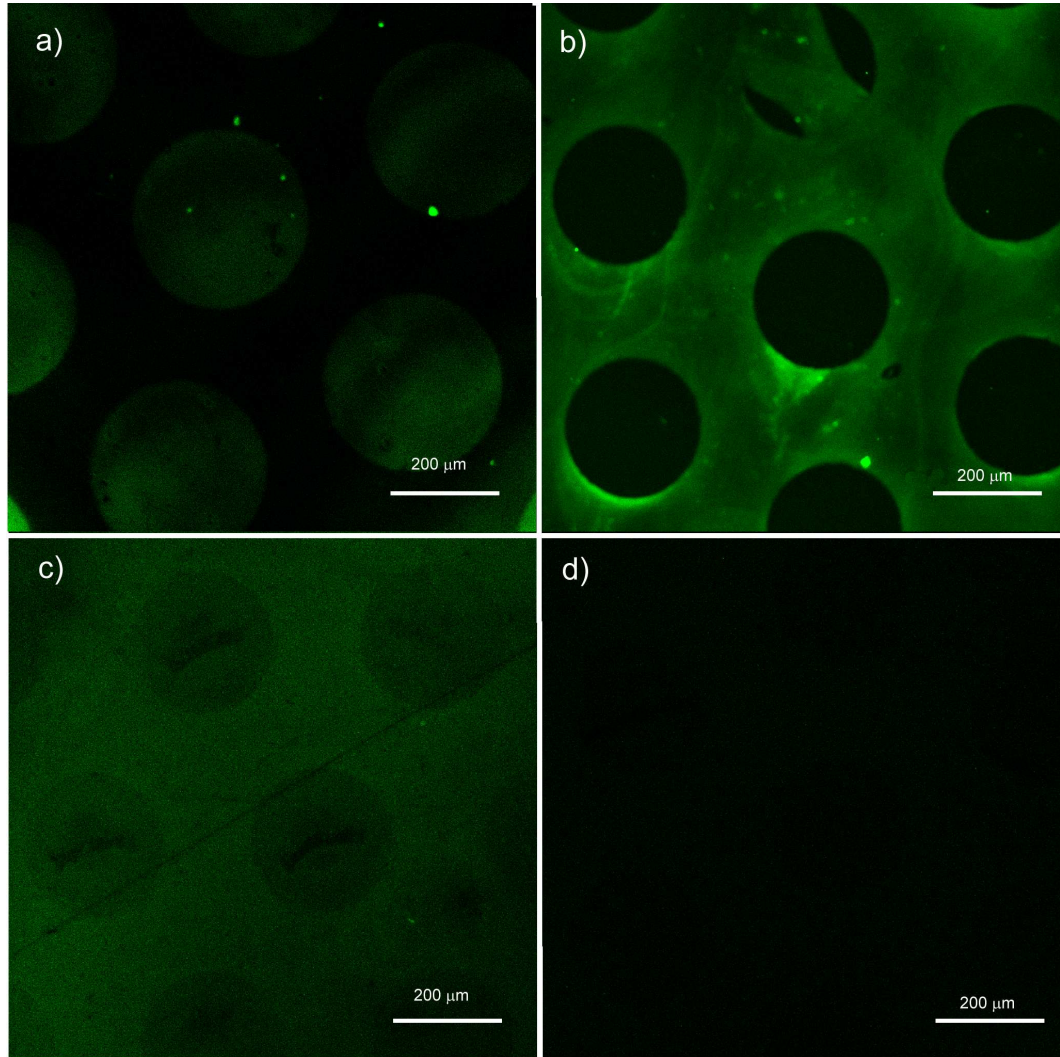


Figure 3.19: Confocal images Fibronectin adsorbed to a) stencil masked, b) photolithographically patterned sample c) ODTMS patterned samples at a concentration of 0.1 mg/mL and labeled for confirmation. d) Confocal image of Fibronectin adsorbed to a ODTMS patterned sample at a concentration of 0.1 mg/mL and labeled for conformation with the removal of HFN7.1 step.

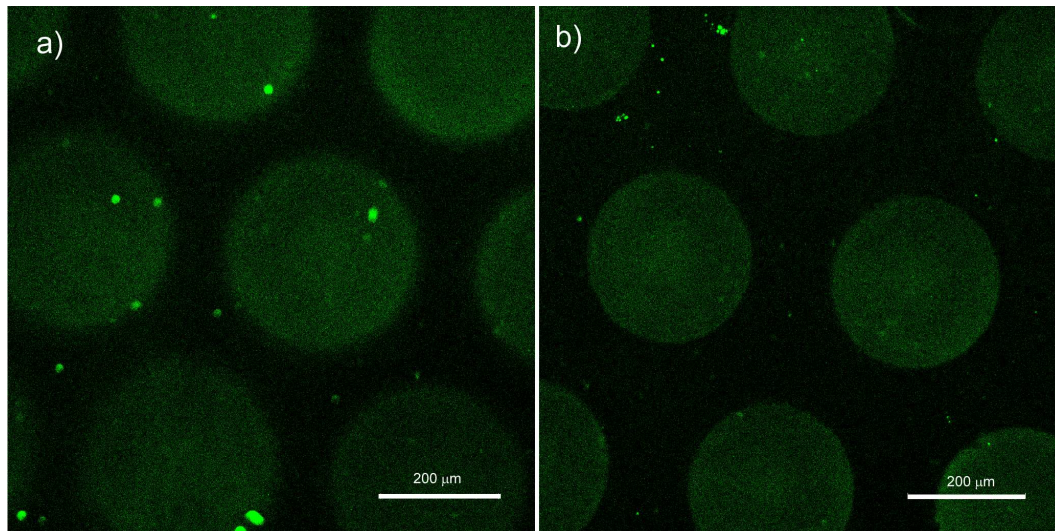


Figure 3.20: Confocal fluorescent images of absorbed onto stencil masked patterned samples and labeled for configuration: a) 50  $\mu\text{g}/\text{mL}$  Fn, b) 50  $\mu\text{g}/\text{mL}$  Fn and 2  $\text{mg}/\text{mL}$  BSA

centration of Fn was lowered to 50  $\mu\text{g}/\text{mL}$ , and when BSA was added on the PDMS-R patterned surfaces (data not shown). The lower concentration of Fn had little effect on the conformation on the PDMS-ODTMS patterned surfaces. Figure 3.21b, shows an increase in fluorescence in the hydrophilic dots over the ODTMS surroundings when BSA was added as a competitive protein.

The conformation of Fn adsorbed on the surface was not only dependent on surface type, but also on the Fn concentration and the presence of a competitive protein, BSA. At higher concentrations (0.1  $\text{mg}/\text{mL}$ ) the relative amount of Fn found in the correct conformation followed the following trend:

$$\text{PDMS-R} > \text{PDMS-ODTMS} > \text{PDMS-AI} > \text{PDMS}.$$

When the concentration was lowered to 50  $\mu\text{g}/\text{mL}$ , the trend changed, such that, PDMS-R and PDMS-AI were equal:

$$\text{PDMS-ODTMS} > \text{PDMS-R} = \text{PDMS-AI} > \text{PDMS}.$$

The ability of Fn to bind the primary HFN7.1 antibody has previously been

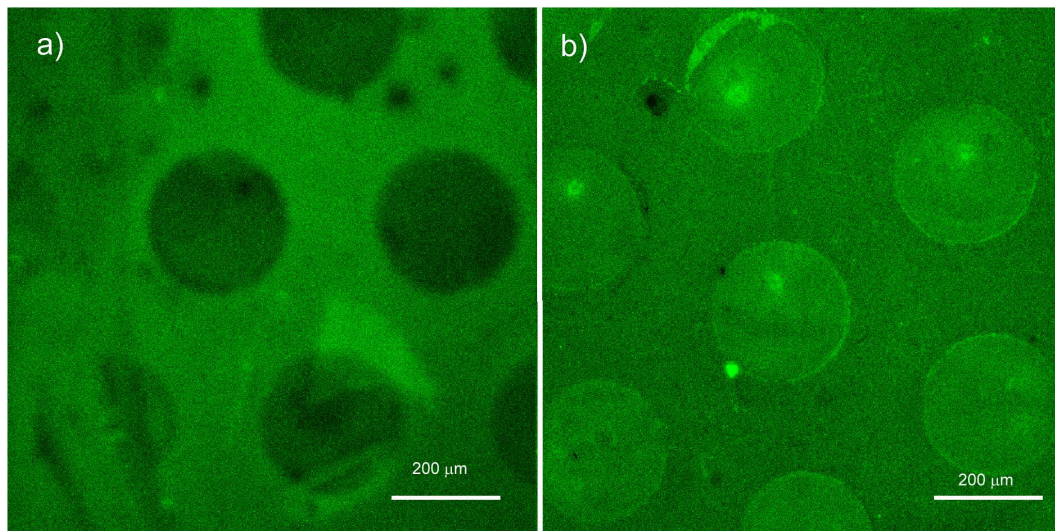


Figure 3.21: Confocal fluorescent images of Fn adsorbed onto stencil masked patterned samples and labeled for configuration: a) 50  $\mu\text{g}/\text{mL}$  Fn-OG, b) 50  $\mu\text{g}/\text{mL}$  Fn-OG and 2  $\text{mg}/\text{mL}$  BSA

shown to be greater on OH terminated SAMs than  $\text{CH}_3$  terminated SAMs [26]. Thus PDMS-Al would be expected to show more fluorescence than PDMS and PDMS-ODTMS. As the PDMS-ODTMS patterned surface does not follow this trend, other surface properties may therefore be affecting protein adsorption.

Finally in the presence of BSA, the trend resembles that seen for cell adhesion:  
PDMS-Al = PDMS-R > ODTMS > PDMS

The BSA/Fn system is the closest environment to that used for cell culturing. These results show the importance of not only adhesion proteins, but also the entire environment, on cell surface interactions.

ECM protein adsorption and conformation were visualized on patterned surfaces. Determining protein adsorption and conformation on the surface gives insight into the interactions between the surface and cells. The effects of protein concentration and the addition of a competitive protein on the relative adsorption and conformation of Fn were explored. BSA plays an important role in determining the

Table 3.3: Summary of cell patterning, protein adsorption, and protein concentration on patterned PDMS. (+) indicates an increase inside of the dots, (-) indicates an increase outside of the dots, and (=) indicates uniformity across the surface.

Surroundings	Proteins	Protein Concentration	Cell Adhesion	Protein Adsorption	Protein Conformation
PDMS	Fg	0.1 mg/mL	+	+	N/A
PDMS-R	Fg	0.1 mg/mL	=	-	N/A
PDMS-ODTMS	Fg	0.1 mg/mL	+	-	N/A
PDMS	Fn	0.1 mg/mL	+	+	+
PDMS-R	Fn	0.1 mg/mL	=	=	-
PDMS-ODTMS	Fn	0.1 mg/mL	+	+	=
PDMS	Fn	0.05 mg/mL	+	-	+
PDMS-R	Fn	0.05 mg/mL	=	-	=
PDMS-ODTMS	Fn	0.05 mg/mL	+	-	-
PDMS	Fn:BSA	0.05 :2 mg/mL	+	+	+
PDMS-R	Fn:BSA	0.05 :2 mg/mL	=	+	=
PDMS-ODTMS	Fn:BSA	0.05 :2 mg/mL	+	+	+

adsorption and conformation of Fn, and thus the ability of cells to attach to the surface. Table 3.3 provides a summary of cell adhesion, protein adsorption and protein conformation on the patterned PDMS surfaces.

### 3.4 Conclusions

The effects of modifying the surface of PDMS on cell attachment and protein adsorption was examined in this chapter. The cell studies showed good agreement between cell adhesion and the observed patterning from Chapter 2. The adsorption of adhesion proteins Fg and Fn, was visualized on the surface through confocal microscopy by conjugating the protein with fluorescent molecules. Adsorption did not directly correlate to cell attachment and was observed to be surface, protein and concentration dependent. The conformation of Fn was also visualized on the surface through the

---

use of a monoclonal antibody specific for the RGD peptide on Fn. A fluorescently labeled secondary antibody was used to create the fluorescent image. The conformation pattern correlated to cell attachment when Fn was adsorbed in the presence of BSA, which is an excellent model system for a cell culturing environment.

# Chapter 4

## Atomic Force Studies of PDMS and Surface Modified PDMS

### 4.1 Introduction

The wettability and chemistry of a surface plays a large role in determining whether cells are capable of adhesion [15, 18, 141]. The hydrophobicity and  $\text{CH}_3$  terminated chemistry of PDMS prevents the attachment and growth of cells. In order to increase bioactivity of the polymer, PDMS has been modified by a magnetron sputter deposition of aluminum. After the aluminum layer was etched away, the surface showed an increase in oxygen by XPS similar to PDMS that has been plasma treated. Modifying the surface also significantly decreased the contact angle.

In order to pattern cell attachment by photolithography, the surface chemistry and wettability must become closer to native PDMS. Both hydrophobic recovery of the modified polymer and a silane reaction with ODTMS have been used. The hydrophobic recovered surface did not fully recover and was still considered hydrophilic, it also showed similar cell attachment to the non-recovered modified surface. The treatment with ODTMS did increase the carbon content of the surface as seen by XPS and the contact angle was close to that of PDMS. The increased contact angle and carbon content did appear to reduce the number of cells adhered to the surface, in comparison to the magnetron modified polymer. The number of cells that adhered



to the surface was still significantly greater than that of native PDMS, despite the similar wettability and chemistry.

Aside from wettability and surface chemistry, other properties such as roughness and stiffness (i.e. elastic modulus), of the surface have been shown to affect cell adhesion [15, 18, 141]. Surface roughness is a measure of the surface texture found by vertical surface deviations [160]. The so called  $R_a$  is the most common value used to describe the surface roughness and is calculated as in (4.1), where  $z$  is the deviation from the average surface height and  $n$  is the number of measurements. Rougher surfaces tend to have increased cellular adhesion and proliferation compared to smooth surfaces [40–43]. The preferred roughness is cell dependent; however roughnesses in the order of a few micrometers is often required to observe an increase in cell attachment.

$$R_a = \frac{1}{n} \sum_{i=1}^n |z_i| \quad (4.1)$$

A material's stiffness is the resistance of the material to deformation, and is described in (4.2). The Young's modulus of a material, also known as the tensile modulus, is a measure of tensile stress over tensile strain. The Young's modulus can be determined by recording the change in an object's length due to an applied force and using (4.3) where  $E$  is the Young's modulus,  $F$  is the applied force,  $A_o$  is the cross sectional area,  $L_o$  is the original length and  $\Delta L$  is the change in length of the material. For many cell types, stiffer material tends to show an increase in cell adhesion over similar materials with lower moduli [51–55]. Materials with moduli lower than 16 to 30 kPa often are unable to support cell adhesion [53–55]. These effects are a generalizations and can vary with different cell types.

$$k = \frac{F}{\delta} \quad (4.2)$$

$$E = \frac{\text{stress}}{\text{strain}} = \frac{FL_o}{Ao\Delta L} \quad (4.3)$$

Since both surface roughness and stiffness may change how cells interact with a surface, it is important to understand what the effect modifying PDMS has on both of these surface properties. PDMS that has been plasma treated has shown both increased surface roughness and stiffness [116,138–140]. As the magnetron deposition of aluminum involves exposing PDMS to an argon plasma, the surface roughness and stiffness should be affected by the plasma. In this chapter, AFM has been used to assess the surface topography and roughness of PDMS and modified PDMS, force curves were collected and used to determine the Young's modulus of PDMS and magnetron treated PDMS, and the interactions between cells and modified PDMS were further analyzed using AFM.

## 4.2 Materials and Methods

### 4.2.1 Reagents

PDMS Sylgard 184A and B were purchased from Dow Corning. The materials used for photolithography, Microposit SC1827 positive photoresist and Microposit MF-319 developer, were purchased from Rohm & Haas Electronic Materials. C2C12 and COS-7 cell line were purchased from ATCC. DMEM, L-glutamine, penicillin streptomycin, FBS, Trypsin/EDTA, and PBS, were all purchased from Invitrogen. All other chemicals were purchased from Sigma-Aldrich and used as received.

## 4.2.2 Preparation of PDMS and Modified PDMS surfaces

Micrometer thick PDMS surfaces were used and prepared through spincoating onto a glass coverslip as described in 2.2.2.2. Modified PDMS-Al surfaces were prepared through the deposition of aluminum in a magnetron sputtering system, followed by etching in orthophosphoric acid as described in 2.2.2.3. PDMS-Al was modified with ODTMS to create PDMS-ODTMS surfaces as described in 2.2.2.5.

## 4.2.3 Preparation of Patterned PDMS Surfaces

Stencil masked patterned samples were created by aluminum deposition through a commercially available steel mesh as described in 2.2.3.1. Aluminum was also patterned on PDMS using photolithography as described in 2.2.3.2.

## 4.2.4 Cell Culture and Patterning

COS-7 fibroblast cells and C2C12 myoblast cells, were cultured on the PDMS substrates. DMEM supplemented with 2 mM L-glutamine, 1% penicillin-streptomycin (Invitrogen) and 10 % FBS was used for all experiments. Cell cultures were incubated at 37 °C , 5 % CO<sub>2</sub> and 100 % humidity.

Samples of patterned PDMS were etched with orthophosphoric acid for 30 min and rinsed 3 times in water prior to sterilization by rinsing with 70% ethanol. Prior to plating, cultured cells were washed with trypsin/EDTA to promote cell detachment from the culture flasks. The cells were mixed into media for transfer. 0.5 mL of the solution was plated onto modified PDMS samples, inside a 3 cm petri dish. An additional 2 mL of fresh media was added to each dish, the cells were then incubated for 24-36 hrs.

Prior to imaging, cells were rinsed 3 times with PBS at pH 7.4 and fixed using a solution of 4.4 % paraformaldehyde in PBS for 10 min. Cells were then rinsed 3 times in PBS and water.

#### 4.2.4.1 Optical Imaging

All optical images were captured using a Zeiss Axioskop2 Mat Microscope with a QImaging Retiga 1300 CCD digital camera or using a Zeiss Axiovert 200M inverted microscope with a Zeiss AxioCam HRM CCD digital Camera.

#### 4.2.5 Atomic Force Microscopy

AFM is a scanning probe technique that characterizes a surface based on the interaction between a tip and the surface. The tip is mounted on a cantilever, and the cantilever's deflection is detected through the use of laser and photodiode detector. Figure 4.1 shows a common AFM setup, the sample is scanned in the  $x,y$  and  $z$  direction through a piezoelectric translator, while the tip position is held constant. Newer instruments designed for biological applications, such as the Bioscope II (Veeco Instruments Inc) are mounted onto an inverted microscope and are unable to move the sample. Instead, the tip holder is attached to the piezo and is moved while the sample position is fixed. The surface characteristics can be measured in several different modes, contact and intermittent tapping being the most typical.

In contact mode, the tip is in contact with the surface. As the tip move across the surface, the cantilever deflects and the  $z$  piezo moves the sample up or down to maintain a constant deflection set point. The change in  $z$  position is recorded and mapped against the  $xy$  position, creating a topographical image of the surface.

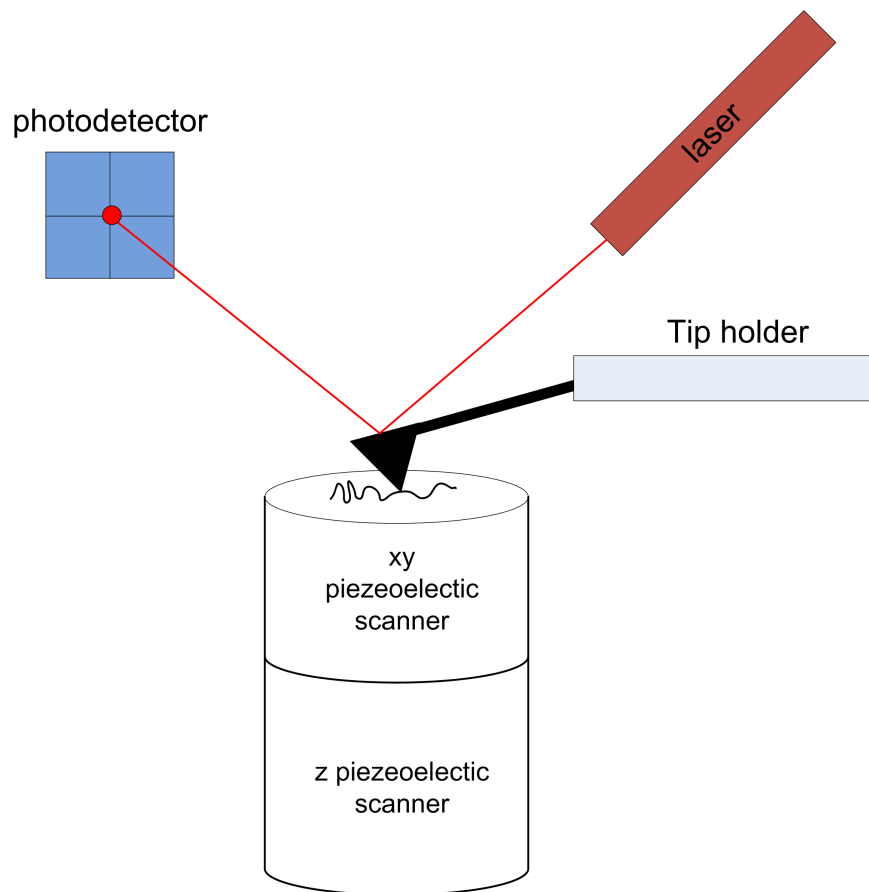


Figure 4.1: Typical setup for an atomic force microscope

In tapping mode, the tip is oscillated at its resonance frequency, typically at least 100 kHz. As the tip makes contact with the surface the oscillation amplitude is reduced. By adjusting the distance between the tip and the sample, a constant amplitude can be maintained. Once again the change in height can be recorded and produces a topographical image. Since the tip taps the surface of the sample rather than drags across it, tapping mode is less destructive than contact mode.

AFM images were collected on a Bioscope II (Veeco Instruments Inc). The AFM was operated at a constant deflection set point 1-2.0 V in contact mode using a NP-S20 gold coated silicon nitride V shaped cantilever. The cantilever was 200  $\mu\text{m}$  in length with a spring constant of 0.06 N/m (Veeco Instruments Inc). Scan rates between 0.1 to 0.5 Hz were used for samples in water. Parameters including feature height and surface roughness were evaluated using Nanoscope Analysis 1.2 software (Veeco Instruments Inc) after first-order flattening of the raw data.

#### 4.2.6 Force Distance Curves

An AFM instrument can also be used to monitor forces during indentation of a surface. The change in deflection of the cantilever versus the change in height can be recorded as the a tip approaches and indents into a surface. If the spring constant of the cantilever is known, the deflection of the cantilever can be used to determine the amount of force being applied by the tip.

The information collected by the AFM is the voltage applied to the piezo and voltage change due to the movement of the laser on the photodiode [161, 162]. The AFM software can convert the voltage applied to the piezo into a change in the height of the cantilever. In order to determine the force applied to the surface the spring constant of the cantilever must be known. The force applied to a surface is determined

by Hooke's Laws (4.4), where  $F$  is the force,  $k$  is the spring constant of the cantilever and  $h$  is the vertical displacement of the free end of the cantilever.

$$F = -k \times h \quad (4.4)$$

Many methods can be used to determine the spring constant of a cantilever, however the thermal tune method is one of the simplest and is automated on most commercial AFMs [162]. This method involves measuring the deflection signal of the cantilever with no driving oscillations, while the cantilever is in thermal equilibrium and suspended away from the surface [161, 162]. A Fourier transformation is applied to the resulting function and the power spectral density (PSD) is determined in the frequency domain. By finding the area under the PSD, the power  $P$ , of the thermal cantilever fluctuations can be determined. Using (4.5), where  $k_B$  is Boltzmann's constant, and  $T$  is the temperature, the spring constant can be determined. It is important to independently determine the spring constant for each cantilever as even the same type of cantilever from the same manufacturer will have slightly different spring constants.

$$k = \frac{k_B T}{P} \quad (4.5)$$

Once the spring constant is known, the deflection sensitivity of the cantilever must be determined. The deflection sensitivity must be redetermined every time the laser beam path is changed. This is done by collecting a force curve against a hard surface and calibrating the instrument.

Figure 4.2 shows a typical force curve. As a tip approaches a sample there should be no force or deflection of the cantilever until contact; however soft cantilevers may show some detectable attractive forces (A). When the tip is close enough to the

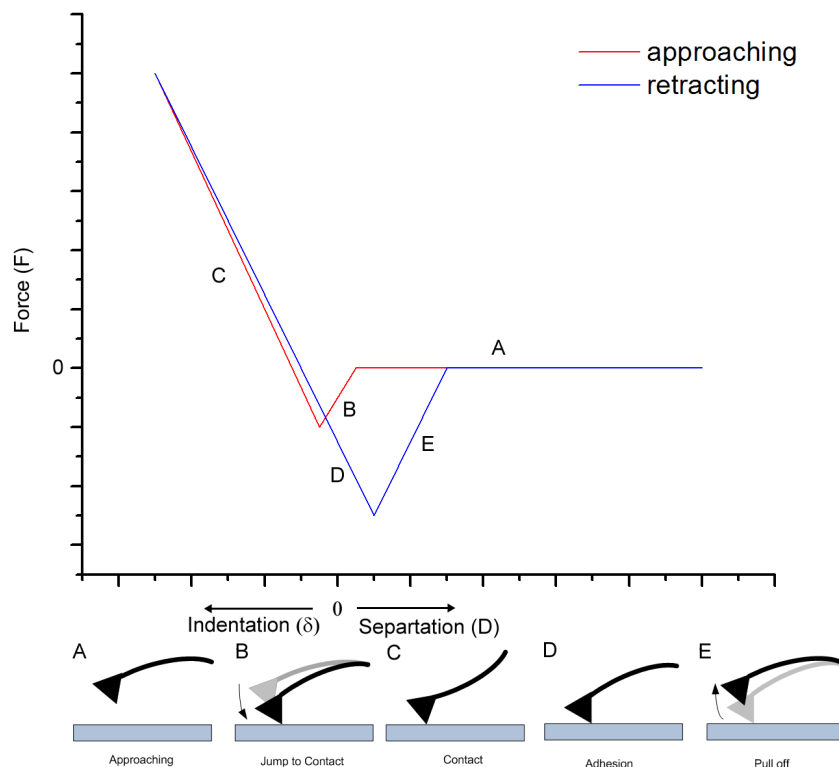


Figure 4.2: Typical force curves and corresponding tip-sample interactions

surface, attractive forces between the tip and the surface will dominate the curve (B). As the tip continues to push into the surface, an increase in force is seen (C). While the tip is being retracted, the curve would be expected to follow the approach curve; this only occurs on perfectly elastic materials. More often a hysteresis is seen between the two curves due to deformation of the material. Due to attractive forces between the tip and the surface, the tip will maintain contact (D). Upon further retraction the tip returns to the no contact position (E). Features in the force-distance curve can be used to determine the Young's modulus of the material.

Force-distance curves were collected on a Bioscope II with a NP-S20 gold coated silicon nitride V shaped cantilever. To convert the cantilever deflection to a force measurement a force curve was taken against a hard glass surface and the spring



constant was determined to be 0.1119 N/m, by measuring the intensity of thermal noise. The force distance curves were analyzed using the Nanoscope Analysis 1.2 software (Veeco Instruments Inc).

### **4.2.7 Interactions Between a Tip-less Cantilever and Modified PDMS**

A tip-less cantilever (NSC12, MIKROMASCH) with a spring constant of 14 N/m was brought into the contact with the surface of PDMS and modified PDMS using a Bioscope II microscope. Images of the surface were taken using the Zeiss Axiovert 200M inverted microscope with a Zeiss AxioCam HRM CCD digital Camera which the Bioscope II was mounted on top of. The cantilever was moved up, down, to the right and left, as well as forward and backward, to observe the effects on the surface. To determine if the cantilever had come into contact with the surface the deflection of the cantilever was monitored. Glass beads of 5  $\mu\text{m}$  to 50  $\mu\text{m}$  were suspended in water and transferred to the polymer surfaces. Once the water evaporated, the glass beads were present on the surface. A tip-less cantilever was aligned over the glass bead and pressed into the surface to observe the effect of an applied force created using a controlled geometry.

## **4.3 Results and Discussion**

### **4.3.1 Topographical Analysis of PDMS and Modified PDMS**

Cell attachment to a surface is not only affected by the surface wettability and chemistry but also the surface roughness and stiffness. Plasma modification and metal

deposition on PDMS have been shown to affect the polymer's surface topography. AFM was used to assess the surface topography of PDMS, PDMS after aluminum deposition through magnetron sputtering, and after aluminum etching. Figure 4.3 shows randomly oriented sinusoidal shaped ripples across the metal coated surface. These ripples had a wavelength of  $2.7 \pm 0.4 \mu\text{m}$  and an amplitude of  $146 \pm 8 \text{ nm}$ . The surface roughness ( $R_a$ ) of the aluminum coated polymer was  $40 \pm 4 \text{ nm}$ , significantly larger than that seen for native PDMS ( $4.9 \pm 0.4 \text{ nm}$ ).

These randomly oriented sinusoidal ripples resemble those observed during thermal deposition of metals onto PDMS [163], and during plasma treatment of PDMS [139, 140], and are commonly referred to as Whiteside patterns. During thermal metal deposition, PDMS heats up and expands [163]. The coefficient of thermal expansion of PDMS is approximately twenty times that of the metal. These differences cause the metal layer to buckle in order to redistribute the compressive stresses during cooling. During plasma treatment the formation of a silica-like layer can also cause the creation of sinusoidal ripples [139, 140]. The silica-like layer is expected to have a lower coefficient of thermal expansion than the bulk polymer [139]. During plasma treatment the polymer is expected to increase in temperature, thus upon cooling the silica-like layer buckles [140].

During magnetron deposition, the bulk argon gas temperature remains between 40 and 70°C, and thus causes some expansion of the bulk polymer. During the first stage the shutter is closed preventing aluminum deposition but allowing interactions between the polymer and the plasma, creating a silica-like layer. After the shutter is opened a thin aluminum layer is deposited onto the surface. Once removed from the plasma the polymer will cool; the combination of the silica and aluminum layers are expected to undergo compressive stress which causes buckling of the aluminum and silica layers.

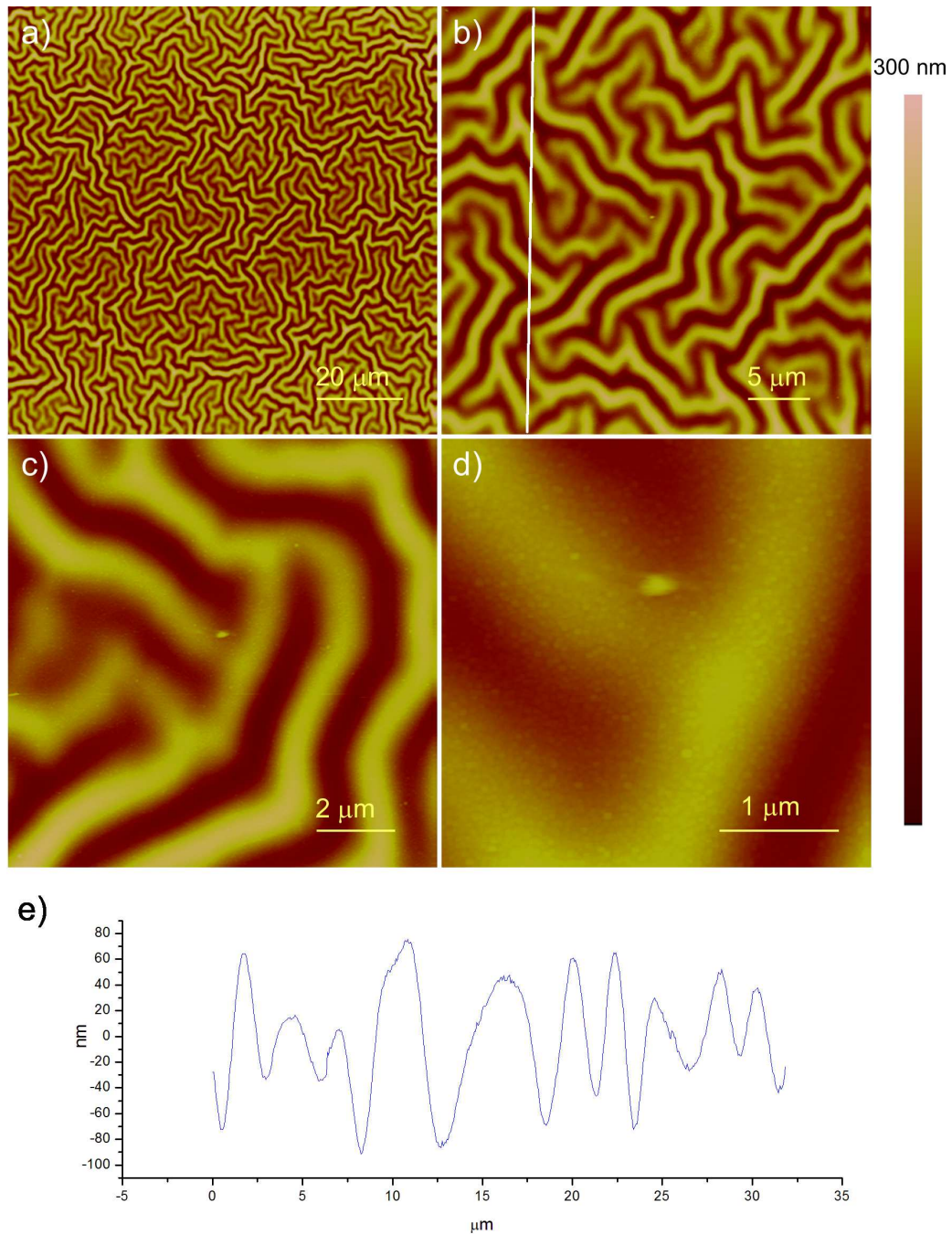


Figure 4.3: AFM contact mode height images of a-d) aluminum coated PDMS, and e) a sectional analysis corresponding to the white line in (b)

If the polymer was unmodified during plasma exposure, it would be expected to relax and return to a flat surface after aluminum etching, as the stress from the metal layer would be removed. If a silica-like layer caused by the plasma modification during deposition did in fact form, it would remain after etching, thus the ripples should still be present. The ripples on the modified PDMS did in fact remain after etching; this gives additional proof that a thin stiff silica-like layer has been formed. The ripples maintained a similar wavelength ( $\lambda = 2.3 \pm 0.2 \mu\text{m}$ ) but showed a reduction in amplitude ( $A = 69 \pm 9 \text{ nm}$ ) in comparison to the aluminum coated surface (Figure 4.4). While the surface roughness has been reduced to  $21 \pm 3 \text{ nm}$ , it is still greater than that of native PDMS. The removal of the aluminum layer may relieve some of the compressive stresses which cause buckling leading to the observed reduction in amplitude.

After further modification with ODTMS, the waves are still present with a wavelength of  $2.6 \pm 0.6 \mu\text{m}$ , and a reduction in amplitude to  $35 \pm 3 \text{ nm}$ , when compared to the aluminum coated polymer both before and after aluminum etching (Figure 4.5). The ODTMS treatment involved heating the polymer to  $100^\circ\text{C}$ . The ripples have been shown to disappear during heating, but reform with the same wavelength and amplitude [163]. During the initial cooling phase after metal deposition, both the aluminum and silica-like layer plays a role in the formation of the ripples. During the ODTMS modification, the aluminum layer has been removed and thus only the silica layer would be responsible for the reformation of the ripples, which may explain the significant decrease in amplitude.

Stencil masked patterned PDMS was also imaged. Figure 4.6, shows aluminum dots on PDMS. The aluminum coated dots show the sinusoidal ripples. These ripples end as soon as they reach the edge of the aluminum dots. The ripples have the same wavelength seen on completely coated PDMS but a slightly reduced amplitude ( $\lambda =$

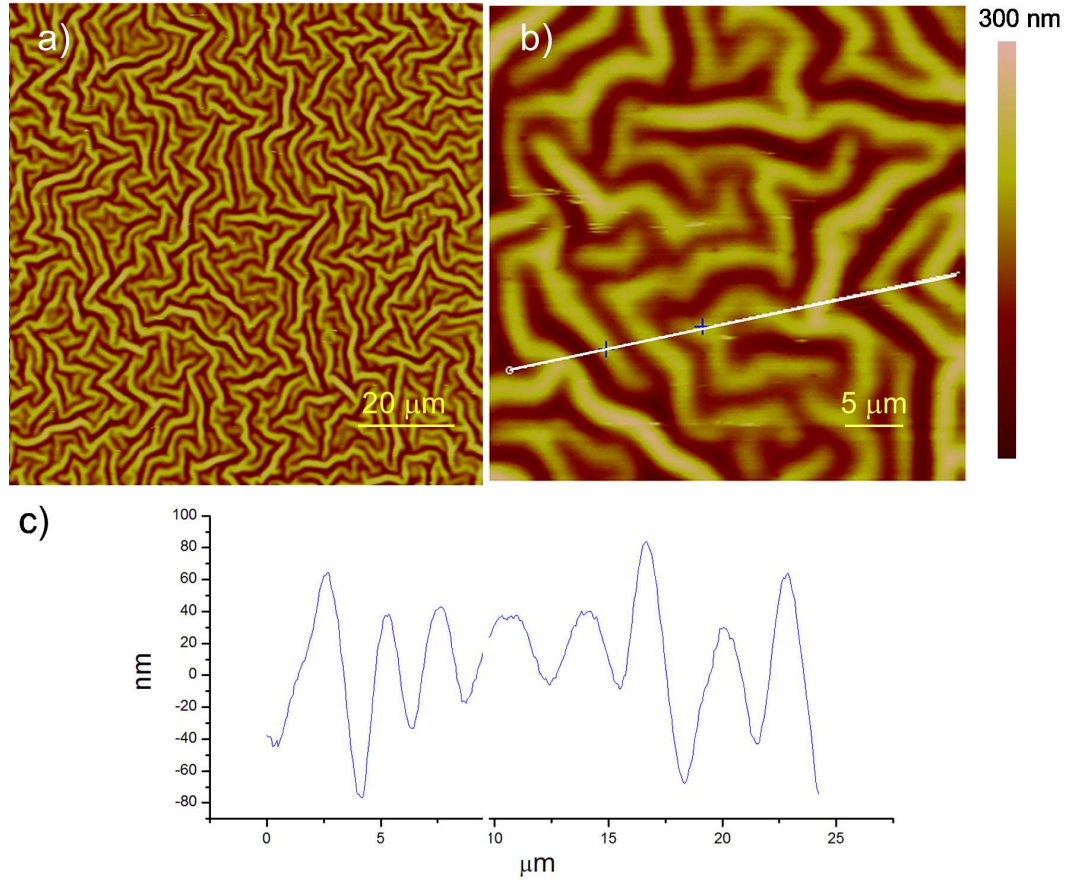


Figure 4.4: AFM contact mode height images of a, b) aluminum treated PDMS surface after aluminum etching and c) a sectional analysis corresponding to the white line in (b)

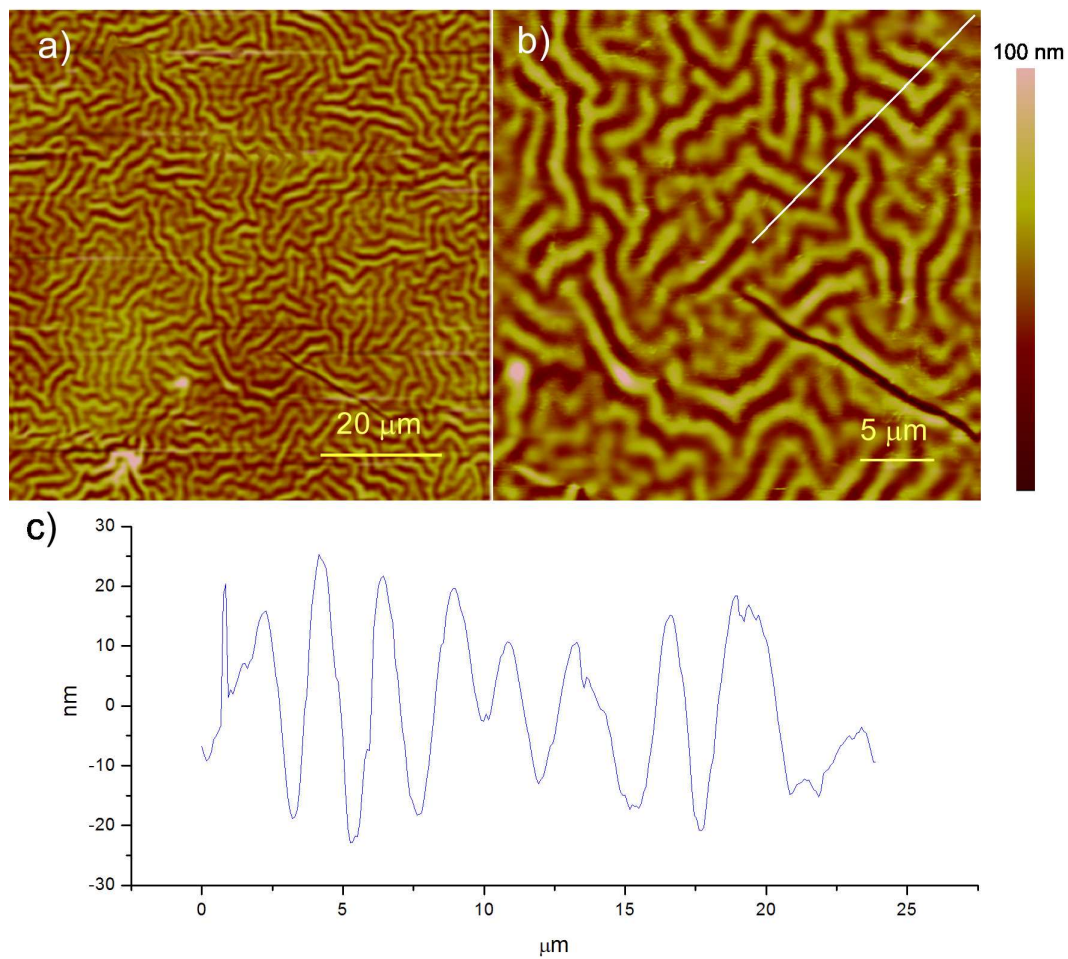


Figure 4.5: AFM contact mode height images of a,b) ODMTS functionalized PDMS-Al and c) a sectional analysis corresponding to the white line in (b)

Table 4.1: Surface topography of PDMS and modified PDMS

Surface	$R_a$ (nm)	$A$ (nm)	$\lambda$ ( $\mu\text{m}$ )
PDMS	$4.9 \pm 0.4$	N/A	N/A
Al on PDMS	$40 \pm 4$	$146 \pm 8$	$2.7 \pm 0.4$
Etched PDMS	$21 \pm 3$	$69 \pm 9$	$2.3 \pm 0.2$
Al dots on PDMS	$20 \pm 1$	$123 \pm 7$	$2.7 \pm 0.4$
Etched dots on PDMS	$13 \pm 1$	$56 \pm 8$	$2.3 \pm 0.4$
ODTMS modified PDMS	$8.6 \pm 0.9$	$35 \pm 3$	$2.6 \pm 0.6$

$2.7 \pm 0.4 \mu\text{m}$ ,  $A = 123 \pm 7 \text{ nm}$ ). After etching, the waves were still located only in the modified dots. Once again a reduction in amplitude occurred ( $A = 56 \pm 8 \text{ nm}$ ) while the wavelength was maintained ( $\lambda = 2.4 \pm 0.4 \mu\text{m}$ ). In both cases, the dots were rougher than the surrounding PDMS with  $R_a$  values of  $20 \pm 1$  and  $13 \pm 1 \text{ nm}$ , for aluminum coated and etched dots respectively. During stencil mask patterning, the aluminum layer was confined to a small region. Upon cooling, the aluminum coated areas are under compressive stresses which causes buckling. Previously, the size and shape of the polymer has been shown to affect the orientation and size of the ripples formed during thermal metal deposition and plasma modification [139, 140, 163]. Similar effects maybe responsible for the decrease in amplitude during stencil mask patterning.

The effects of aluminum treatment, etching and ODTMS treatment are summarized in Table 4.1. All modified surfaces showed an increase in roughness over native PDMS. It is possible that the increase in roughness is responsible for the increase in cell attachment; however, the roughness of all the modified surfaces is on the order of tens of nanometers. Roughened surfaces that have been shown to increase cell attachment are generally on the order of several micrometers. Thus, the increase in roughness would not be expected to significantly affect cell attachment.

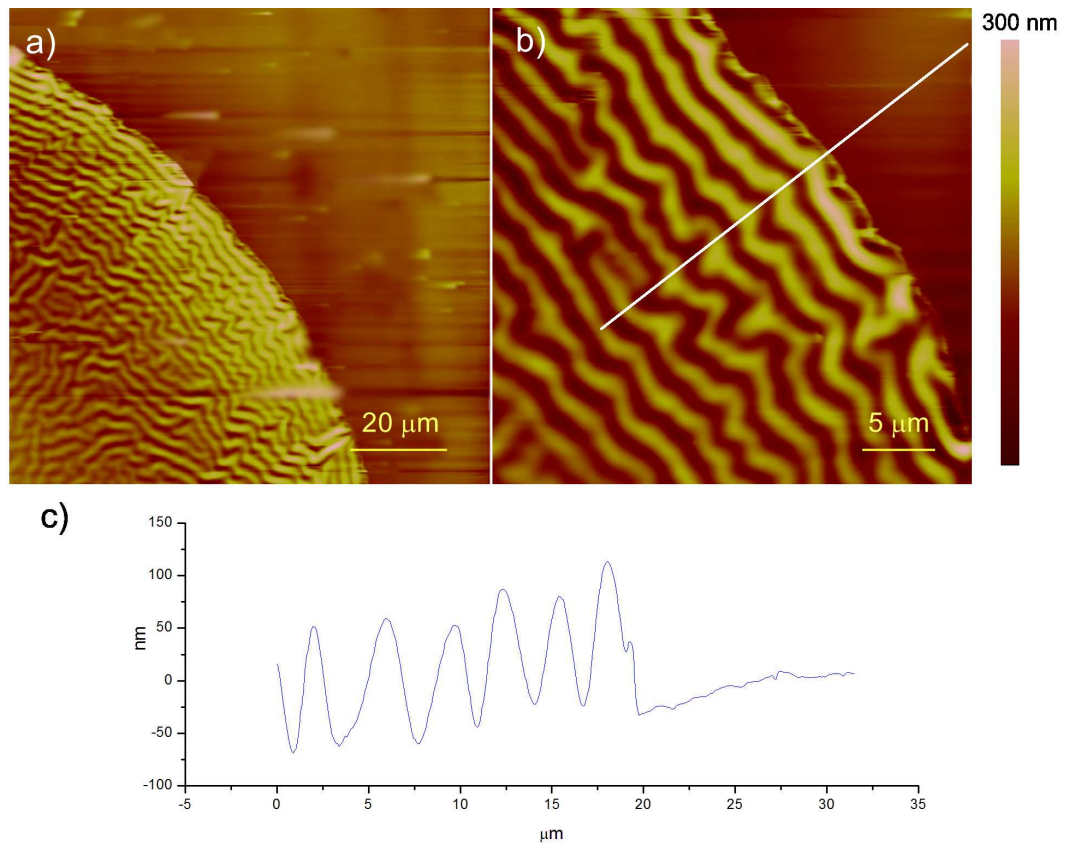


Figure 4.6: AFM contact mode height images of a,b) aluminum deposited through a stencil mask on PDMS, c) a sectional analysis corresponding to the white line in (b)



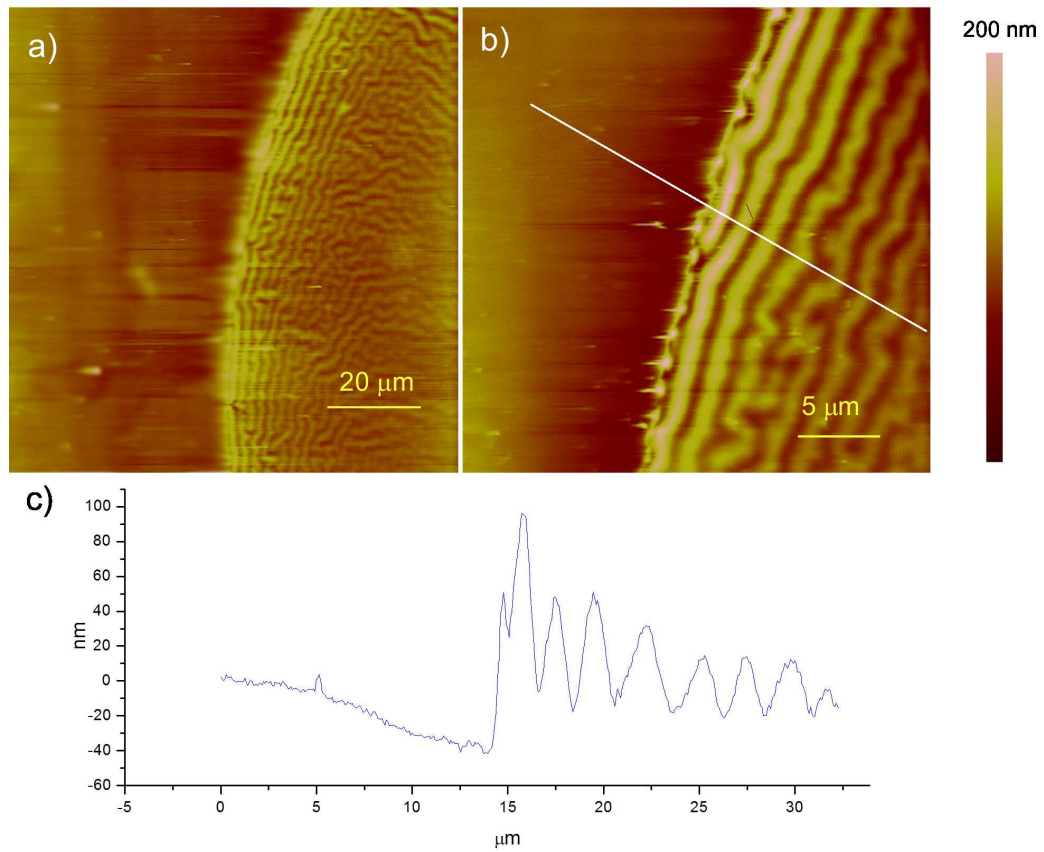


Figure 4.7: AFM contact mode height images of a,b) stencil masked patterned PDMS after etching, c) a sectional analysis corresponding to the white line in (b)

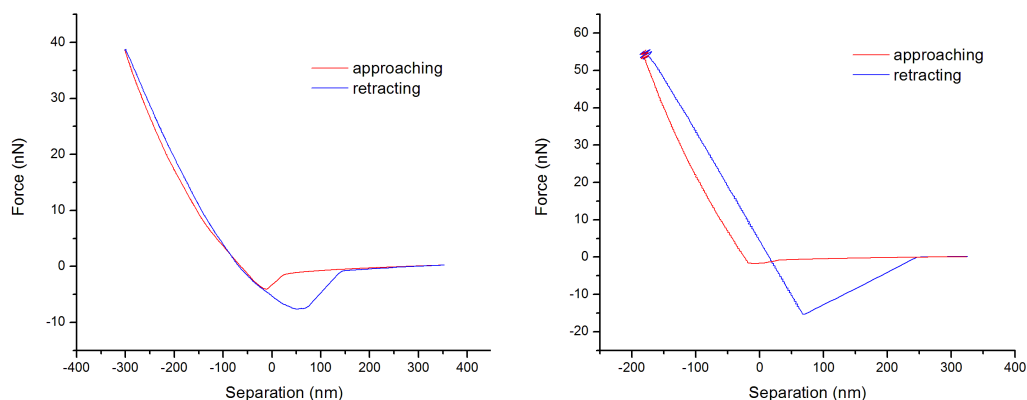


Figure 4.8: Force curves for a) PDMS and b) PDMS-Al

### 4.3.2 Surface Stiffness of PDMS and Magnetron Modified PDMS

From the contact regime of a force-displacement curve it is possible to draw information about the elastic-plastic behavior of the material. On an ideal elastic material, the tip deforms the sample by a depth of  $\delta$ , and the loading and unloading curves overlap. Many materials undergo plastic deformation and do not regain their shape during the unloading curve. Thus, the loading and unloading curves do not overlap and a hysteresis occurs. Figure 4.8 shows both the loading and unloading curves for PDMS (a) and PDMS-Al (b). Since PDMS is elastic, the hysteresis is quite small. PDMS-Al shows a larger hysteresis which implies there is more deformation. Thus PDMS-Al does not maintain the same elastic behaviour as PDMS.

Force distance curves can give both qualitative and quantitative data about a material's stiffness. The stiffer a material, the steeper the force distance curve will appear. To obtain quantitative data about the surface, contact mechanics models can be used to fit the curve. The Hertz model describes a system where two spheres of different radii come into contact. Indentation measurements normally occurs between a spherical tip and a flat plane, thus the plane is treated as a sphere with an infinite

radius. The Hertz model describes the relationship between the indentation distance and the force as (4.6), where  $a$  is the contact radius,  $\delta$  is the sample deformation,  $R$  is the tip radius,  $F$  is the force exerted by the tip on the surface, and  $E_{tot}$  is the reduced Young's modulus. The reduced Young's modulus is described as (4.7), where  $E_s$  and  $E_t$  are the Young's moduli of the surface and the tip, and  $\nu_s$  and  $\nu_t$  are the Poisson's ratio of the surface and the tip respectively.

$$\delta = \frac{a^2}{R} = \left( \frac{F^2}{RE_{tot}^2} \right)^{1/3} \quad (4.6)$$

$$\frac{1}{E_{tot}} = \frac{3}{4} \left( \frac{1 - \nu_s^2}{E_s} + \frac{1 - \nu_t^2}{E_t} \right) \quad (4.7)$$

Since the Young's modulus of the tip will be significantly larger than that of the surface and the Poisson's ratio is always less than 0.5,  $E_{tot} = E_s$ . The force curves for both PDMS and PDMS-Al were fitted using the Hertz model by the nanoscope analysis software. From the fit, the Young's moduli were calculated to be 2.2 MPa and 6.8 MPa for PDMS and PDMS-Al, respectively. Typical values for the Young's modulus of PDMS are between 360 kPa and 4 MPa [164–166], and the Young's modulus of plasma treated PDMS has been found to be 8 MPa [116]. The Young's modulus of PDMS may change, depending on the degree of crosslinking and base-cure ratio. Using nanoindentation and a 10:1 base-cure ratio, the Young's modulus for PDMS has been found to be 2.39 MPa when fitted using the Hertz model [165]. The Young's modulus has also been reported to be up to 4 MPa for PDMS formed using a 10:1 base cure ratio and extended bake time [166]. Thus the conditions used to crosslink PDMS can have an effect on the polymer's Young's modulus. Both polymer samples were from the same PDMS mixture and baked at the same time to eliminate experimental errors. Thus the difference in the Young's modulus can only

be attributed to the surface treatment.

The Young's modulus for the magnetron treated PDMS after etching is more than three times that of native PDMS; thus, all the modified polymer surfaces are stiffer than native PDMS. This is not surprising due to the increased oxidation after magnetron treatment as seen through XPS. As many cells typically prefer to grow on stiffer more ridged surfaces this could explain why cells are able to attach to the ODTMS surface even though it has similar surface chemistry and wettability as PDMS.

#### **4.4 Interactions of Cells and a Tip-less Cantilever with Magnetron Modified PDMS**

To better assess the morphology of cells grown on stencil masked patterned PDMS, cells located on the modified dots were imaged using AFM. Figure 4.9 a and b show C2C12 mouse muscle cells on the modified dot. Wrinkles in the polymer surface appear to extend from the cluster of cells on the modified dot. Whiteside patterns seen on our modified surfaces have always been disordered; however, these wrinkles appear to radiate outward from the cells located on the modified surface. These wrinkles greatly resemble those seen by Burton *et. al.* when they grew goldfish keratocytes and Swiss 3T3 fibroblast cells on a silicone rubber substrate [167]. They used the wrinkles to determine the forces generated by cells with nanoNewton precision and submicrometer spatial resolution. Other information, including the direction of the cell motion and the mechanism by which the cell moves can be obtained by looking at the change in these wrinkles over time. In this case, a thin crosslinked silicone layer rested above an uncrosslinked silicone fluid. The PDMS-Al surface consists of a

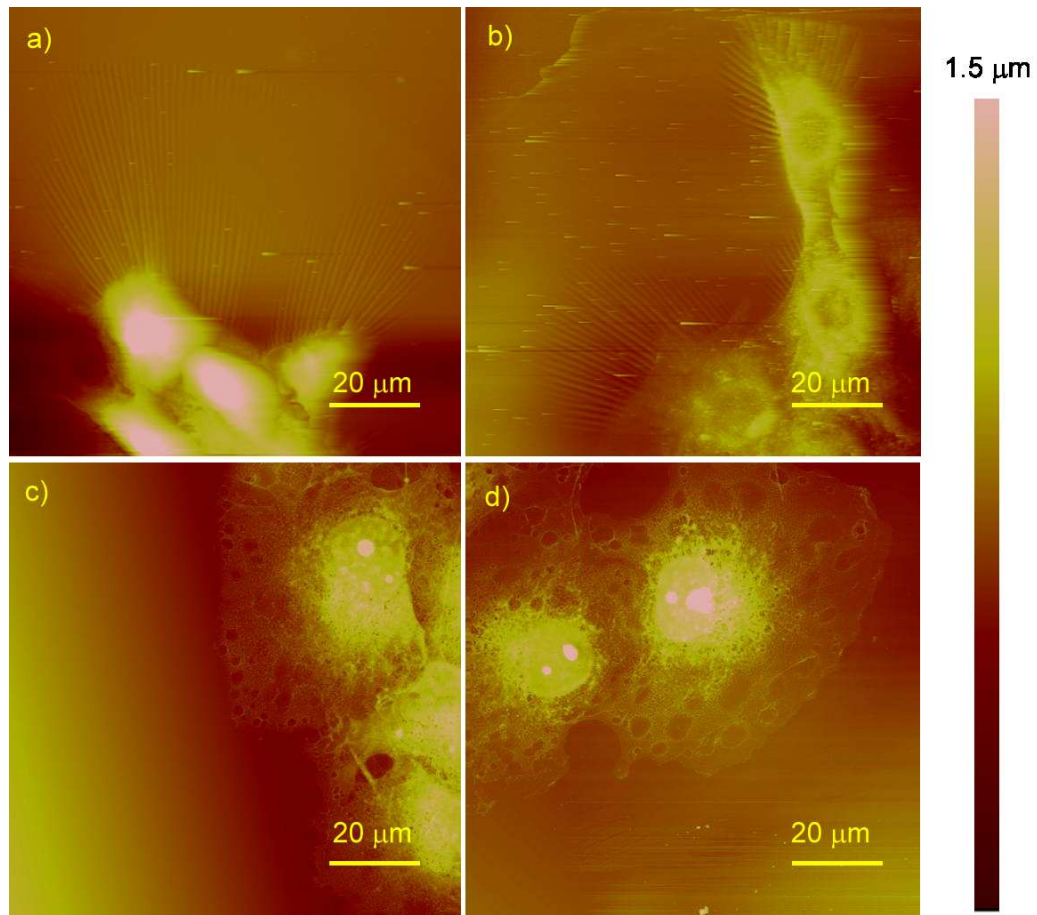


Figure 4.9: AFM contact mode height images of a-b) C2C12 c-d) COS-7 cells grown on stencil masked patterned PDMS

thin silica-like layer over a solid silicone polymer, however, it has been reported that a thin fluid like layer exists between the bulk polymer and the silica-like layer [110]. Thus it is possible that the surface wrinkles are caused by tractional forces from the cells.

Surface wrinkles do not form when COS-7 kidney cells are grown on modified polymer (Figure 4.9 c and d). The lack of wrinkles does not mean that the cell is not exhibiting a force, only that the force is not great enough to wrinkle the polymer surface. COS-7 cells are expected to exhibit less force than C2C12 cells, and thus may not be able to exert enough force to cause wrinkling.

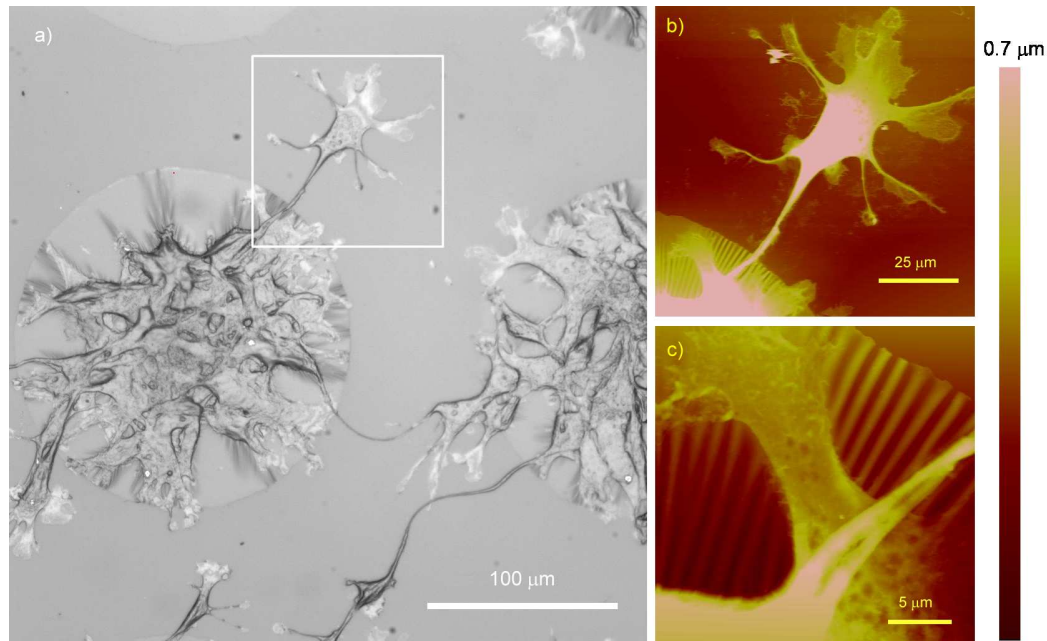


Figure 4.10: a) Bright field optical image and b-c) AFM contact mode height images of C2C12 cells on stencil masked patterned PDMS

Figure 4.10 shows cells located near and beyond the edge of a modified dot. The surface wrinkles appear as blurry edges by optical microscopy (Figure 4.10 a). The cell located outside of the modified dot, does not have a normal morphology for a C2C12 cell, rather it appears to be unhealthy (Figure 4.10 b). No surface wrinkles are associated with the outlying cell, indicating that either the PDMS surface cannot display wrinkles or that the cell is not exhibiting enough force. Since the PDMS surface does not have the same layer structure as the modified polymer or as the thin silicon layer above a fluid, it would not be expected to show wrinkles. The wrinkles created by the cells inside the dot abruptly end once they reach the edge of the modified region (Figure 4.10 c), also indicating that the bulk polymer is unable to propagate the wrinkles.

In some cases the C2C12 cells appear to be tearing the silica-like layer. Figure 4.11 a show a single cell inside of a modified region which appears to be tearing the

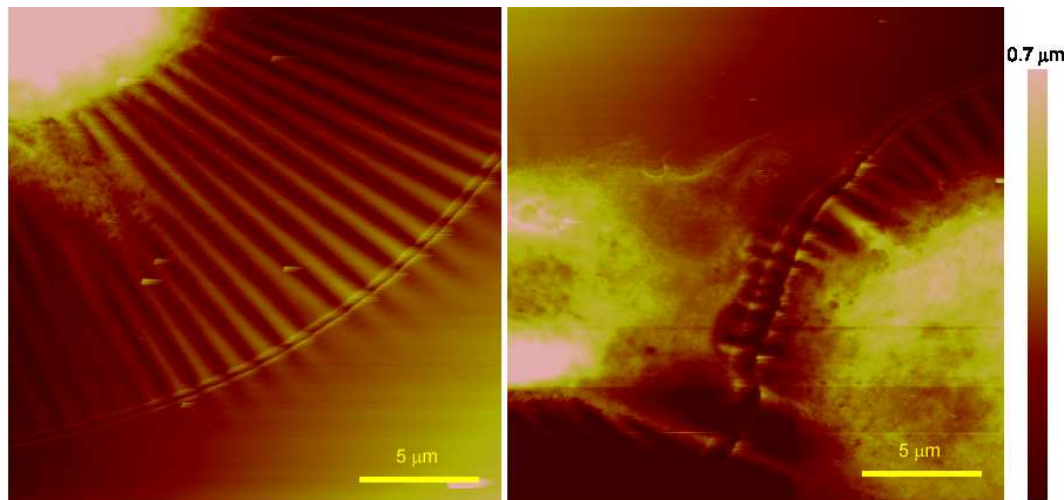


Figure 4.11: AFM contact mode height images of C2C12 cells on stencil masked patterned PDMS

surface of the polymer. Wrinkles once again are radiating outward from the cell, while the tear is perpendicular to the wrinkles. This indicates the the force exerted by the cell is directed towards the cell. Figure 4.11 b shows cells that appear to have ripped the polymer surface between them. Again the surface wrinkles are perpendicular to the rip, indicating that the cells are exhibiting forces on the material in opposite directions and towards themselves.

If the changes in surface wrinkles can be monitored during live cell movement, then the aluminum modified surface could be used to assess cell propagation and forces. However, it was observed that the surface wrinkles were not visible by optical microscopy when the substrate was wet. Since the refractive indices of PDMS and water are much closer than that of PDMS and air, the wrinkles may still be present, but not detectable. Since AFM on live cells can be difficult and time consuming, AFM was performed on fixed cells in an aqueous environment to determine if the wrinkles were still present.

Figure 4.12 show the AFM image of the same cell in air (a) and in water (b).

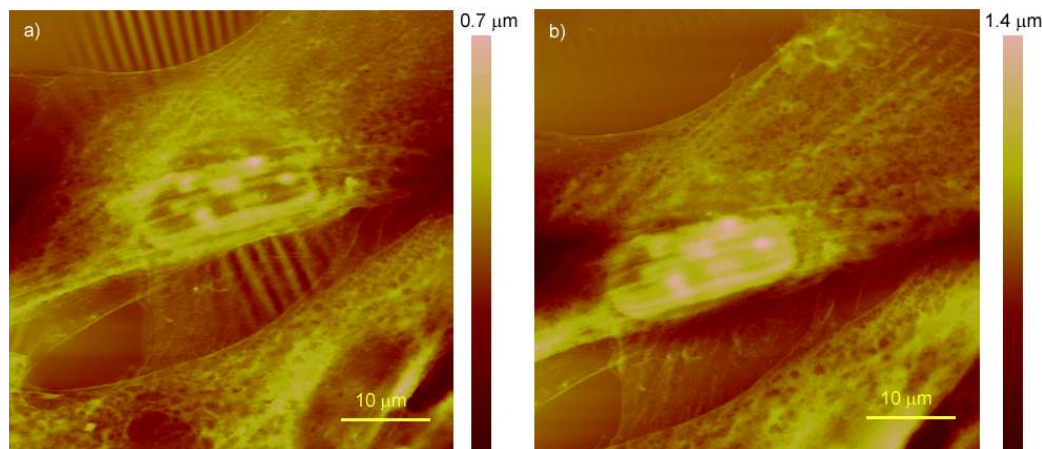


Figure 4.12: AFM contact mode height images of C2C12 cells on stencil masked patterned PDMS taken in a) air and b) water

In water the surface wrinkles are no longer easily visible in the image. However, cross sectional analysis shown in the right hand side of Figure 4.13, detects residual wrinkling with the same periodicity but greatly reduced amplitude.

The surface wrinkles may be caused by the dehydration of the fixed cell, or due to the dehydration of the polymer. The wrinkles are only visible due to the difference in the stiffness of the silica-like layer and the intermediate fluid like layer. If the polymer is hydrated, it is possible that the mechanical properties of the polymer change and prevent wrinkle formation. It is also possible that when the fixed cell is dehydrated it contracts, which would put force onto the silica-like layer and thus the wrinkles would be caused by dehydration of the cell and not tractile forces. Figure 4.14 shows the sectional analysis across the cell in air and in water. When dry, the cell appears to have decreased in height indicating that it has in fact shrunk during dehydration and potentially contracted. The dehydration of the cell would also explain why the wrinkles always radiate outward from the cell.

To better understand how the polymer surface responds to forces, a tip-less cantilever was used to apply forces to polymer surface. When the cantilever was



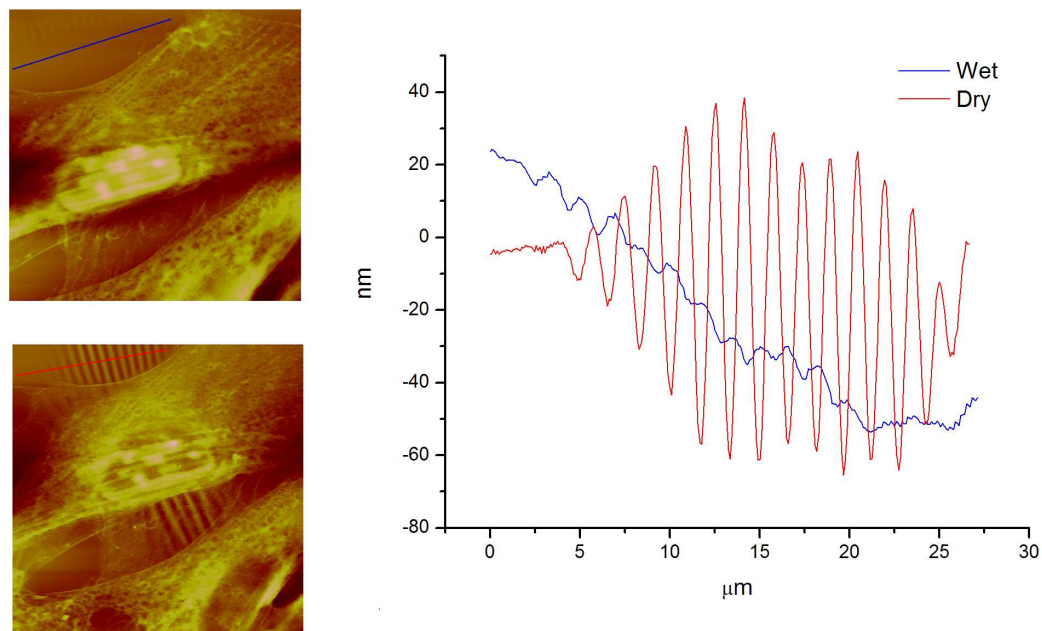


Figure 4.13: Topographical cross-sectional analysis of surface wrinkles from AFM images of C2C12 cells on wet and dry stencil masked patterned PDMS

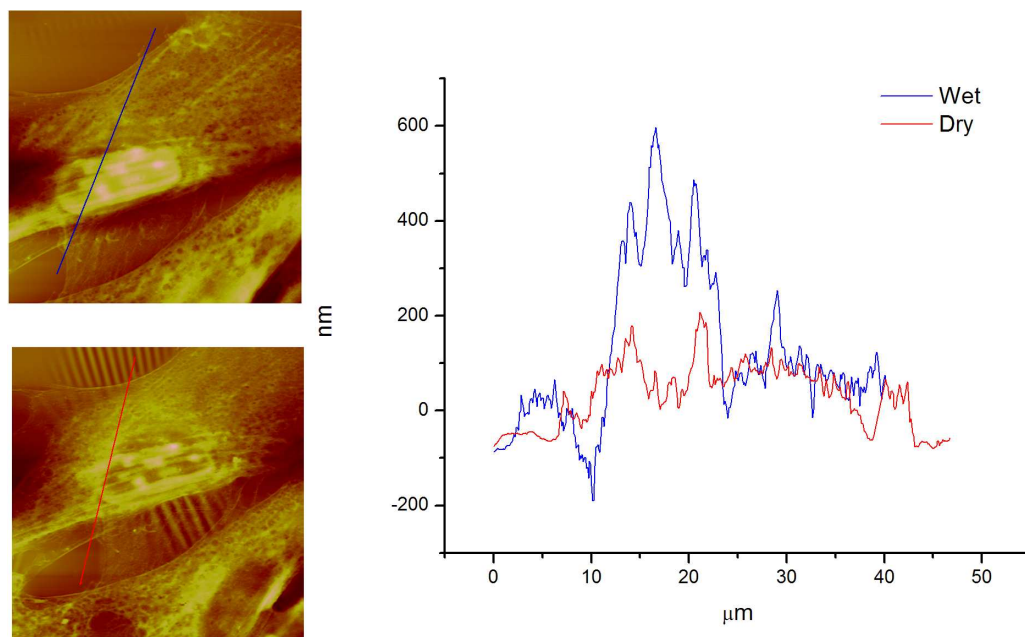


Figure 4.14: Cross-sectional analysis of C2C12 cells from AFM images taken in air and water

pushed into the polymer surface, wrinkles formed parallel to the edges of the cantilever (Figure 4.15 a). When the cantilever was pulled away from the surface, the wrinkles changed direction, extending radially outward from the cantilever (Figure 4.15 b). Once the cantilever was in contact with the surface, it was moved to the left and right (Figure 4.15 c, d). The wrinkles that formed in the direction of cantilever movement formed parallel to the edge of the cantilever. On the other side of the cantilever the wrinkles appeared perpendicular to the cantilever edge. Thus when the polymer surface is compressed, circular wrinkles form, and when the polymer surface is stretched, radial wrinkles form. This suggests that the cells are either pulling up on the surface, inwards towards the center of the cell or both. If the force is in fact caused by contraction of the cell due to dehydration, it would be expected to produce the observed radial wrinkles. The tip-less cantilever was also pressed into a native PDMS sample and imaged (not shown). Even after moving the cantilever to the left and right during contact, no wrinkles were formed on the PDMS.

To determine whether the modified surface can still show surface wrinkles in an aqueous environment, a cantilever was pressed against a surface to form wrinkles in air (Figure 4.16 a). The same surface was then placed in water and the cantilever again pressed into the surface. After several attempts, no surface wrinkles are visible by optical microscopy, as demonstrated in Figure 4.16 b. As the surface was unable to produce wrinkles in a aqueous environment, it is possible that the wrinkles are caused by cell forces; however, this is not definitive.

So far, the tip-less cantilever has produced qualitative information on the interaction between the polymer surfaces and the force applied by the cantilever. To obtain quantitative data a more controlled geometry is required. Glass beads were placed on the modified surface by suspending them in water and allowing the water to evaporate off the surface. Once a bead was located by optical microscopy, the tip-less

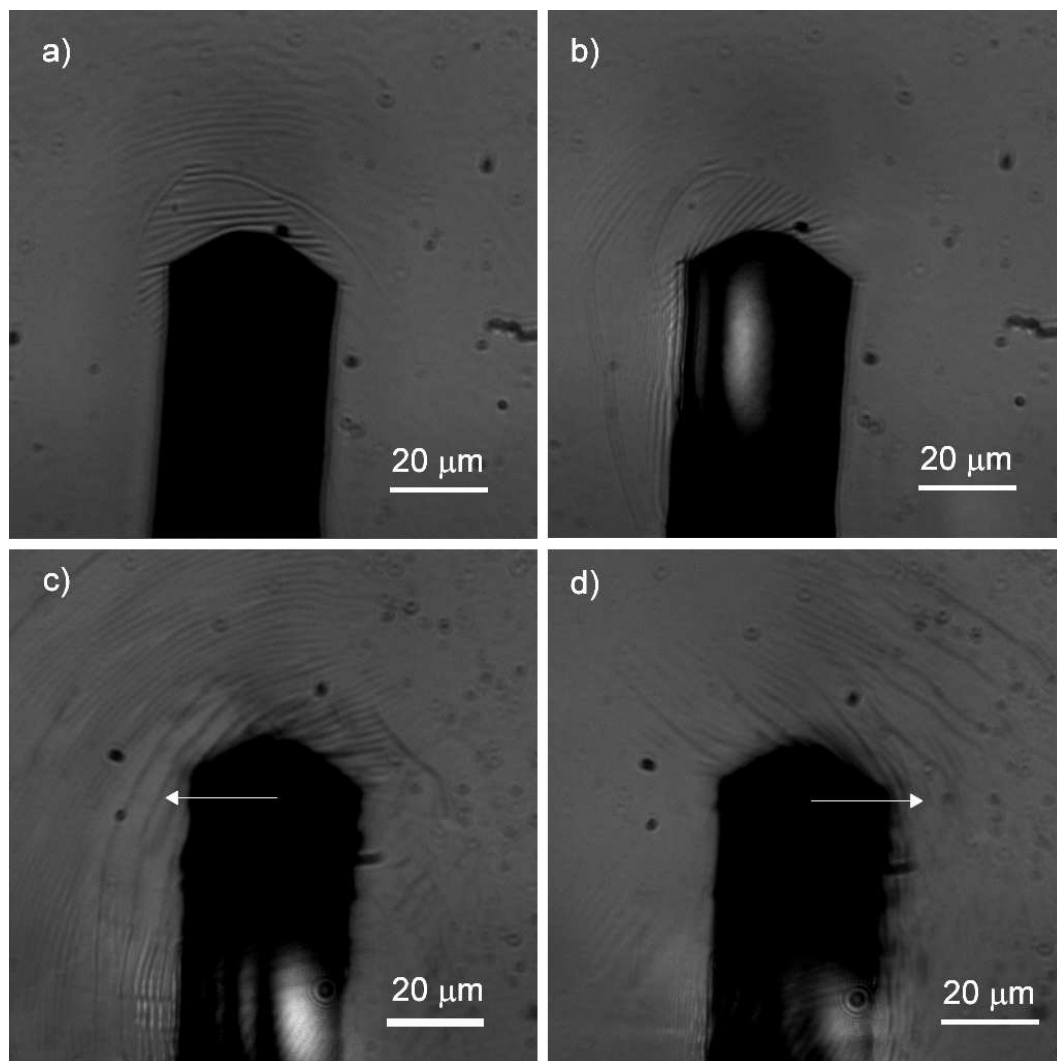


Figure 4.15: Imaging of a tip-less cantilever interacting with PDMS. The cantilever is a) pushed into the surface, b) pulled up from the surface, c) pushed to the left and d) right while in contact with the surface)

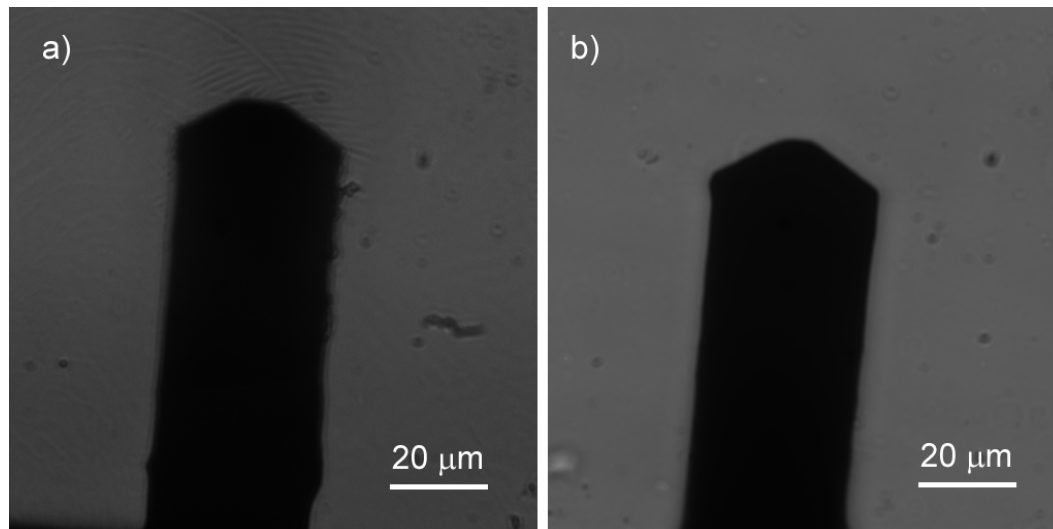


Figure 4.16: A tip-less cantilever pushing into modified PDMS in a) air and b) after immersion in water

cantilever was aligned over the bead and brought towards the surface. Figure 4.17 shows a  $40\ \mu\text{m}$  bead being pressed in the PDMS-Al surface. After applying the maximum force allowed by our AFM system and the tip-less cantilever, the wrinkles only begin to become visible on the side of the bead. Similar effects were seen with beads of different sizes, from  $5\ \mu\text{m}$  to  $50\ \mu\text{m}$ . The wrinkles are most likely forming under the sphere and extending outward; however, they are being covered by the portion of the bead that is not in contact with the surface. In order to obtain quantitative information a different tip geometry is required.

Fixed cells are able to produce surface wrinkles on the magnetron modified polymer surface that form radially from the centre of the cell or group of cells under dry conditions. These surface wrinkles are not present when the cell is in a aqueous environment and only appear once the cell and surface has dried. Fixed cells appear to dehydrate and shrink when dried, and thus the surface wrinkles may be due to the contractile forces this shrinking produces. The modified surface can exhibit wrinkles when forces are applied by a tip-less cantilever in air. Wrinkles do not occur when

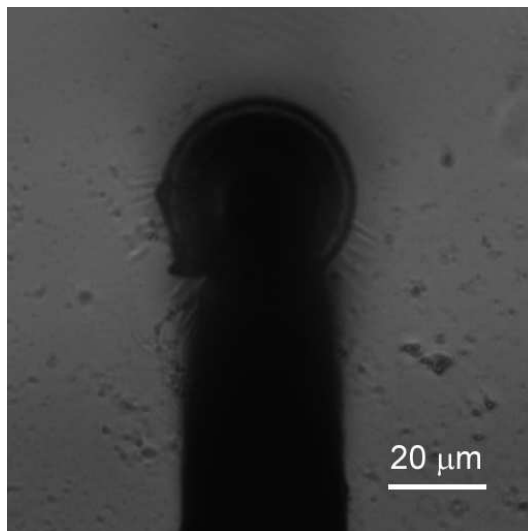


Figure 4.17: A tip-less cantilever pushing on a 40  $\mu\text{m}$  glass bead into modified PDMS

forces are applied in an aqueous environment, implying that some physical change maybe occurring to the surface upon hydration, or that wrinkles are not visible in an aqueous environment. No surface wrinkles were seen on PDMS when forces were applied by a tip-less cantilever, most likely due to the lack of a layered structure.

## 4.5 Conclusions

Magnetron aluminum deposition onto PDMS exposed the polymer to an argon plasma before deposition. The plasma modifies the polymers surface creating a oxygen rich stiff silica-like layer that is revealed upon aluminum etching. The plasma heats and expands the polymer during deposition, and when the polymer cools, it contracts, creating compression forces on the silica-like layer and the aluminum layer. These layers buckle and form surface ripples as observed by AFM. Even after the aluminum is etched away the silica-like layer maintain the ripples. These ripples increase the roughness of the polymer surface.

The stiffness of the both PDMS and magnetron treated PDMS after aluminum etching was determined by analyzing force curves for both materials. PDMS-Al was found to have a Young's modulus three times greater than that of PDMS. This increase in modulus is attributed to the silica-like layer.

Both stiffness and roughness have been correlated to increased cell adhesion such that, stiffer and rougher surfaces often show an increase in cell attachment. All modified PDMS surfaces used for cell patterning have the underlying silica layer structure and thus are rougher and stiffer than native PDMS. The roughness increase is on the order of a few nanometers, this is much smoother than surfaces whose roughness has been previously reported to increase cell adhesion. Thus, the surface roughness of modified PDMS is not likely to play an important role in increasing cell adhesion.

Previously, a transition point near the cell modulus has been reported, where cells are able to spread on surfaces stiffer than this transition point, and remained unattached on surfaces with lower moduli [53–55]. PDMS has a stiffness large enough to maintain cell attachment, as it is stiffer than this transition point. The previous studies have all been performed on surfaces with chemistries and wettabilities that are ideal for cell adhesion. PDMS and the PDMS-ODTMS surface both present methyl-terminated hydrophobic surfaces. Aside from the slight increase in roughness the main difference between the two surfaces is the increase in the Young's modulus. Although, this increase in stiffness does not cross the conventional transition point, it is possible that it is responsible for the increase in cell attachment, as neither surface present reasonable surface chemistry for cell adhesion.

AFM was used to look at the interactions between cells and the stencil masked patterned surfaces. New surface wrinkles appeared to radiate outward from cells fixed on the polymer surface. These wrinkles only occur in air and were not observed when

imaged in an aqueous environment. The fixed cells shrink when dehydrated, which may be responsible for the wrinkles. The formation of the wrinkles supports a layer like structure for plasma treated PDMS. Also no observable wrinkles were formed when the polymer was pressed with a tip-less cantilever in a aqueous environment using similar force that produced wrinkles in air. This indicates that either the wrinkles are not visible by optical imaging methods or a change in the physical properties of the modified layers has occurred.

# Chapter 5

## Fabrication of Patterned Microfluidic Channels

### 5.1 Introduction

One goal of our research group is to create a microfluidic device that uses cells as biosensors. Cell based biosensors offer advantages over conventional biomolecular-based sensors as they are not specific to certain compounds but are able to respond to a wide variety of biologically active compounds [2]. Cell based biosensors have been used for high throughput drug discovery, clinical diagnostics, and to detect toxic agents. This device must be capable of controlling cells' environments, and must allow for the integration of analytical techniques in order to monitor cell responses. Microfluidic channels patterned for cell adhesion can allow cells to be located in a particular environment and to be positioned over sensors used to detect changes in the cell. It can also allow for easier alignment for off chip detection methods. By controlling the size of the patterned regions the number of cells being studied can be controlled. Smaller regions can allow for single cell studies while larger regions allow for the study of small cell clusters.

Microfluidic devices contain micron-scale channels that control the flow of minute amounts of liquids. For biological purposes, microfluidic devices demonstrate great promise, because they allow for the control over the cells' environment in a fashion



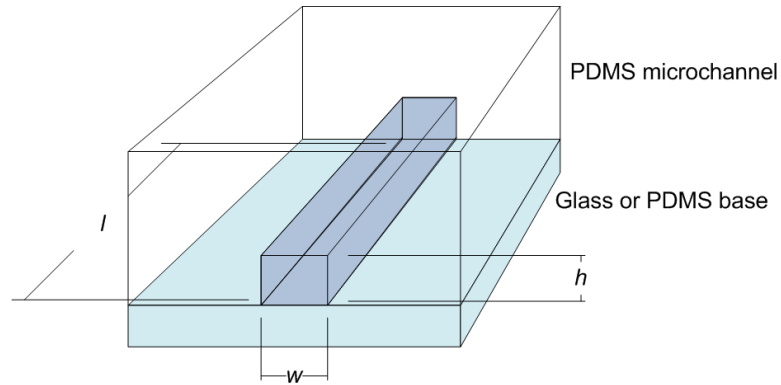


Figure 5.1: Section of a microfluidic channel

not obtainable by standard cell culturing methods [2, 119, 168]. Their small size and the ability to perform multiple processes on a single chip, give them a great advantage over standard lab techniques, including reduced consumption of reagents and faster analysis and response times [2, 118, 119].

Microfluidic devices typically contain a network of channels, valves, and pumps. Figure 5.1 shows a section of a microfluidic channel. The channels have heights ( $h$ ) and widths ( $w$ ) between 1 and 1000  $\mu\text{m}$ , and lengths ( $l$ ) many millimeters. The geometry of the channels allows for a low Reynolds number ( $Re$ ) [118]. The Reynolds number can be expressed as a function of density  $\rho$ , velocity  $U$ , characteristic length  $L$  and dynamic viscosity  $\mu$ :

$$Re = \frac{\rho U L}{\mu} \quad (5.1)$$

For a typical microfluidic channel the Reynolds number is much less than threshold conditions for turbulent versus laminar flow. Thus the fluid in a microchannel is under laminar flow, meaning that fluids flowing side by side only mix by diffusion, creating more uniform and controllable reaction conditions and environments [118].

For biological applications, PDMS microfluidic devices are becoming the standard. PDMS is inexpensive, easily molded to form micron scale shapes, optically transparent at wavelengths greater than 280 nm, is produced by low temperature polymerization, is nontoxic, and can be readily sealed to many other materials by making molecular (van der Waals) contact with the surface [90,92]. Often the seal formed through molecular contact is not robust and thus irreversible bonding is preferred. PDMS can be irreversibly bonded to itself, glass, silicon, silicon oxide, and oxidized polystyrene by plasma treating both surfaces and immediately bringing them into contact [90,92,118,119].

Early chapters in this thesis have demonstrated different cell patterning methods. The most promising method involved the deposition of aluminum through a stencil mask. This present chapter demonstrates the fabrication of both reversibly and irreversibly bonded patterned microfluidic channels using the stencil mask patterning technique. The reversibly bonded channels take advantage of the seal that forms when two pieces of PDMS are brought into contact. When creating irreversibly bonded channels, the use of the typical plasma bonding method would undo the stencil mask patterning. Also the two polymer surfaces must come into contact within 1 min of plasma exposure, not allowing enough time to align the channel over the patterned surface. To overcome this, a new PDMS bonding method, exploiting the chemical changes that occur during aluminum deposition, was developed. In order to create an irreversibly patterned channel new custom stencil masks were fabricated and chromium was used as a protective layer during the bonding process.

## 5.2 Materials and Methods

### 5.2.1 Reagents

PDMS Sylgard 184A and B were purchased from Dow Corning. Microposit SC1827 positive photoresist and Microposit MF-319 developer were purchased from Rohm & Haas Electronic Materials. SU-8 2010 and SU-8 developer were purchased from MicroChem. Epoxy 907 was purchased from Miller-Stephenson Chemical. Octafluorocyclobutane gas was purchased from BOC Edwards. Crystalbond 509 from Aremco Products Inc. Cr etchant 1020 was purchased from Transene Company Inc. Nanostrip was purchased from Cyantek Corporation. C2C12 cell line was purchased from ATCC. DMEM, L-glutamine, penicillin streptomycin, FBS, trypsin/EDTA and PBS were all purchased from Invitrogen. All other chemicals were purchased from Sigma-Aldrich and used as received.

### 5.2.2 Preparation of PDMS Substrates

#### 5.2.2.1 Bulk PDMS

To allow for easy removal of PDMS, silica wafers were exposed to HMDS vapor in a vacuum oven (YES-3TA HMDS Oven) at 150°C and 1 torr for 5 min. To remove water vapor and oxygen from the sample and the chamber, the chamber was purged 3 times with nitrogen gas by evacuating the chamber to 10 torr and refilling the chamber with nitrogen gas to 600 torr. PDMS precursors, Sylgard 184A and B (Dow Corning), were combined in a 10:1 mass ratio, poured onto a silica wafer to a thickness of 3 to 5 mm. The prepolymer was then degassed under vacuum for 60 min and cured for 60 min at 70°C. After curing the PDMS was peeled from the wafer.

### 5.2.2.2 Molded PDMS by Soft Lithography

The application of soft lithography to form PDMS microfluidic devices was first introduced in 1998 by Whitesides *et al.* [90]. Soft lithography has revolutionized microfluidics, reducing the need for a clean room environment, putting microfluidics within the reach of biology-focused laboratories [168].

Microfluidic channels were created using a soft lithography technique. In order to form the channels, molds were created on glass microscope slides or silicon wafers, through photolithography. Figure 5.2 illustrates the fabrication method used to create PDMS microfluidic channels by soft lithography. A negative photoresist (SU-8) was cast onto either glass microscope slides or silicon wafers at 500 rpm for 5 s and 1000 rpm for 30 s. Before coating the glass slides, they were cleaned in isopropanol for 60 min and the silicon wafer HMDS vapor primed in a vacuum oven (YES-3TA HMDS Oven) at 150°C and 1 torr for 5 min. A final thickness of 20  $\mu\text{m}$  was obtained (determined using a Dektak profilometer, Veeco Instruments Inc). The substrate was baked to remove excess solvent at 65°C for 1 min, and then 90°C for 3 min. The photoresist was exposed through a photomask using 12.5 mW/cm<sup>2</sup> of 365 nm light produced by a 350 W Hg Arc lamp on a Karl Suss MJB3 Mask Aligner for 17.5 s. The photomask was designed in L-edit (Tanner EDA) and printed onto an acetate file using a high resolution commercial printer (PhotoplotStore). A post exposure bake at 65°C for 1 min and 90°C for 3 min, was carried out immediately after exposure and before developing in SU-8 developer for 2.5 min. After rinsing with isopropanol and then water, the substrates were dried with a stream of air and hard baked for 10 min at 200°C .

PDMS precursors, Sylgard 184A and B (Dow Corning), were combined in a 10:1 mass ratio, and poured onto the master. The prepolymer was then degassed under

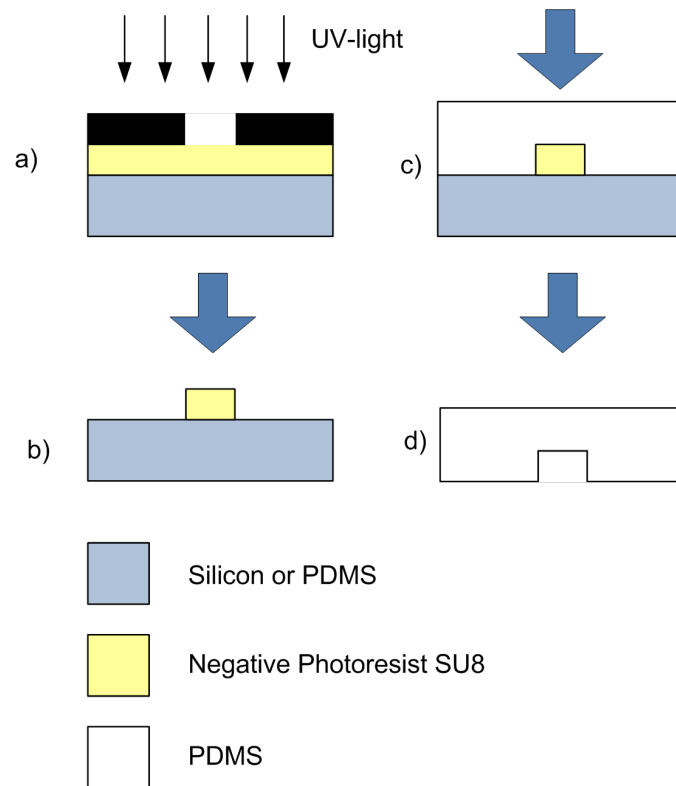


Figure 5.2: Fabrication of microfluidic channels in PDMS by soft lithography. a) a thin layer of SU8 is exposed to UV-light through a photomask. b) the unexposed SU8 is removed by the developer. c) uncrosslinked PDMS is mixed and poured over the mold d) PDMS is cured and removed from the mold.

vacuum for 60 min and cured for 60 min at 70°C . After curing, the PDMS replica was peeled from the master and ports punched into the ends of the channels to allow for the addition of liquids.

### 5.2.2.3 Preparation of Thin PDMS Films

PDMS precursors, Sylgard 184A and B (Dow Corning), were combined in a 10:1 mass ratio. Thin PDMS samples were generated by casting the PDMS mixture onto glass microscope slides at 500 rpm for 5 s then 2000 rpm for 30 s with a Solitec 850 spin coater (Solitec Wafer Processing). The thickness of the PDMS layer was  $33 \pm 3 \mu\text{m}$ , determined using a Dektak profilometer.

### 5.2.2.4 Magnetron Surface Modification of PDMS

Aluminum was sputtered onto the PDMS substrates to a thickness of  $44 \pm 3 \text{ nm}$  using an Edwards Auto 500 Magnetron Sputtering System. The thickness was determined using a Dektak profilometer (Veeco Instruments Inc). The sputtering system was operated at 300 W, 4.8 mTorr, with argon gas flowing at a rate of 15 sccm. The plasma was generated using a RF power supply with an operation frequency of 13.56 MHz. Prior to metal deposition, the samples were kept in the chamber with the plasma struck and the source shutter closed for 4 min.

## 5.2.3 PDMS Bonding

### 5.2.3.1 PDMS-Glass Bonding

The aluminum layer was etched from bulk PDMS and molded PDMS by 1.8 M orthophosphoric acid for 30 min. The polymer was then rinsed 3 times in water and dried by a stream of air. After 3 min the samples were quickly immersed in water and

immediately the treated side was brought into contact with a glass microscope slide. The system was heated to 85°C for 10 min and light pressure applied to the top of the polymer. Before bonding, the glass slide was cleaned with 20% (v/v) hydrochloric acid for 60 min and rinsed with deionized water.

### 5.2.3.2 PDMS-PDMS Bonding

The aluminum layer was etched from bulk or molded PDMS, and thin PDMS by 1.8 M orthophosphoric acid for 30 min. The polymer was then rinsed 3 times in water. The bulk or molded PDMS was dried under a stream of air while the thin substrate remained wet. The treated side of the bulk or molded PDMS was brought into contact with the treated side of the thin PDMS and heated at 110°C for 10 min with light pressure.

### 5.2.3.3 Tensile Testing

Bulk PDMS samples were punched in 20 mm diameter circles for tensile testing. Bonding was performed both 24 hrs and 7 days after initial modification. Measurements were taken for 4 samples for each PDMS-PDMS and PDMS-glass bonding at each time point. To assess the pull-off strength, a pneumatic adhesion tensile testing instrument (PATTI 110, F2 Piston; SEMicro Inc) was used. In order to fix the pull-stub to the PDMS, both sides of the bulk PDMS were treated with aluminum. After bonding, the top aluminium layer was etched away using 1.8 M orthophosphoric acid for 30 min, and the polymer was then rinsed in water and dried under a stream of air. Once the modified top layer was exposed, an epoxy was used to affix a clean pull stub to the polymer. A light pressure was maintained on the stub until complete curing, approximately 24 hrs. A load was applied to the pull-stub by the instrument, until bond failure. Figure 5.4 shows the experimental set-up of the tensile bonding test.

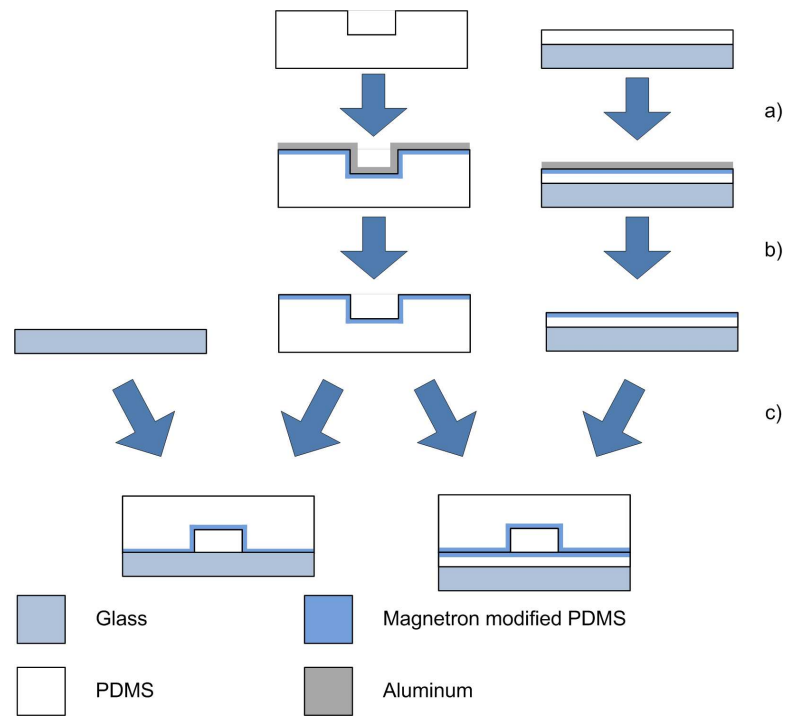


Figure 5.3: Schematic illustration of the bonding procedures of PDMS-glass and PDMS-PDMS. a) Aluminum is deposited over PDMS; b) aluminum is etched away, revealing modified PDMS; c) the surfaces to be bonded are brought into contact and heated.



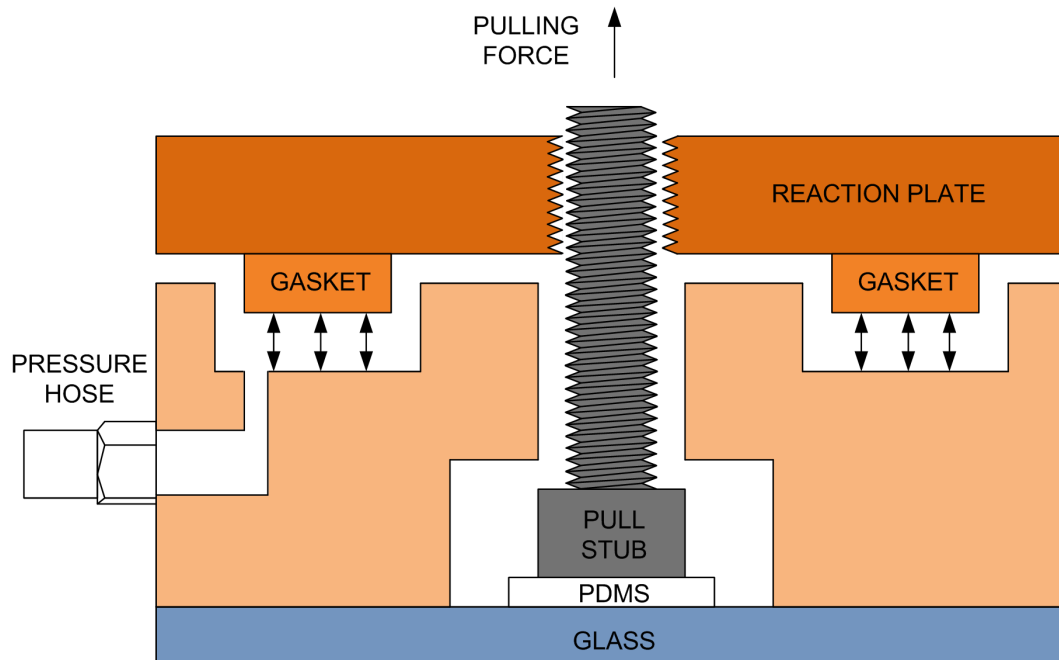


Figure 5.4: Experimental set-up of the tensile bonding pull-off test, showing the fully assembled PATTI tensile testing apparatus

#### 5.2.3.4 Leakage Testing

Blue coloured dye was pumped through sealed PDMS-glass and PDMS-PDMS channels using a syringe pump (Harvard Apparatus). These channels were formed by bonding molded PDMS to either a glass slide or thin PDMS. The channel had a length of 25 mm, a width of  $300\ \mu\text{m}$  and a height of  $20\ \mu\text{m}$ . The fluid ports had a diameter of 2.5 mm. Capillary tubing was used to connect the syringe pump to the fluid ports. The tubing was connected to the needle of the syringe through a needle-capillary connector. The dye was pumped through the channel at an initial flow rate of 0.025 mL/min and increased by 0.025 mL/min every 30 s until failure occurred.

### 5.2.4 Stencil Mask Fabrication

Reactive ion etching (RIE) is one of the most common methods used to etch high ratio features into a silicon substrate [118, 169].  $\text{SF}_6$  is used to create a reactive plasma, forming fluorine radicals ( $\text{F}^\bullet$ ), positive ions ( $\text{SF}_5^+$ ) and negative ions ( $\text{F}^-$ ). The reactive fluorine species will adsorb onto the Si surface and will produce  $\text{SiF}_4$  and  $\text{SiF}_x$  (where  $x < 4$ ); since these species are volatile they will desorb from the surface. To prevent the species from dissociating and redepositing onto the surface, they must be removed from the system. To create straight edges an inhibiting layer is needed. Typically, a carbon fluorine gas is used to create a plasma which then deposits a fluorocarbon polymer onto the silicon surface, including the sidewalls. Since the walls are not directly bombarded with ions, the polymer will remain on the wall and protect it from etching. Thus the RIE process involves alternating steps between etching and deposition of an inhibiting layer. This alternation also allows for the evacuation of the system to remove  $\text{SiF}_x$  ( $x \leq 4$ ) species.

To create custom stencil masks, 100  $\mu\text{m}$  thick silicon wafers were patterned using photolithography and etched using a RIE system. Figure 5.5 illustrates the fabrication procedures used to form stencil masks. 100  $\mu\text{m}$  silicon wafers were attached to oxidized Silicon carrier wafers using the mounting medium, CrystalBond. CrystalBond was dissolved in acetone and a small amount spin coated onto the carrier wafer at 500 rpm for 5 s and 2500 rpm for 45 s. The wafer was heated to 110°C to melt the media and the 100  $\mu\text{m}$  wafer aligned carefully over the carrier wafer. After alignment, both wafers were removed from the heat source and allowed to cool to room temperature. During cooling, the CrystalBond solidifies and seals the two wafers together.

A positive photoresist, Microposit S1827, was spin coated on to the mounted

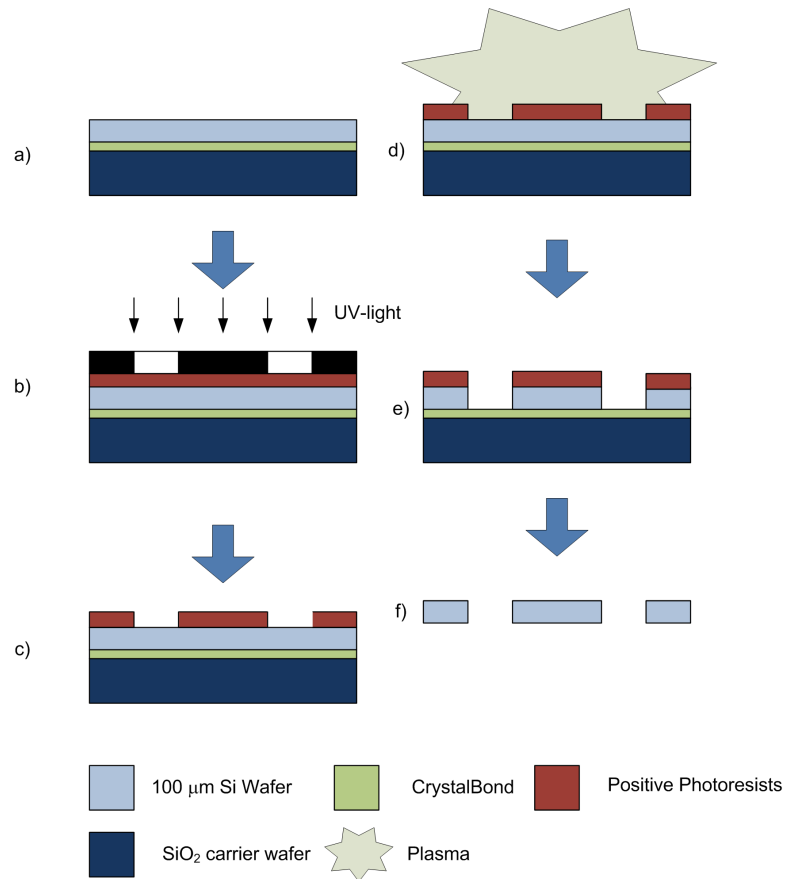


Figure 5.5: Fabrication procedure used to form stencil masks: a) a 100  $\mu\text{m}$  Si wafer is glued to a  $\text{SiO}_2$  carrier wafer using CrystalBond; b) a photoresist is spin coated over the wafer and exposed to UV-light through a photomask; c) after development, the exposed photoresist is removed; d) RIE of the 100  $\mu\text{m}$  Si wafer; e) the wafer is then immersed in acetone overnight and the patterned Si wafer removed

silicon wafer using a Solitec 5110 spin coater, at 500 rpm for 5 s and 2000 rpm for 45 s to obtain a thickness of 4.0  $\mu\text{m}$ . The sample was soft baked at 115 $^{\circ}\text{C}$  for 4 min to remove solvent, care was taken to maintain alignment between the two wafers during heating. The photoresist was then exposed to 405 nm UV light through an acetate photomask for 22 s using a Karl Suss MJB3 optical lithography system (Suss MicroTec) at a power of 18 mW/cm $^2$ . The photoresist was developed using Microposit MF-319 developer for 75 s, dissolving the exposed photoresist. The exposed silicon was etched using an Alcatel 601E Deep Silicon Etching system (Alcatel MicroMachining Systems). The system was operated with an inductively coupled plasma (ICP) RF source of 1800 W and a substrate power of 120 W. Each cycle contained two steps, first an etch using SF $_6$  gas with a flow rate of 300 sccm for 8 s, the second a passivating step using C $_2$ F $_8$  gas with a flow rate of 150 sccm for 3 s. The two steps were cycled continuously for a total process time of 30 min.

Both wafers were immersed in acetone overnight to dissolve the remaining photoresist and CrystalBond. Once the CrystalBond was dissolved, the individual stencil masks were carefully removed and rinsed with fresh acetone and water. To remove any excess CrystalBond the masks were cleaned with Nanostrip for 5 min, followed by thorough washing with deionized water and dried with a stream of air.

## 5.2.5 Fabrication and Testing of Patterned Microfluidic Channels

### 5.2.5.1 Reversible Bonded Patterned Channels

To create a single row of aluminum dots, a commercial steel mesh was taped off using electrical tape, only exposing a single row of 180  $\mu\text{m}$  diameter circular holes. The mesh was aligned over a PDMS coated glass coverslip such that the exposed holes were

near the center of the coverslip. Aluminum was deposited onto the polymer through the mesh using an Edwards Auto 500 Magnetron Sputtering System as described above. A piece of molded PDMS containing a single channel were aligned over the row of aluminum dots using a Leica MZ12.5 Stereozoom microscope. The channels dimensions were: length = 10 mm, width = 250  $\mu\text{m}$ , height = 20  $\mu\text{m}$ , and the fluid ports diameter = 2.5 mm.

### 5.2.5.2 Chromium Protection of Aluminum Coated PDMS

Aluminum was sputtered onto PDMS substrates and PDMS substrates covered by a steel mesh, using an Edwards Auto 500 Magnetron Sputtering System as described above. To prevent etching of aluminum in selected areas during an orthophosphoric acid etch, chromium was deposited over the the aluminum through a steel mesh using an Edwards Auto 500 Magnetron Sputtering System. When aluminum had previously been deposited through a steel mesh, the mesh remained in place until after chromium deposition. The sputtering system was operated at 300 W, 4.8 mTorr, with an argon gas flow rate of 15 sccm. The shutter was immediately opened and deposition occurred for 1 min 15 s, giving a chromium thickness of  $30 \pm 4 \mu\text{m}$ , as determined using a Dektak profilometer. To test the efficiency of chromium as a capping layer, the substrates were immersed in 1.8 M orthophosphoric acid for 30 min and examined.

The substrates were immersed in Cr etchant 1020 for 1 min 10 s to remove the chromium layer, rinsed 3 times with water and examined. After the chromium etch, the substrates were further etched with 1.8 M orthophosphoric acid to expose the modified PDMS surface. To insure that the biocompatibility of the modified surface was not affected by the chromium layer, C2C12 cells were plated onto the substrates. First the etched substrates were sterilized by rinsing with 70% ethanol. Prior to plating, cultured cells were washed with trypsin/EDTA to promote cell detachment

from the culture flasks. The cells were mixed into 10 mL media for transfer. 0.5 mL of the solution was plated onto modified PDMS samples, in a 3 cm petri dish. An additional 2 mL of fresh media was added to each dish, the cells were then incubated for 24-36 hrs. Prior to imaging, cells were rinsed 3 times with PBS (pH 7.4) and fixed using a solution of 4.4% paraformaldehyde in PBS for 10 min. Cells were then rinsed 3 times in PBS and water.

### 5.2.5.3 Irreversible Bonded Channels

To create an irreversible bonded patterned channel, the pattern must be protected from the plasma treatment needed to form an irreversible seal. Ideally, a stencil mask in the shape of the channel with selected regions removed would be used. Since the channel is only a few hundred micrometers wide this mask would be very fragile and difficult to work with. To overcome this problem, two custom stencil masks were created. The first, the half channel mask, creates a shadow of half of a channel (Figure 5.6 a). The second, was a square mask the same size as a coverslip (22 x 22 mm), with 100  $\mu\text{m}$  circular holes down the center of the mask (Figure 5.6 b). Both masks were fabricated as described earlier.

The half channel mask was aligned with the edges of a glass coverslip coated with a thin PDMS layer. Aluminum was deposited onto the exposed PDMS, while the polymer surface under the mask remained protected. The half channel mask was then flipped over and aligned with the other edge of the coverslip, and aluminum deposited once again onto the substrate. A stencil mask consisting of etched circles in a row down the center, was aligned such that the row of dots was above the non-aluminum-coated polymer. Aluminum was deposited through the holes onto the PDMS surface. Chromium was then deposited over the aluminum dots. The stencil mask was not

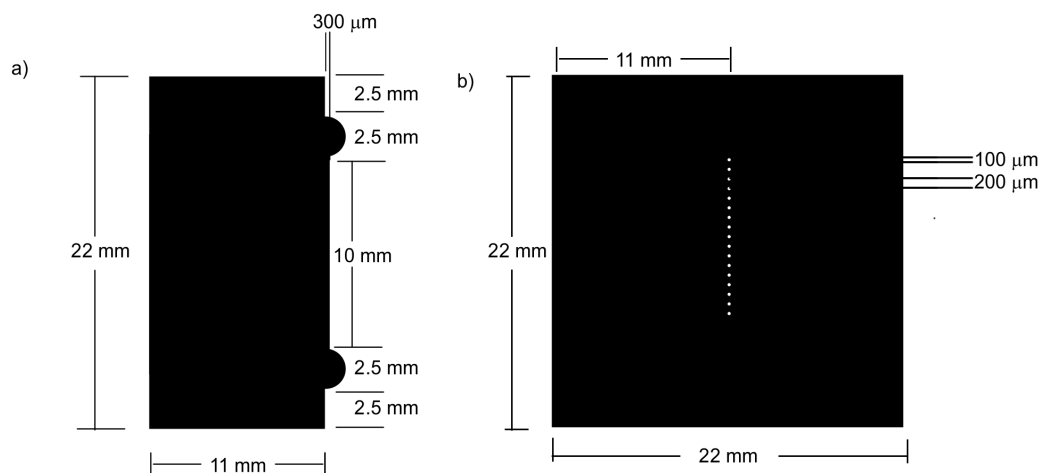


Figure 5.6: Stencil masked used to pattern microfluidic channels: a) the half channel mask, b) a mask used to create a single row of dots

moved between aluminum and chromium depositions. The fabrication steps used to create the patterned surface are illustrated in Figure 5.7.

The substrate was immersed in 1.8 M orthophosphoric acid for 30 min to etch away the non-chromium coated aluminum. A microfluidic channel was also aluminum treated and etched with orthophosphoric acid. Both the coverslip and the microfluidic channel were rinsed 3 times in water and dried with a stream of air. The channel was then aligned over the aluminum-chromium dots using a Leica MZ12.5 Stereozoom microscope and brought into contact with the surface. Once contact was made the system was heated to  $110^{\circ}\text{C}$  for 10 min with light pressure holding the two substrates together, forming an irreversible bond. The channels dimensions were: length = 10 mm, width =  $250\ \mu\text{m}$ , height =  $20\ \mu\text{m}$ , and the fluid ports diameter = 2.5 mm. To reveal the patterned channel the chromium and aluminum are etched away using Cr etchant 1020 for 2 min with a flow rate of  $5\ \mu\text{L}/\text{min}$ . Figure 5.8 shows the final fabrication steps used to form the irreversibly bonded patterned microfluidic channel.

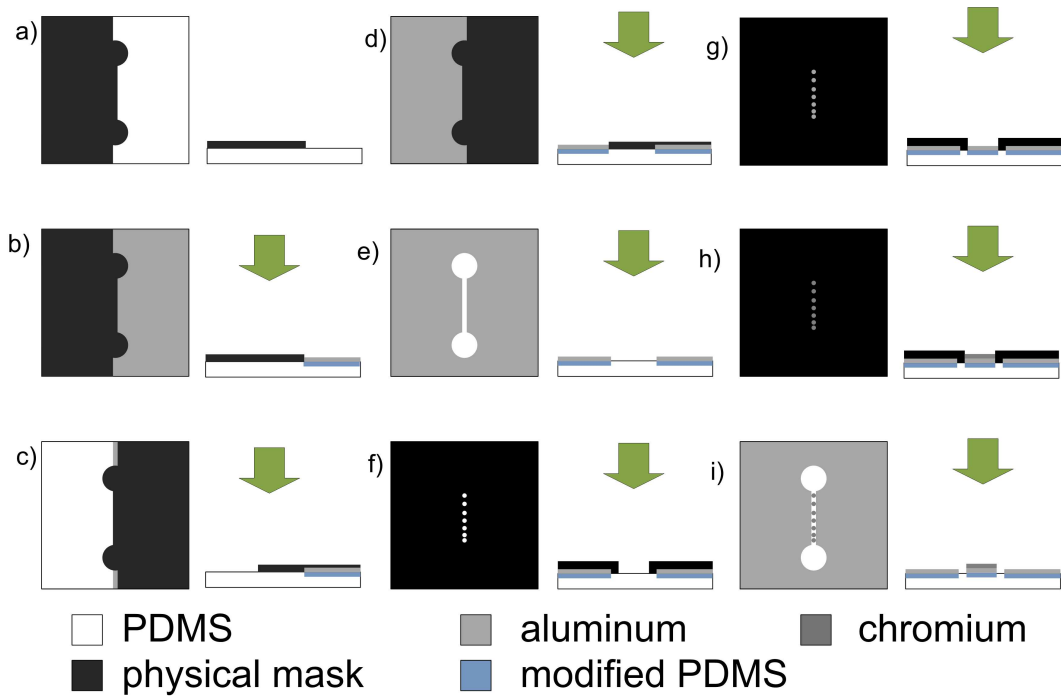


Figure 5.7: Fabrication procedure used to create the patterned bottom of the microfluidic device: a-b) the half channel mask is aligned with the cover slip and aluminum is deposited onto the exposed polymer; c-e) the half channel mask is flipped over and aligned with the other edge of the cover slip; aluminum is deposited onto the exposed surface; f-i) aluminum and chromium are deposited through another stencil mask aligned over the non-treated polymer



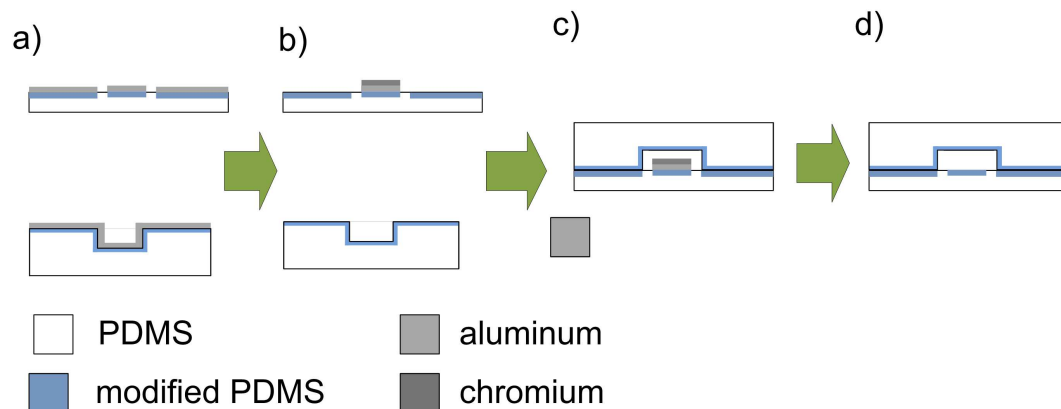


Figure 5.8: Fabrication procedure used to create irreversibly bonded patterned microfluidic channels: a) The bottom is patterned using stencil masks and the channel is treated with aluminum; b) aluminum is etched from both the top and the bottom; c) the channel is aligned over the patterned bottom and the two are bonded together; d) the chromium and the aluminum are etched away to reveal the patterned channel

#### 5.2.5.4 Fibrinogen Patterned Microfluidic Channels

To obtain protein patterned microfluidic channels, Alexa Fluor 488 conjugated fibrinogen (Fg-488) was adsorbed to modified PDMS dots inside of both the reversibly bonded and irreversibly bonded patterned microfluidic channels. For the reversibly bonded channels, orthophosphoric acid was flowed through the channel using a syringe pump for 10 min. The channel was then rinsed with water for 1 hr. A 1 mg/mL solution of Fn-488 was then flowed through the channel for 15 min and then washed with water for 2 hrs. For the irreversibly bonded channels, the chromium and aluminum were etched by rinsing with Cr etchant 1020 for 2 min. The channel was then washed with water for 1 hr, followed by 1 mg/mL Fn-488 for 15 min. The channel was rinsed with water for 2 hrs before imaging. Each step was performed with a flow rate of 5  $\mu\text{L}/\text{min}$ . To connect the syringe pump to the channel a blunt tip needle was used as an interconnect. The blunt tip needle was connected to the syringe pump

through Luer-lock connectors and tubing.

### 5.2.6 Imaging

All optical microscope images were captured using a Zeiss Axioskop2 Mat Microscope with a QImaging Retiga 1300 CCD digital camera. Confocal images were acquired using a Zeiss 510 LSM confocal (Zeiss, Thornwood, NY) with an excitation wavelength of 488 nm corresponding to the  $\lambda_{max}$  for FITC.

## 5.3 Results and Discussion

### 5.3.1 Reversibly Bonded Patterned Channels

The simplest method to create patterned microfluidic channels is to simply align a molded PDMS channel over a patterned surface. The seal that forms between PDMS and PDMS through van der Waals forces is sufficient to allow for the flow of liquid. Figure 5.9 a, shows aluminum dots inside of a PDMS channel. The dots were deposited in a row onto a thin layer of PDMS. In order to create the single row of aluminum dots, the steel mesh was taped, only exposing a single row of holes.

The PDMS channel was aligned over the patterned surface using an optical microscope. In order to remove the aluminum layer, orthophosphoric acid was flowed through the channel with a low flow rate. The continuous flow of etchant reduced the etching time from 30 min to 10 min. To visualize the bioactive regions a solution of Fg-488 was then flowed into the channel. In Chapter 3, Fg-488 only adsorbed to the aluminum treated surface on stencil masked patterned substrates, thus the bright areas in a fluorescent image, indicate the modified regions. Figure 5.9 b and c, show the microfluidic channel after Fg-488 adsorption. The dots in the centre of

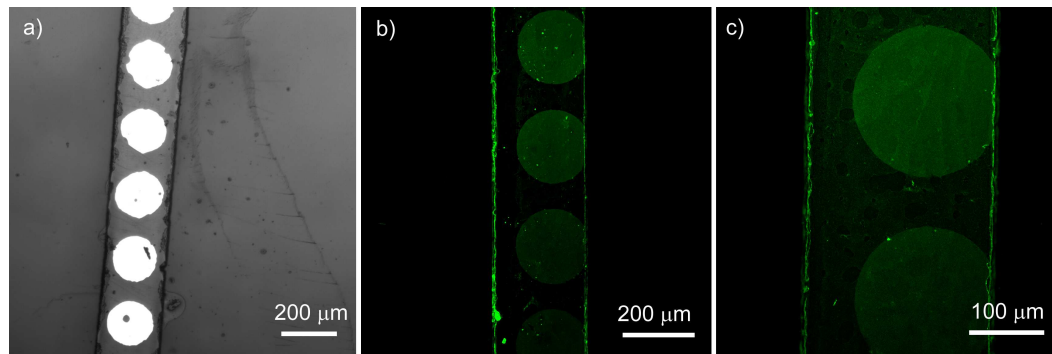


Figure 5.9: Bright field reflection mode optical images a) aluminum dots inside of a PDMS reversibly bonded microfluidic channel. Confocal fluorescent images of b,c) Fn-488 absorbed in a reversibly bonded patterned microfluidic channel

the channel are bright while the surrounding areas are dark. The channel edge is also visible indicating that Fn has adsorbed to edge between channel wall and patterned surface.

Channel leakage is a common problem with all microfluidic systems. Channels created through reversible bonding between PDMS and PDMS or PDMS and glass are more prone to this problem, as the seal is not as strong as an irreversible bond. Leaks become more common with increased flow rate and when forces are applied to the interconnects which connect the channel to a pump. The interconnects in this system were blunt tips needles which connected a syringe pump to the channel. Each time there was a solution change the needle was removed and replaced with new needle to reduce contamination of the bulk solution. Cell culture inside of a microfluidic device involves several solution changes, thus reversible bonding is not robust enough for cell culture

## 5.3.2 Irreversibly Bonded Patterned Channels

### 5.3.2.1 PDMS-PDMS and PDMS-Glass bonding

When PDMS is exposed to a gaseous plasma, the surface is bombarded with high energy ions and electrons. These oxidize the polymer, resulting in a hydroxyl-terminated surface. When two of these surfaces come into contact, they can form an irreversible seal at their interface through the formation of bridging Si-O-Si bonds [90,92,118,119]. This type of irreversible bond is typically used to seal PDMS to PDMS, and to glass. If the bond is successful the bulk polymer will tear before the bond fails. Due to hydrophobic recovery of PDMS the bond must be formed less than one minute after plasma treatment to be successful. The speed required to successfully form a bond makes aligning the polymer channel over a patterned surface difficult. Also, both PDMS surfaces must be plasma treated, which would increase the bioactivity of the surface and undo any patterning.

A new bonding method for PDMS-PDMS and PDMS-glass has been developed. This method activates the PDMS surface through magnetron sputtering of a thin aluminum film. The polymer is exposed to an argon plasma before and during film deposition. The aluminum film acts as a capping layer, preventing hydrophobic recovery as long as it remains intact. After etching away the aluminum layer, the hydroxy-rich surface is exposed and able to form an irreversible bond.

To create a PDMS-glass bond, the polymer is aluminum treated while the glass is cleaned with hydrochloric acid. Once the aluminum layer is etched away, the treated polymer surface is brought into contact with the glass surface and the two are slightly heated. Similarly to form a PDMS-PDMS bond, both polymer surfaces are aluminum treated. After etching both surfaces, the two are brought into contact and heated. A

Table 5.1: Bonding efficiency, pull-off strength, maximum flow rate and channel pressure for PDMS-glass and PDMS-PDMS sealed devices

<b>Bonding property</b>	<b>Materials</b>	<b>24 hrs</b>	<b>7 days</b>
Bonding Success rate (%)	PDMS-glass	92	83
	PDMS-PDMS	85	79
Pull-off Strength (MPa)	PDMS-glass	$5.7 \pm 0.4$	$3.5 \pm 0.2$
	PDMS-PDMS	$1.9 \pm 0.2$	$1.3 \pm 0.3$
Max. Flow Rate (mL/min)	PDMS-glass	$1.1 \pm 0.7$	$0.6 \pm 0.3$
	PDMS-PDMS	$0.24 \pm 0.09$	$0.17 \pm 0.06$
Max. Channel Pressure (MPa)	PDMS-glass	$2 \pm 1$	$1.2 \pm 0.6$
	PDMS-PDMS	$0.5 \pm 0.2$	$0.3 \pm 0.1$

few minutes can elapse between etching and contact, allowing for time to align the channel over a patterned substrate.

To test the efficiency of bond formation, tensile testing and leakage testing were performed. The tensile test involved pulling up on the thick polymer layer with controlled force until failure occurred in the bond using a pneumatic tensile testing instrument. The results of the tensile tests are compiled in Table 5.1. Bonding occurred 24 hrs and 7 days after aluminum treatment. After 24 hrs, the pull-off strength was  $5.7 \pm 0.4$  and  $1.9 \pm 0.2$  MPa for PDMS-glass and PDMS-PDMS respectively. After 7 days of storage, the pull-off strength decreased to  $3.5 \pm 0.2$  and  $1.3 \pm 0.3$  MPa for PDMS-glass and PDMS-PDMS respectively. Typical values for PDMS-glass and PDMS-PDMS pull off strengths have been reported to be on the order of 0.5 MPa [170]. Even after 7 days of storage, the pull-off strength are larger than those perviously reported.

A leakage test was used to assess the integrity of the bond under flow conditions. A blue aqueous dye was pumped through a straight channel with an increasing flow rate until leakage occurred inside of the channel or the fluid ports (Figure 5.10). The

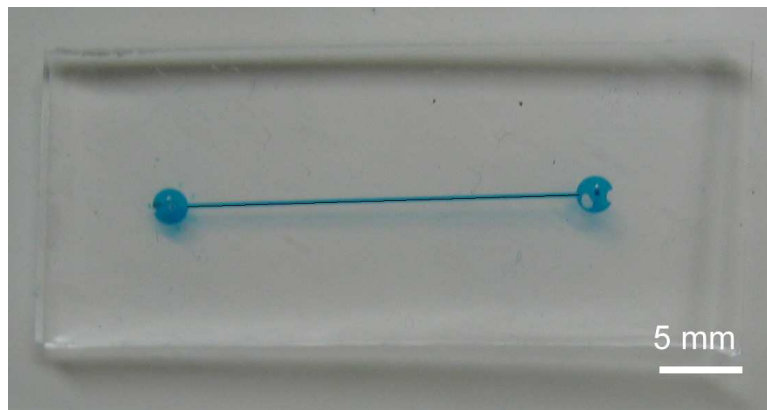


Figure 5.10: Straight channel used for leakage test

maximum flow rates for PDMS-glass and PDMS-PDMS bonded 24 hrs after aluminum deposition were  $1.1 \pm 0.7$  and  $0.24 \pm 0.09$  mL/min respectively, before failure. The maximum flow rate decreased when bonding occurred 7 days after aluminum deposition, to  $0.6 \pm 0.3$  and  $0.17 \pm 0.06$  mL/min. During typical microfluidic applications, flow rates of only a few microliters per minute are used, thus the seals established by this bonding technique greatly exceed the required flow rates. Table 5.1 compiles the maximum flow rate as well as the maximum channel pressure. The maximum channel pressure was calculated using the observed maximum flow rates and the equation for laminar flow in conduits with rectangular transverse cross-sections [171].

### 5.3.2.2 Physical Mask Fabrication

The stencil masks used in previous chapters were commercially available steel mesh. This mesh was only available in limited geometry and sizes. In order to obtain the geometry necessary to create patterned microfluidic devices and increase the versatility of the stencil mask patterning method, customized stencil masks were required. The masks were formed from 100  $\mu\text{m}$  silicon wafer. A thin substrate was used to minimize shadowing during the aluminum deposition. Silicon was chosen as it can be etched

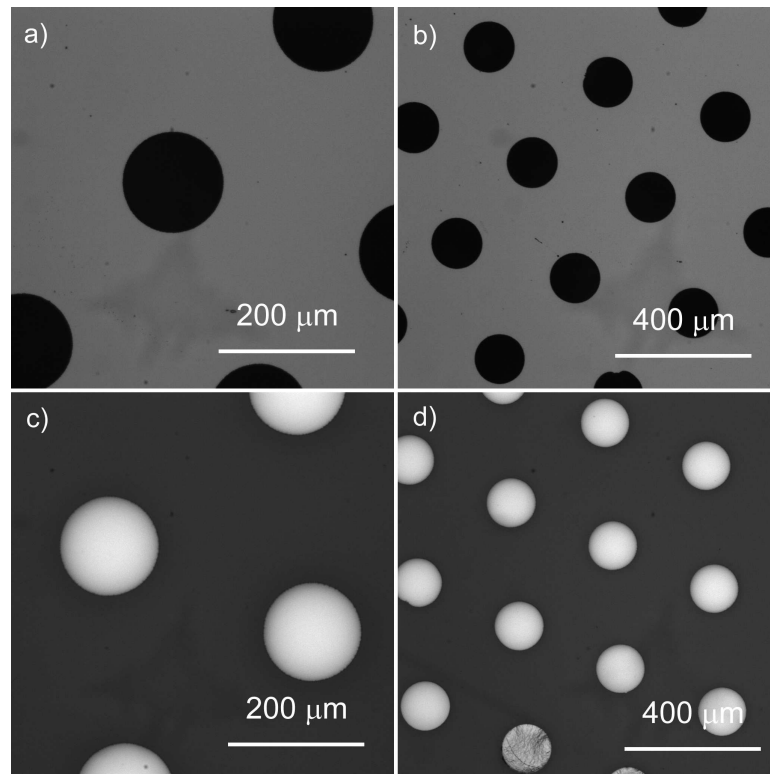


Figure 5.11: Bright field reflection mode optical images of a, b) custom stencil masks made from 100  $\mu\text{m}$  silicon wafers, c, d) Aluminum deposited on PDMS through custom stencil masks

with straight walls using the RIE system available at the Western Nanofabrication facility.

Figure 5.11 a and b, shows a top view of custom stencil masks with 120  $\mu\text{m}$  circular holes etched through them. Figure 5.11 c and d, show aluminum deposited through the same stencil masks onto PDMS. As the aluminum dots maintain the size and shape of the etched holes, little shadowing occurs. PDMS is able to form a seal with silicon allowing for complete contact between the mask and PDMS. As the stencil mask is 100  $\mu\text{m}$  thick the resolution of the stencil mask technique will be limited. While the stencil masks could be reused many times, they are very fragile, limiting their lifetime.

### 5.3.2.3 Chromium Masking

To determine if chromium would act as an effective protective layer for aluminum, the effects of aluminum etching on chromium were tested. Aluminum was deposited through a metal mesh onto the PDMS surface and capped with chromium without moving the metal mesh (Figure 5.12 a). Aluminum was also deposited over the entire PDMS surface and chromium patterned over the surface through a metal mesh (Figure 5.12 b). These surfaces were then etched with orthophosphoric acid to remove aluminum. On both surface the chromium layer remained intact and did not delaminate, indicating that the aluminum layer remained intact underneath (Figure 5.12 c and d).

To ensure that the additional chromium layer and chromium etch would not affect the bioactivity of the modified and unmodified regions on the polymer surface, cells were grown over the new substrates. Figure 5.13 shows cells grown on PDMS surface that have been patterned by depositing aluminum and then chromium through a stencil mask. The metals were removed to exposed the modified polymer surface by first etching away chromium and then aluminum. Cells appear to grow only in the regions that were originally coated with metal, thus the patterning does not appear to be affected by the addition chromium layer or etch.

### 5.3.2.4 Channel Fabrication

The first step in fabricated irreversible bonded patterned channels, is to create a patterned surface. The surface needs to have a non-modified channel shaped feature which is surrounded by aluminum deposited through a magnetron sputtering system. The aluminum can be etched away and the modified surface used to create the irreversible bond. The channel shaped feature also needs to be patterned and



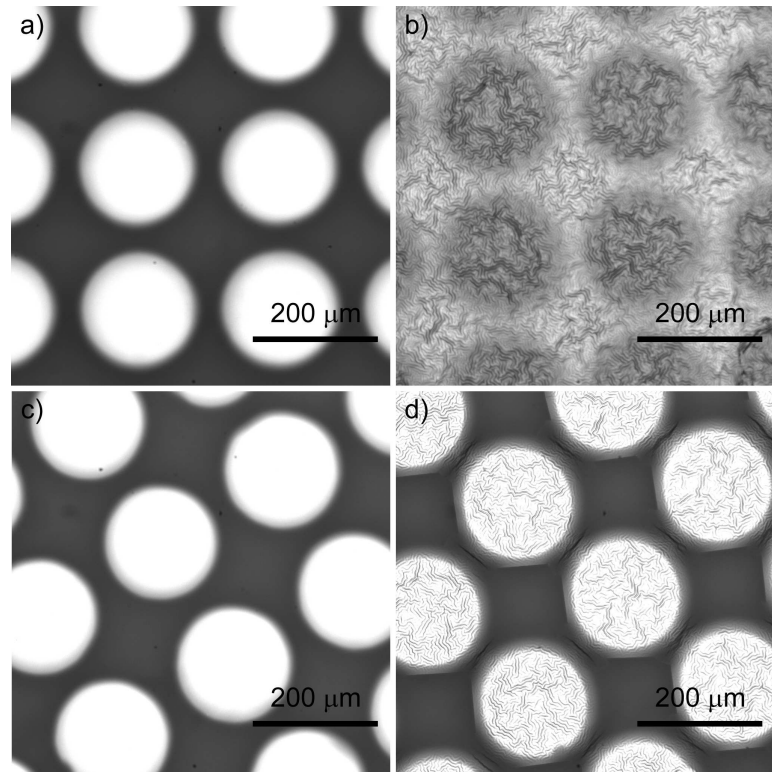


Figure 5.12: Bright field reflection mode optical images of a) chromium dots deposited directly over aluminum dots, b) chromium dots deposited over a non-patterned aluminum layer, c) chromium dots deposited directly over aluminum dots which underwent aluminum etching after chromium deposition d) chromium dots deposited over a non-patterned aluminum layer, which underwent aluminum etching after chromium deposition

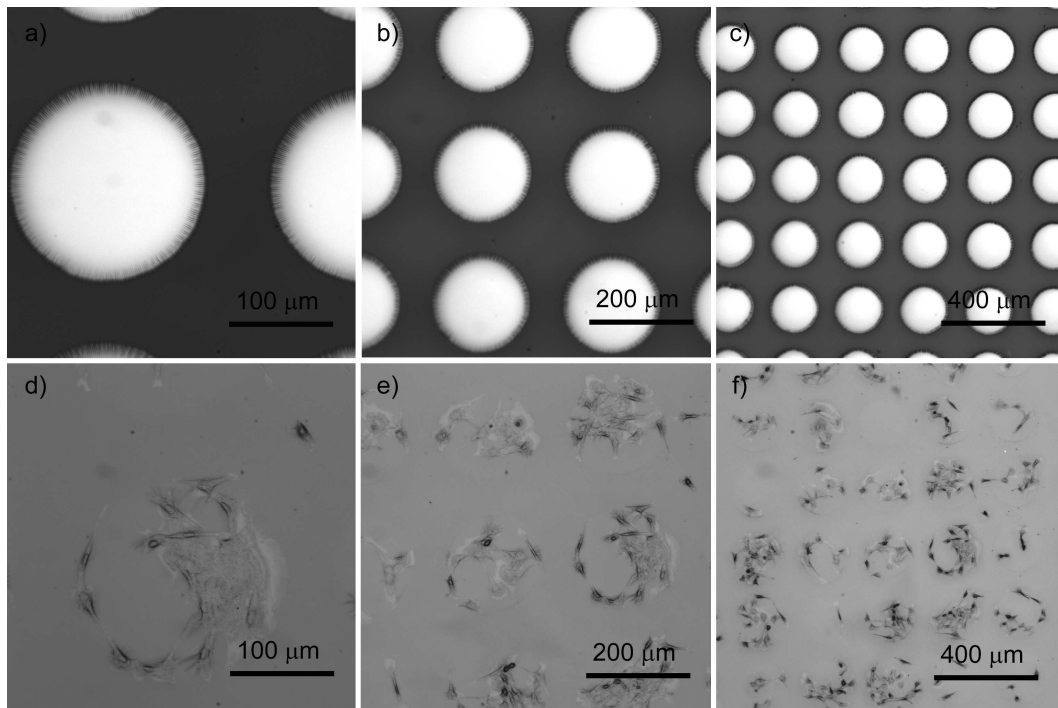


Figure 5.13: Bright field reflection mode optical images a-c) chromium coated aluminum dots on PDMS and d-f) C2C12 cells grown the patterned surface after metal etching

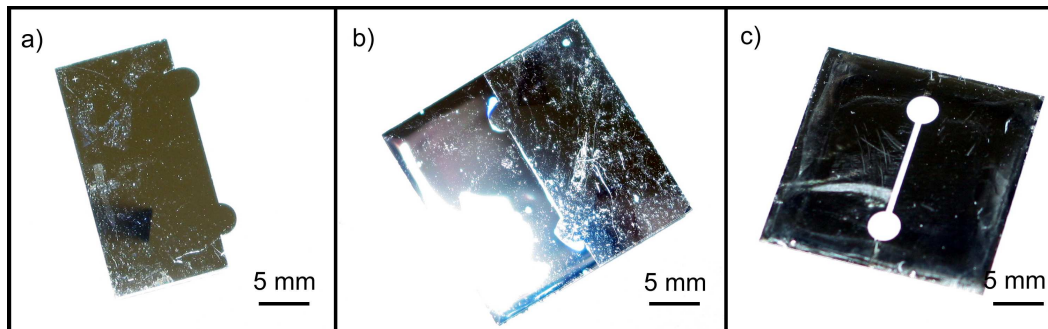


Figure 5.14: Photographs of a) the half channel mask, b) the half channel mask on PDMS after aluminum deposition c) aluminum deposited onto PDMS through two subsequent depositions of aluminum forming a unmodified channel shape region

that pattern protected against aluminum etching. The half channel mask was used to create the channel shaped feature (Figure 5.14). Aluminum and chromium were then deposited through a second mask into the centre of the channel shaped feature (Figure 5.15 a).

Once a patterned surface is created, the second step in the fabrication of irreversibly bonded patterned channels is to bond a molded PDMS channel to the patterned surface. Figure 5.15 b, shows a PDMS channel aligned over the patterned surface. The metal dots are slightly to the side of the channel. This is due to the short alignment time and shifting of the channel when the device was moved from the microscope to the hot plate.

Chromium etchant was then flowed through the channel to remove the chromium layer; after only 30 sec, both the chromium and aluminum layers were removed. This allows for the elimination of one step when preparing the devices. To visualize the patterned channel, Fg-488 was absorbed to the channel surfaces (Figure 5.15 c). Fg-488 absorbed not only in the dots as expected, but also to a band on the left hand side of the channel. This additional band is part of the polymer surface which was meant to be placed under the PDMS and not inside of the channel. Since the dots

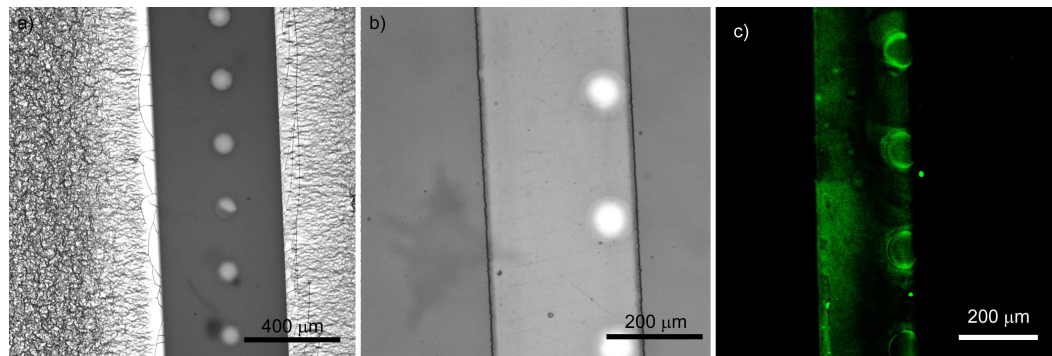


Figure 5.15: Straight channel used for leakage test

were misaligned slightly to the right, this modified area was moved into the channel.

This fabrication method has seven major steps: the two aluminum depositions over the half channel, the aluminum deposition to create dots, the chromium deposition, the first aluminum etch, the bonding of the channel and the final metal etch. The first four steps involve alignment, which needs to be accurate within a few micrometers. This fabrication process is very time consuming and suffers from low yields. The use of a photolithographic patterned method would simplify the fabrication process by reducing the need for three aluminum deposition and one chromium deposition to only one aluminum deposition. Also instead of aligning the stencil mask and the channel, only channel alignment would be required. Since neither photolithographic cell patterning method provides complete control over cell adhesion, a more effective photolithographic based patterning method is needed.

## 5.4 Conclusion

Both reversibly and irreversibly sealed patterned PDMS microfluidic channels were fabricated. The reversibly sealed devices were simple to fabricate but were not robust enough for cell culture or transport. The fabrication of irreversibly sealed devices was more complex, but once created they were more robust.

A new PDMS-PDMS and PDMS-glass bonding technique was established. This technique utilized the chemical changes that occurred during aluminum treatment to form Si-O-Si links between the two surfaces. The aluminum layer allowed bonding to occur several days after initial treatment. Once etched, a few minutes could elapse between etching and bonding, allowing more time for alignment than provided by conventional bonding methods.

New custom stencil masks were created from 100  $\mu\text{m}$  thick silicon wafers using photolithography and RIE. These masks allowed for a variety of geometries and sizes, but were significantly more fragile than commercially available steel mesh.

Chromium was shown to be an effective protecting layer for aluminum during aluminum etching. This allowed aluminum dots to remain intact during bonding of the irreversibly sealed devices.

The irreversibly sealed devices were time consuming to fabricate due to the significant number of steps. Their fabrication also suffered from a low yield due to alignment issues. The use of a photolithographic patterning method could greatly reduce the fabrication time and increase the fabrication yield.

## Chapter 6

### Thesis Summary and Future Work

Micropatterning cellular adhesion is important in many research applications, including fundamental studies of cell interactions, cellular microarrays and cell based biosensors. Controlling cell positions in order to align them with microdetectors is necessary for cell based biosensors, which are often integrated into microfluidic environments. Thus the ability to not only pattern cells on flat substrates, but also inside microfluidic channels, is important for cell based biosensor advancement.

There are many surface properties which affect the ability of cells to adhere: chemistry, wettability, charge, roughness and material stiffness. Patterning these properties allows for spatial control over cell attachment. Of these properties, wettability is often considered the most important as it directly affects the conformation of mediating proteins on the surface.

This thesis reported three methods of patterning surface wettability on an important biomaterial, PDMS. PDMS is naturally hydrophobic and limits cell adhesion due to closely packed methyl groups at its surface. A modified plasma technique was used to oxidize the surface, creating a silica-like hydrophilic layer. This technique involved the deposition of aluminum by a magnetron sputtering system. The aluminum layer prevented hydrophobic recovery of the polymer surface while it remained intact. Once the aluminum layer was etched away the silica-like layer was exposed. The silica-like layer showed an increase in oxygen and decrease in carbon

content by XPS, and was found to be three times stiffer than native PDMS. The modification also increased the surface roughness due to the formation of random sinusoidal ripples as seen by AFM.

To pattern this aluminum surface treatment, aluminum was deposited onto the surface through a stencil mask. The mask prevented the covered PDMS regions from undergoing oxidation, allowing them to remain hydrophobic. After aluminum etching, the surface contained hydrophilic silica-like regions surrounded by hydrophobic PDMS. Water droplets formed only in the modified regions when the surface was dipped in water. These pattern surface showed good cell patterning, with cells only being able to adhere to the modified regions.

While the stencil mask technique proved successful, it was limited in its geometry and feature size. To overcome these deficiencies, two patterning methods were developed, which allowed for photolithography patterning of the surface wettability. As PDMS is not compatible with most conventional photoresists, photolithography could not be performed directly on the polymer. Instead, the entire polymer was coated with aluminum. Under the aluminum, the polymer was modified and formed a hydrophilic silica-like layer. Photolithography was used to enable the removal of selected portions of the aluminum layer. The exposed portions were made hydrophobic by one of two methods: i) allowing them to recover their hydrophobicity; and ii) reacting with a methyl terminated alkyl silane. After the exposed surface was made hydrophobic, the remaining aluminum layer was etched away to reveal hydrophilic silica-like regions. Both methods proved successful at patterning surface wettability and only formed water droplets in the freshly exposed polymer regions when dipped in water. However, only the second method, i.e. reacting the surface with a methyl terminated alkyl silane, proved effective at controlling cell adhesion. Even so, this method was not as successful at controlling cell adhesion as the stencil mask approach,

as cells were able to adhere and spread on the hydrophobic surface.

The hydrophobically recovered surface did not fully recover and remained slightly hydrophilic even after several days in air. Once placed in an aqueous environment, it became even more hydrophilic, and thus cells could interact with a slightly hydrophilic, not a hydrophobic surface. The alkyl silane modified surface was hydrophobic with a contact angle only slightly less than that of native PDMS. Even so, it maintained the surface topography and stiffness of the silica-like layer.

The number of cells attached to each surface was determined. PDMS showed the smallest number of cells attached, followed by the methyl terminated alkyl silane surface. The aluminum treated surface and its hydrophobically recovered counterpart, showed very similar cell interactions, showing the greatest number of cells.

To further understand the interaction of cells with the patterned surface, the relative amount of protein adsorption was visualized on the patterned surfaces. Protein adsorption did not correlate with cellular adhesion, for either protein studied, Fn and Fg. The adsorption was found to be surface, protein and concentration dependent. Fn was tested for conformation using a monoclonal antibody specific for the RGD peptide sequence found on Fn binding sites. Using immunofluorescent labeling, the relative amount of Fn in an appropriate binding configuration was determined for each patterned surface. The conformation pattern correlated to cell attachment when Fn was adsorbed in the presence of BSA, which is a reasonable model system for a cell culturing environment.

As the stencil mask patterning technique was the most successful, it was used to pattern microfluidic channels. Using reversibly sealed devices, formed when two pieces of PDMS are brought into contact, simple patterned channels were developed. These channels were not able to maintain high flow rates, and often failed during fluid changes. To prevent this, an irreversible seal was desired. As conventional



plasma methods would destroy any sample patterning and did not provide enough time to align the channel over the patterned surface, a new bonding technique was developed which allowed the two surface to bond using the magnetron deposition of aluminum. This technique allowed for patterning the bonding areas and thus did not interfere with the patterns designed for cell adhesion. To do this, custom stencil masks were fabricated from 100  $\mu\text{m}$  thick silicon wafers, and chromium was used to protect the regions meant for cell patterning during bonding. Irreversibly bonded patterned microfluidic channels were thereby fabricated. This fabrication took many steps and suffered from alignment issues. The use of photolithographic patterning could substantially reduce the number of steps required for fabrication.

While stencil mask patterning was more effective at controlling cell attachment, photolithographic methods are desirable. Not only do photolithographic methods provide better resolution, and can form any two dimensional shape, they can reduce the number of fabrication steps required to form irreversibly bonded patterned microfluidic channels. To improve our current photolithographic methods the bioactivities of the surrounding regions must be further reduced. This can be accomplished by further increasing the surfaces' hydrophobicity or incorporating chemistries known to significantly reduce bioactivity, such as PEG.

In addition to the use of PDMS for the production of patterned bioactivity, PDMS is optically transparent it is an ideal material when optical detection techniques are used for cell based biosensors. Further, PDMS is commonly used in the creation of microfluidic devices, which are important in controlling the chemical environment of cells. PDMS will continue to play a important role in the medical and bio-device industries, making the ability to control the surface chemistry and bioactivity important for future development.

## References

- [1] R. Freshney, *Culture of Animal Cells: A Manual of Basic Technique*, 5th ed. New York: Wiley-Liss, 2005. 1, 3, 6
- [2] T. Park and M. Shuler, "Integration of cell culture and microfabrication technology," *Biotechnology Progress*, vol. 19, no. 2, pp. 243–253, 2003. 1, 2, 26, 127, 128
- [3] D. Falconnet, G. Csucs, H. Michelle Grandin, and M. Textor, "Surface engineering approaches to micropattern surfaces for cell-based assays," *Biomaterials*, vol. 27, no. 16, pp. 3044–3063, 2006. 2, 8, 9, 26
- [4] F. Yap and Y. Zhang, "Protein and cell micropatterning and its integration with micro/nanoparticles assembly," *Biosensors and Bioelectronics*, vol. 22, no. 6, pp. 775–788, 2007. 2, 8, 9, 11, 13, 26
- [5] R. Kane, S. Takayama, E. Ostuni, D. Ingber, and G. Whitesides, "Patterning proteins and cells using soft lithography," *Biomaterials*, vol. 20, pp. 2363–2376, 1999. 2, 11, 13, 26
- [6] R. Singhvi, A. Kumar, G. Lopez, G. Stephanopoulos, D. Wang, G. Whitesides, and D. Ingber, "Engineering cell shape and function," *Science*, vol. 264, no. 5159, pp. 696–698, 1994. 2, 13, 26
- [7] C. Chen, M. Mrksich, S. Huang, G. Whitesides, and D. Ingber, "Geometric control of cell life and death," *Science*, vol. 276, no. 5317, pp. 1425–1428, 1997. 2, 26
- [8] M. Bailly, L. Yan, G. Whitesides, J. Condeelis, and J. Segall, "Regulation of Protrusion Shape and Adhesion to the Substratum during Chemotactic Responses of Mammalian Carcinoma Cells\* 1," *Experimental Cell Research*, vol. 241, no. 2, pp. 285–299, 1998. 2, 26
- [9] S. Bhatia, M. Yarmush, and M. Toner, "Controlling cell interactions by micropatterning in co-cultures: hepatocytes and 3T3 fibroblasts," *Journal of Biomedical Materials Research Part A*, vol. 34, no. 2, pp. 189–199, 1997. 2, 11
- [10] C. Chen, M. Mrksich, S. Huang, G. Whitesides, and D. Ingber, "Micropatterned surfaces for control of cell shape, position, and function," *Biotechnology Progress*, vol. 14, no. 3, pp. 356–363, 1998. 2, 12

- [11] F. Asphahani, M. Thein, O. Veisoh, D. Edmondson, R. Kosai, M. Veisoh, J. Xu, and M. Zhang, "Influence of cell adhesion and spreading on impedance characteristics of cell-based sensors," *Biosensors and Bioelectronics*, vol. 23, no. 8, pp. 1307–1313, 2008. 2
- [12] A. Aravanis, B. DeBusschere, A. Chruscinski, K. Gilchrist, B. Kobilka, and G. Kovacs, "A genetically engineered cell-based biosensor for functional classification of agents," *Biosensors and Bioelectronics*, vol. 16, no. 7-8, pp. 571–577, 2001. 2
- [13] A. Rudolph and J. Reasor, "Cell and tissue based technologies for environmental detection and medical diagnostics," *Biosensors and Bioelectronics*, vol. 16, no. 7-8, pp. 429–431, 2001. 2
- [14] J. Pancrazio, J. Whelan, D. Borkholder, W. Ma, and D. Stenger, "Development and application of cell-based biosensors," *Annals of Biomedical Engineering*, vol. 27, no. 6, pp. 697–711, 1999. 2
- [15] K. Anselme, "Osteoblast adhesion on biomaterials," *Biomaterials*, vol. 21, no. 7, pp. 667–681, 2000. 3, 6, 62, 64, 80, 83, 95, 96
- [16] C. Wilson, R. Clegg, D. Leavesley, and M. Percy, "Mediation of biomaterial-cell interactions by adsorbed proteins: a review," *Tissue Engineering*, vol. 11, no. 1-2, pp. 1–18, 2005. 3, 4, 6, 7, 64, 80, 83
- [17] C. Haynes and W. Norde, "Globular proteins at solid/liquid interfaces," *Colloids and Surfaces B: Biointerfaces*, vol. 2, no. 6, pp. 517–566, 1994. 4
- [18] J. Vitte, A. Benoliel, A. Pierres, and P. Bongrand, "Is there a predictable relationship between surface physical-chemical properties and cell behaviour at the interface," *European Cells and Materials*, vol. 7, pp. 52–63, 2004. 4, 62, 64, 95, 96
- [19] H. Elwing, L. Li, A. Askendal, G. Nimeri, and J. Brash, *Protein displacement phenomena in blood plasma and serum studied by the wettability gradient method and the lens-on-surface method*. Washington DC: American Chemical Society, 1995, vol. 602, ch. 10, pp. 138–149. 4
- [20] U. Jonsson, B. Ivarsson, I. Lundstrom, and L. Bergheim, "Adsorption behavior of fibronectin on well-characterized silica surfaces," *Journal of Colloid and Interface Science*, vol. 90, no. 1, pp. 148–163, 1982. 4
- [21] D. MacDonald, N. Deo, B. Markovic, M. Stranick, and P. Somasundaran, "Adsorption and dissolution behavior of human plasma fibronectin on thermally and chemically modified titanium dioxide particles," *Biomaterials*, vol. 23, no. 4, pp. 1269–1279, 2002. 4

- [22] W. Norde and C. Giacomelli, "BSA structural changes during homomolecular exchange between the adsorbed and the dissolved states," *Journal of Biotechnology*, vol. 79, no. 3, pp. 259–268, 2000. 4
- [23] W. Norde and C. Giacomelli, "Conformational changes in proteins at interfaces: from solution to the interface and back," *Macromolecular Symposia*, vol. 145, pp. 125–136, 1999. 4
- [24] C. Giacomelli and W. Norde, "The adsorption-desorption cycle. Reversibility of the BSA-silica system," *Journal of Colloid and Interface Science*, vol. 233, no. 2, pp. 234–240, 2001. 4
- [25] B. Keselowsky, D. Collard, and A. García, "Surface chemistry modulates fibronectin conformation and directs integrin binding and specificity to control cell adhesion," *Journal of Biomedical Materials Research Part A*, vol. 66, no. 2, pp. 247–259, 2003. 4, 65, 88
- [26] K. Michael, V. Vernekar, B. Keselowsky, J. Meredith, R. Latour, and A. Garcia, "Adsorption-induced conformational changes in fibronectin due to interactions with well-defined surface chemistries," *Langmuir*, vol. 19, no. 19, pp. 8033–8040, 2003. 4, 64, 65, 88, 92
- [27] C. Barrias, M. Martins, G. Almeida-Porada, M. Barbosa, and P. Granja, "The correlation between the adsorption of adhesive proteins and cell behaviour on hydroxyl-methyl mixed self-assembled monolayers," *Biomaterials*, vol. 30, no. 3, pp. 307–316, 2009. 4, 6
- [28] A. Garcia, M. Vega, and D. Boettiger, "Modulation of cell proliferation and differentiation through substrate-dependent changes in fibronectin conformation," *Molecular biology of the cell*, vol. 10, no. 3, p. 785, 1999. 6, 64, 65, 88
- [29] B. Dalton, C. McFarland, T. Gengenbach, H. Griesser, and J. Steele, "Polymer surface chemistry and bone cell migration," *Journal of Biomaterials Science, Polymer Edition*, vol. 9, no. 8, pp. 781–799, 1998. 6
- [30] K. Webb, V. Hlady, and P. Tresco, "Relationships among cell attachment, spreading, cytoskeletal organization, and migration rate for anchorage-dependent cells on model surfaces," *Journal of Biomedical Materials Research Part A*, vol. 49, no. 3, pp. 362–368, 1999. 6, 61
- [31] K. Webb, V. Hlady, and P. Tresco, "Relative importance of surface wettability and charged functional groups on NIH 3T3 fibroblast attachment, spreading, and cytoskeletal organization," *Journal of Biomedical Materials Research Part A*, vol. 41, no. 3, pp. 422–430, 1998. 6

- [32] G. Altankov, F. Grinnell, and T. Groth, "Studies on the biocompatibility of materials: fibroblast reorganization of substratum-bound fibronectin on surfaces varying in wettability," *Journal of Biomedical Materials Research Part A*, vol. 30, no. 3, pp. 385–391, 1998. 6
- [33] T. Ruardy, J. Schakenraad, H. Van der Mei, and H. Busscher, "Adhesion and spreading of human skin fibroblasts on physicochemically characterized gradient surfaces," *Journal of Biomedical Materials Research*, vol. 29, no. 11, pp. 1415–1423, 2004. 6
- [34] Z. Yang, J. Galloway, and H. Yu, "Protein interactions with poly (ethylene glycol) self-assembled monolayers on glass substrates: diffusion and adsorption," *Langmuir*, vol. 15, no. 24, pp. 8405–8411, 1999. 6
- [35] E. Tziampazis, J. Kohn, and P. Moghe, "PEG-variant biomaterials as selectively adhesive protein templates: model surfaces for controlled cell adhesion and migration," *Biomaterials*, vol. 21, no. 5, pp. 511–520, 2000. 6
- [36] J. Dames, B. Causton, Y. Bovell, K. Davy, and C. Sturt, "The migration of osteoblasts over substrata of discrete surface charge," *Biomaterials*, vol. 7, no. 3, pp. 231–233, 1986. 6, 7
- [37] R. Shelton, A. Rasmussen, and J. Davies, "Protein adsorption at the interface between charged polymer substrata and migrating osteoblasts," *Biomaterials*, vol. 9, no. 1, pp. 24–29, 1988. 6, 7
- [38] A. Kishida, H. Iwata, Y. Tamada, and Y. Ikada, "Cell behaviour on polymer surfaces grafted with non-ionic and ionic monomers," *Biomaterials*, vol. 12, no. 8, pp. 786–792, 1991. 6
- [39] Y. Arima and H. Iwata, "Effects of surface functional groups on protein adsorption and subsequent cell adhesion using self-assembled monolayers," *Journal of Materials Chemistry*, vol. 17, no. 38, pp. 4079–4087, 2007. 6, 61
- [40] M. Lampin, R. Warocquier-Clerout, C. Legris, M. Degrange, and M. Sigot-Luizard, "Correlation between substratum roughness and wettability, cell adhesion, and cell migration," *Journal of Biomedical Materials Research Part A*, vol. 36, no. 1, pp. 99–108, 1998. 7, 96
- [41] D. Deligianni, N. Katsala, P. Koutsoukos, and Y. Missirlis, "Effect of surface roughness of hydroxyapatite on human bone marrow cell adhesion, proliferation, differentiation and detachment strength," *Biomaterials*, vol. 22, no. 1, pp. 87–96, 2001. 7, 96

- [42] H. Huang, C. Ho, T. Lee, T. Lee, K. Liao, and F. Chen, "Effect of surface roughness of ground titanium on initial cell adhesion," *Biomolecular Engineering*, vol. 21, no. 3-5, pp. 93–97, 2004. 7, 96
- [43] K. Bowers, J. Keller, B. Randolph, D. Wick, and C. Michaels, "Optimization of surface micromorphology for enhanced osteoblast responses in vitro." *The International Journal of Oral & Maxillofacial Implants*, vol. 7, no. 3, p. 302, 1992. 7, 96
- [44] M. Costa, H. Rodríguez, M. Machado, J. Mano, R. Gómez, P. Monleón, and S. Salmerón, "Human chondrocyte morphology, its dedifferentiation, and fibronectin conformation on different PLLA microtopographies." *Tissue Engineering, Part A*, vol. 14, no. 10, p. 1751, 2008. 7
- [45] E. Martines, K. Seunarine, H. Morgan, N. Gadegaard, C. Wilkinson, and M. Riehle, "Superhydrophobicity and superhydrophilicity of regular nanopatterns," *Nano Letters*, vol. 5, no. 10, pp. 2097–2103, 2005. 7
- [46] B. Wojciak-Stothard, A. Curtis, M. McGrath, I. Sommer, C. Wilkinson, and W. Monaghan, "Role of the cytoskeleton in the reaction of fibroblasts to multiple grooved substrata," *Cell Motility and the Cytoskeleton*, vol. 31, no. 2, pp. 147–158, 1995. 7
- [47] A. Green, J. Jansen, J. Van der Waerden, and A. Von Recum, "Fibroblast response to microtextured silicone surfaces: Texture orientation into or out of the surface," *Journal of biomedical materials research*, vol. 28, no. 5, pp. 647–653, 1994. 7
- [48] F. Luthen, R. Lange, P. Becker, J. Rychly, U. Beck, and J. Nebe, "The influence of surface roughness of titanium on [beta] 1-and [beta] 3-integrin adhesion and the organization of fibronectin in human osteoblastic cells," *Biomaterials*, vol. 26, no. 15, pp. 2423–2440, 2005. 7
- [49] T. Kunzler, T. Drobek, M. Schuler, and N. Spencer, "Systematic study of osteoblast and fibroblast response to roughness by means of surface-morphology gradients," *Biomaterials*, vol. 28, no. 13, pp. 2175–2182, 2007. 7
- [50] P. Janmey, J. Winer, M. Murray, and Q. Wen, "The hard life of soft cells," *Cell Motility and the Cytoskeleton*, vol. 66, no. 8, pp. 597–605, 2009. 8
- [51] S. Nemir and J. West, "Synthetic materials in the study of cell response to substrate rigidity," *Annals of Biomedical Engineering*, vol. 38, no. 1, pp. 2–20, 2010. 8, 96
- [52] J. Wong, J. Leach, and X. Brown, "Balance of chemistry, topography, and mechanics at the cell-biomaterial interface: issues and challenges for assessing

- the role of substrate mechanics on cell response,” *Surface Science*, vol. 570, no. 1-2, pp. 119–133, 2004. 8, 96
- [53] J. Wong, A. Velasco, P. Rajagopalan, and Q. Pham, “Directed Movement of Vascular Smooth Muscle Cells on Gradient-Compliant Hydrogels,” *Langmuir*, vol. 19, no. 5, pp. 1908–1913, 2003. 8, 96, 125
- [54] N. Zaari, P. Rajagopalan, S. Kim, A. Engler, and J. Wong, “Photopolymerization in microfluidic gradient generators: Microscale control of substrate compliance to manipulate cell response,” *Advanced Materials*, vol. 16, no. 23-24, pp. 2133–2137, 2004. 8, 96, 125
- [55] T. Yeung, P. Georges, L. Flanagan, B. Marg, M. Ortiz, M. Funaki, N. Zahir, W. Ming, V. Weaver, and P. Janmey, “Effects of substrate stiffness on cell morphology, cytoskeletal structure, and adhesion,” *Cell Motility and the Cytoskeleton*, vol. 60, no. 1, pp. 24–34, 2005. 8, 96, 125
- [56] Z. Cui, *Micro-Nanofabrication: Technologies and Applications*. Beijing, China: Higher Education Press, 2005. 8, 13, 47
- [57] B. Spargo, M. Testoff, T. Nielsen, D. Stengerf, J. Hickman, and A. Rudolph, “Spatially controlled adhesion, spreading, and differentiation of endothelial cells on self-assembled molecular monolayers,” *Proceedings of the National Academy of Sciences of the United States of America*, vol. 91, no. 23, p. 11070, 1994. 9
- [58] S. Britland, P. Clark, P. Connolly, and G. Moores, “Micropatterned substratum adhesiveness: a model for morphogenetic cues controlling cell behavior,” *Experimental Cell Research*, vol. 198, no. 1, pp. 124–129, 1992. 9
- [59] S. Britland, E. Perez-Arnaud, P. Clark, B. McGinn, P. Connolly, and G. Moores, “Micropatterning proteins and synthetic peptides on solid supports: a novel application for microelectronics fabrication technology,” *Biotechnology Progress*, vol. 8, no. 2, pp. 155–160, 1992. 9
- [60] K. Healy, C. Thomas, A. Reznia, J. Kim, P. McKeown, B. Lom, and P. Hockberger, “Kinetics of bone cell organization and mineralization on materials with patterned surface chemistry,” *Biomaterials*, vol. 17, no. 2, pp. 195–208, 1996. 9
- [61] D. Kleinfeld, K. Kahler, and P. Hockberger, “Controlled outgrowth of dissociated neurons on patterned substrates,” *Journal of Neuroscience*, vol. 8, no. 11, pp. 4098–4120, 1988. 9
- [62] B. Lom, K. Healy, and P. Hockberger, “A versatile technique for patterning biomolecules onto glass coverslips,” *Journal of Neuroscience Methods*, vol. 50, no. 3, pp. 385–397, 1993. 9

- [63] C. Scotchford, M. Ball, M. Winkelmann, J. Voros, C. Csucs, D. Brunette, G. Danuser, and M. Textor, "Chemically patterned, metal-oxide-based surfaces produced by photolithographic techniques for studying protein-and cell-interactions. II: Protein adsorption and early cell interactions," *Biomaterials*, vol. 24, no. 7, pp. 1147–1158, 2003. 11
- [64] M. Veiseh, B. Wickes, D. Castner, and M. Zhang, "Guided cell patterning on gold-silicon dioxide substrates by surface molecular engineering," *Biomaterials*, vol. 25, no. 16, pp. 3315–3324, 2004. 11
- [65] M. Mrksich, L. Dike, J. Tien, D. Ingber, and G. Whitesides, "Using microcontact printing to pattern the attachment of mammalian cells to self-assembled monolayers of alkanethiolates on transparent films of gold and silver," *Experimental Cell Research*, vol. 235, no. 2, pp. 305–313, 1997. 12
- [66] Y. Xia, M. Mrksich, E. Kim, and G. Whitesides, "Microcontact printing of octadecylsiloxane on the surface of silicon dioxide and its application in micro-fabrication," *Journal of the American Chemical Society*, vol. 117, no. 37, pp. 9576–9577, 1995. 13
- [67] A. Bernard, E. Delamarche, H. Schmid, B. Michel, H. Bosshard, and H. Biebuyck, "Printing patterns of proteins," *Langmuir*, vol. 14, no. 9, pp. 2225–2229, 1998. 13
- [68] G. Fiorini and D. Chiu, "Disposable microfluidic devices: fabrication, function, and application," *Biotechniques*, vol. 38, no. 3, pp. 429–446, 2005. 13
- [69] D. Chiu, N. Jeon, S. Huang, R. Kane, C. Wargo, I. Choi, D. Ingber, and G. Whitesides, "Patterned deposition of cells and proteins onto surfaces by using three-dimensional microfluidic systems," *Proceedings of the National Academy of Sciences*, vol. 97, no. 6, pp. 2408–2413, 2000. 13, 26
- [70] W. Tan and T. Desai, "Microfluidic patterning of cells in extracellular matrix biopolymers: effects of channel size, cell type, and matrix composition on pattern integrity," *Tissue Engineering*, vol. 9, no. 2, pp. 255–267, 2003. 13, 26
- [71] A. Folch, A. Ayon, O. Hurtado, M. Schmidt, and M. Toner, "Molding of deep polydimethylsiloxane microstructures for microfluidics and biological applications," *Journal of Biomechanical Engineering*, vol. 121, pp. 28–35, 1999. 13
- [72] A. Folch and M. Toner, "Cellular micropatterns on biocompatible materials," *Biotechnology Progress*, vol. 14, no. 3, pp. 388–392, 1998. 13
- [73] M. De Silva, R. Desai, and D. Odde, "Micro-patterning of animal cells on PDMS substrates in the presence of serum without use of adhesion inhibitors," *Biomedical Microdevices*, vol. 6, no. 3, pp. 219–222, 2004. 13



- [74] E. Delamarche, A. Bernard, H. Schmid, B. Michel, and H. Biebuyck, "Patterned delivery of immunoglobulins to surfaces using microfluidic networks," *Science*, vol. 276, no. 5313, pp. 779–781, 1997. 13
- [75] E. Delamarche, A. Bernard, H. Schmid, A. Bietsch, B. Michel, and H. Biebuyck, "Microfluidic networks for chemical patterning of substrates: design and application to bioassays," *Journal of the American Chemical Society*, vol. 120, no. 3, pp. 500–508, 1998. 13, 22, 26
- [76] N. Patel, R. Padera, G. Sanders, S. Cannizzaro, M. Davies, R. Langer, C. Roberts, S. Tendler, P. Williams, and K. Shakesheff, "Spatially controlled cell engineering on biodegradable polymer surfaces," *The Journal of the Federation of American Societies for Experimental Biology*, vol. 12, no. 14, pp. 1447–1454, 1998. 13
- [77] A. Folch, B. Jo, O. Hurtado, D. Beebe, and M. Toner, "Microfabricated elastomeric stencils for micropatterning cell cultures," *Journal of Biomedical Materials Research Part A*, vol. 52, no. 2, pp. 346–353, 2000. 15
- [78] E. Ostuni, R. Kane, C. Chen, D. Ingber, and G. Whitesides, "Patterning mammalian cells using elastomeric membranes," *Langmuir*, vol. 16, no. 20, pp. 7811–7819, 2000. 15
- [79] H. Hatakeyama, A. Kikuchi, M. Yamato, and T. Okano, "Patterned biofunctional designs of thermoresponsive surfaces for spatiotemporally controlled cell adhesion, growth, and thermally induced detachment," *Biomaterials*, vol. 28, no. 25, pp. 3632–3643, 2007. 15
- [80] G. Kim, B. Kim, and J. Brugger, "All-photoplastic microstencil with self-alignment for multiple layer shadow-mask patterning," *Sensors and Actuators A: Physical*, vol. 107, no. 2, pp. 132–136, 2003. 15
- [81] A. Tourovskaia, T. Barber, B. Wickes, D. Hirdes, B. Grin, D. Castner, K. Healy, and A. Folch, "Micropatterns of chemisorbed cell adhesion-repellent films using oxygen plasma etching and elastomeric masks," *Langmuir*, vol. 19, no. 11, pp. 4754–4764, 2003. 15
- [82] C. Thomas, J. Lhoest, D. Castner, C. McFarland, and K. Healy, "Surfaces designed to control the projected area and shape of individual cells," *Journal of Biomechanical Engineering*, vol. 121, p. 40, 1999. 15
- [83] L. Pardo, W. Wilson Jr, and T. Boland, "Characterization of Patterned Self-Assembled Monolayers and Protein Arrays Generated by the Ink-Jet Method," *Langmuir*, vol. 19, no. 5, pp. 1462–1466, 2003. 16

- [84] E. Roth, T. Xu, M. Das, C. Gregory, J. Hickman, and T. Boland, "Inkjet printing for high-throughput cell patterning," *Biomaterials*, vol. 25, no. 17, pp. 3707–3715, 2004. 16
- [85] N. Sanjana and S. Fuller, "A fast flexible ink-jet printing method for patterning dissociated neurons in culture," *Journal of Neuroscience Methods*, vol. 136, no. 2, pp. 151–163, 2004. 16
- [86] F. Turcu, K. Tratsk-Nitz, S. Thanos, W. Schuhmann, and P. Heiduschka, "Inkjet printing for micropattern generation of laminin for neuronal adhesion," *Journal of Neuroscience Methods*, vol. 131, no. 1-2, pp. 141–148, 2003. 16
- [87] W. Wilson Jr and T. Boland, "Cell and organ printing 1: protein and cell printers," *The Anatomical Record Part A: Discoveries in Molecular, Cellular, and Evolutionary Biology*, vol. 272, no. 2, pp. 491–496, 2003. 16
- [88] J. McDonald, D. Duffy, J. Anderson, D. Chiu, H. Wu, O. Schueller, and G. Whitesides, "Fabrication of microfluidic systems in poly (dimethylsiloxane)," *Electrophoresis*, vol. 21, no. 1, pp. 27–40, 1999. 16, 25
- [89] H. Makamba, J. Kim, K. Lim, N. Park, and J. Hahn, "Surface modification of poly (dimethylsiloxane) microchannels," *Electrophoresis*, vol. 24, no. 21, pp. 3607–3619, 2003. 16, 19, 20, 21, 25
- [90] D. Duffy, J. McDonald, O. Schueller, and G. Whitesides, "Rapid prototyping of microfluidic systems in poly (dimethylsiloxane)," *Analytical Chemistry*, vol. 70, no. 23, pp. 4974–4984, 1998. 17, 19, 22, 25, 26, 129, 131, 147
- [91] J. McDonald and G. Whitesides, "Poly (dimethylsiloxane) as a material for fabricating microfluidic devices," *Accounts of Chemical Research*, vol. 35, no. 7, pp. 491–499, 2002. 17, 19, 25
- [92] S. Sia and G. Whitesides, "Microfluidic devices fabricated in poly (dimethylsiloxane) for biological studies," *Electrophoresis*, vol. 24, no. 21, pp. 3563–3576, 2003. 17, 22, 25, 129, 147
- [93] S. Hu and N. Dovichi, "Capillary electrophoresis for the analysis of biopolymers," *Analytical Chemistry*, vol. 74, no. 12, pp. 2833–2850, 2002. 19, 25
- [94] J. Lahann, M. Balcels, H. Lu, T. Rodon, K. Jensen, and R. Langer, "Reactive polymer coatings: a first step toward surface engineering of microfluidic devices," *Analytical Chemistry*, vol. 75, no. 9, pp. 2117–2122, 2003. 19, 25
- [95] Y. Dou, N. Bao, J. Xu, and H. Chen, "A dynamically modified microfluidic poly (dimethylsiloxane) chip with electrochemical detection for biological analysis," *Electrophoresis*, vol. 23, no. 20, pp. 3558–3566, 2002. 19, 25

- [96] S. Hu, D. Michels, A. Fazal, C. Ratisoontorn, M. Cunningham, and N. Dovichi, "Capillary sieving electrophoresis/micellar electrokinetic capillary chromatography for two-dimensional protein fingerprinting of single mammalian cells," *Analytical Chemistry*, vol. 76, pp. 4044–4049, 2004. 19
- [97] J. McDonald, D. Duffy, J. Anderson, D. Chiu, H. Wu, O. Schueller, and G. Whitesides, "Fabrication of microfluidic systems in poly (dimethylsiloxane)," *Electrophoresis*, vol. 21, no. 1, pp. 27–40, 2000. 19
- [98] J. Fritz and M. Owen, "Hydrophobic recovery of plasma-treated polydimethylsiloxane," *The Journal of Adhesion*, vol. 54, no. 1, pp. 33–45, 1995. 19, 20, 21, 25, 26, 79
- [99] T. Yang, O. Baryshnikova, H. Mao, M. Holden, and P. Cremer, "Investigations of bivalent antibody binding on fluid-supported phospholipid membranes: the effect of hapten density," *Journal of the American Chemical Society*, vol. 125, no. 16, pp. 4779–4784, 2003. 19
- [100] K. Ro, W. Chang, H. Kim, Y. Koo, and J. Hahn, "Capillary electrochromatography and preconcentration of neutral compounds on poly (dimethylsiloxane) microchips," *Electrophoresis*, vol. 24, no. 18, pp. 3253–3259, 2003. 19
- [101] V. Linder, E. Verpoorte, W. Thormann, N. de Rooij, and H. Sigrist, "Surface biopassivation of replicated poly (dimethylsiloxane) microfluidic channels and application to heterogeneous immunoreaction with on-chip fluorescence detection," *Analytical Chemistry*, vol. 73, no. 17, pp. 4181–4189, 2001. 19
- [102] B. Slentz, N. Penner, and F. Regnier, "Capillary electrochromatography of peptides on microfabricated poly (dimethylsiloxane) chips modified by cerium (IV)-catalyzed polymerization," *Journal of Chromatography A*, vol. 948, no. 1-2, pp. 225–233, 2002. 19
- [103] A. Papra, A. Bernard, D. Juncker, N. Larsen, B. Michel, and E. Delamarche, "Microfluidic networks made of poly (dimethylsiloxane), Si, and Au coated with polyethylene glycol for patterning proteins onto surfaces," *Langmuir*, vol. 17, no. 13, pp. 4090–4095, 2001. 19
- [104] N. Patrito, C. McCague, S. Chiang, P. Norton, and N. Petersen, "Photolithographically patterned surface modification of poly (dimethylsiloxane) via UV-initiated graft polymerization of acrylates," *Langmuir*, vol. 22, no. 8, pp. 3453–3455, 2006. 19, 26, 49
- [105] A. Bubendorfer, X. Liu, and A. Ellis, "Microfabrication of PDMS microchannels using SU-8/PMMA moldings and their sealing to polystyrene substrates," *Smart Materials and Structures*, vol. 16, pp. 367–371, 2007. 19, 21

- [106] C. Séguin, J. McLachlan, P. Norton, and F. Lagugné-Labarthet, "Surface modification of poly (dimethylsiloxane) for microfluidic assay applications," *Applied Surface Science*, vol. 24, no. 21, pp. 3607–3619, 2009. 19, 57
- [107] J. Lai, Y. Lin, Y. Denq, S. Shyu, and J. Chen, "Surface modification of silicone rubber by gas plasma treatment," *Journal of Adhesion Science and Technology*, vol. 10, no. 3, pp. 231–242, 1996. 20
- [108] K. Efimenko, W. Wallace, and J. Genzer, "Surface modification of Sylgard-184 poly (dimethyl siloxane) networks by ultraviolet and ultraviolet/ozone treatment," *Journal of Colloid and Interface Science*, vol. 254, no. 2, pp. 306–315, 2002. 20
- [109] H. Hillborg and U. Gedde, "Hydrophobicity recovery of polydimethylsiloxane after exposure to corona discharges," *Polymer*, vol. 39, no. 10, pp. 1991–1998, 1998. 20
- [110] J. Kim, M. Chaudhury, and O. M.J., "Hydrophobic recovery of polydimethylsiloxane elastomer exposed to partial electrical discharge," *Journal of Colloid and Interface Science*, vol. 226, no. 2, pp. 231–236, June 2000. 20, 21, 79, 116
- [111] F. Katzenberg, "Topographic processing of silicone surfaces," *Surface and Coatings Technology*, vol. 200, no. 1-4, pp. 1097–1100, 2005. 20
- [112] H. Hillborg, J. Ankner, U. Gedde, G. Smith, H. Yasuda, and K. Wikstrom, "Crosslinked polydimethylsiloxane exposed to oxygen plasma studied by neutron reflectometry and other surface specific techniques," *Polymer*, vol. 41, no. 18, pp. 6851–6863, 2000. 20
- [113] H. Hillborg, N. Tomczak, A. Olah, H. Schonherr, and G. Vancso, "Nanoscale hydrophobic recovery: a chemical force microscopy study of UV/ozone-treated cross-linked poly (dimethylsiloxane)," *Langmuir*, vol. 20, no. 3, pp. 785–794, 2004. 20
- [114] A. Olah, H. Hillborg, and G. Vancso, "Hydrophobic recovery of UV/ozone treated poly (dimethylsiloxane): adhesion studies by contact mechanics and mechanism of surface modification," *Applied Surface Science*, vol. 239, no. 3-4, pp. 410–423, 2005. 20
- [115] G. Bausch, J. Stasser, J. Tonge, and M. Owen, "Behavior of plasma-treated elastomeric polydimethylsiloxane coatings in aqueous environment," *Plasmas and Polymers*, vol. 3, no. 1, pp. 23–34, 1998. 20
- [116] G. Bar, L. Delineau, A. Hafele, and M. Whangbo, "Investigation of the stiffness change in, the indentation force and the hydrophobic recovery of

- plasma-oxidized polydimethylsiloxane surfaces by tapping mode atomic force microscopy,” *Polymer*, vol. 42, no. 8, pp. 3627–3632, 2001. 20, 21, 62, 79, 97, 114
- [117] M. Morra, E. Occhiello, R. Marola, F. Garbassi, P. Humphrey, and D. Johnson, “On the aging of oxygen plasma-treated polydimethylsiloxane surfaces,” *Journal of Colloid and Interface Science*, vol. 137, no. 1, pp. 11–24, 1990. 20, 22, 26, 79
- [118] S. Lee and N. Sundararajan, *Microfabrication for Microfluidics*, ser. Intergrated Microsystems Series. Norwood, MA: Actech House Inc., 2010. 22, 128, 129, 137, 147
- [119] J. Zahn, Ed., *Biomicrofabrication and Biomicrofluidics*, ser. Methods in Bioengineering. Altech House Inc., 2010. 22, 128, 129, 147
- [120] N. Patrito, C. McCague, P. Norton, and N. Petersen, “Spatially controlled cell adhesion via micropatterned surface modification of poly (dimethylsiloxane),” *Langmuir*, vol. 23, no. 2, pp. 715–719, 2007. 22, 27, 42, 55, 61
- [121] G. Ocvirk, M. Munroe, T. Tang, R. Oleschuk, K. Westra, and D. Harrison, “Electrokinetic control of fluid flow in native poly (dimethylsiloxane) capillary electrophoresis devices,” *Electrophoresis*, vol. 21, no. 1, pp. 107–115, 1999. 25
- [122] A. Toth, I. Bertoti, B. M., G. Banhegyi, A. Bogнар, and P. Szaplanczay, “oxidative damage and recovery of silicone rubber surface. I. X-ray photoelectron spectroscopic study,” *Journal of Applied Polymer Science*, vol. 52, no. 9, pp. 1293–1307. 25
- [123] L. Sweeney, M. Shuler, J. Babish, and A. Ghanem, “A cell culture analogue of rodent physiology: Application to naphthalene toxicology,” *Toxicology in vitro*, vol. 9, no. 3, pp. 307–316, 1995. 26
- [124] M. Shuler, A. Ghanem, D. Quick, M. Wong, and P. Miller, “A self-regulating cell culture analog device to mimic animal and human toxicological responses,” *Biotechnology and Bioengineering*, vol. 52, no. 1, pp. 45–60, 2000. 26
- [125] R. Langer and J. Vacanti, “Tissue Engineering,” *Science*, vol. 260, no. 5110, pp. 920–926. 26
- [126] S. Rhee, A. Taylor, C. Tu, D. Cribbs, C. Cotman, and N. Jeon, “Patterned cell culture inside microfluidic devices,” *Lab on a Chip*, vol. 5, no. 1, pp. 102–107, 2005. 26
- [127] W. Flack, D. Soong, A. Bell, and D. Hess, “A mathematical model for spin coating polymer resins,” *Journal of Applied Physics*, vol. 56, no. 4. 29

- [128] M. Kazuhisa, *Surface Characterization Techniques*, ser. NASA technical memorandum; 211497. Glenn Research Centre, Cleveland, Ohio: National Aeronautics and Space Administration, July 2002. 30
- [129] E. Irene, *Surfaces, Interfaces, and Thin Films for Microelectronics*. Hoboken, New Jersey: John Wiley and Sons, Inc., 2008. 30
- [130] S. Zhang, L. Li, and A. Kumar, *Materials Characterization Techniques*, 1st ed. 6000 Broken Sound Parkway NW, Suite 300, Boca Raton, FL 33487-2742: CRC Press, 2009. 35, 38, 54
- [131] J. Kiernan, "Formaldehyde, formalin, paraformaldehyde and glutaraldehyde: what they are and what they do," *Microscopy Today*, vol. 1, pp. 8–12, 2000. 40
- [132] D. Rozkiewicz, Y. Kraan, M. Werten, F. de Wolf, V. Subramaniam, B. Ravoo, and D. Reinhoudt, "Covalent microcontact printing of proteins for cell patterning," *Chemistry-A European Journal*, vol. 12, no. 24, pp. 6290–6297, 2006. 45
- [133] D. Eddington, J. Puccinelli, and D. Beebe, "Thermal aging and reduced hydrophobic recovery of polydimethylsiloxane," *Sensors and Actuators B*, vol. 114, pp. 170–172, 2006. 50
- [134] C. Lam, R. Wu, D. Li, M. Hair, and A. Neumann, "Study of the advancing and receding contact angles: liquid sorption as a cause of contact angle hysteresis," *Advances in Colloid and Interface Science*, vol. 96, no. 1-3, pp. 169–191, 2002. 54
- [135] R. Sedev, J. Petrov, and A. Neumann, "Effect of swelling of a polymer surface on advancing and receding contact angles," *Journal of Colloid and Interface Science*, vol. 180, no. 1, pp. 36–42, 1996. 54
- [136] L. Ressier, B. Viallet, J. Grisolia, and J. Peyrade, "Chemical patterns of octadecyltrimethoxysilane monolayers for the selective deposition of nanoparticles on silicon substrate," *Ultramicroscopy*, vol. 107, no. 10-11, pp. 980–984, 2007. 58
- [137] L. Ressier, C. Martin, B. Viallet, J. Grisolia, and J. Peyrade, "Control of micro- and nanopatterns of octadecyltrimethoxysilane monolayers using nanoimprint lithography and atmospheric chemical vapor deposition," *Journal of Vacuum Science & Technology B: Microelectronics and Nanometer Structures*, vol. 25, no. 1, pp. 17–20, 2007. 58
- [138] A. Tserepi, E. Gogolides, K. Tsougeni, V. Constantoudis, and E. Valamontes, "Tailoring the surface topography and wetting properties of oxygen-plasma

- treated polydimethylsiloxane,” *Journal of Applied Physics*, vol. 98, no. 11, p. 113502, 2005. 62, 79, 97
- [139] N. Bowden, W. Huch, K. Paul, and G. Whitesides, “The controlled formation of ordered, sinusoidal structures by plasma oxidation of an elastomeric polymer,” *Applied Physics Letters*, vol. 75, pp. 2557–2559, 1999. 62, 97, 105, 110
- [140] D. Chua, H. Ng, and S. Li, “Spontaneous formation of complex and ordered structures on oxygen-plasma-treated elastomeric polydimethylsiloxane,” *Applied Physics Letters*, vol. 76, pp. 721–723, 2000. 62, 97, 105, 110
- [141] P. Vadgama, “2 Surface biocompatibility,” *Annual Reports Section “C” (Physical Chemistry)*, vol. 101, pp. 14–52, 2005. 62, 64, 95, 96
- [142] M. Bergkvist, J. Carlsson, and S. Oscarsson, “Surface-dependent conformations of human plasma fibronectin adsorbed to silica, mica, and hydrophobic surfaces, studied with use of Atomic Force Microscopy,” *Journal of Biomedical Materials Research Part A*, vol. 64, no. 2, pp. 349–356, 2002. 65
- [143] S. Cheng, K. Chittur, C. Sukenik, L. Culp, and K. Lewandowska, “The conformation of fibronectin on self-assembled monolayers with different surface composition: an FTIR/ATR study,” *Journal of Colloid and Interface Science*, vol. 162, no. 1, pp. 135–143, 1994. 65
- [144] K. Chittur, “FTIR/ATR for protein adsorption to biomaterial surfaces,” *Biomaterials*, vol. 19, no. 4-5, pp. 357–369, 1998. 65
- [145] D. Togashi, A. Ryder, and G. Heiss, “Quantifying adsorbed protein on surfaces using confocal fluorescence microscopy,” *Colloids and Surfaces B: Biointerfaces*, vol. 72, no. 2, pp. 219–229, 2009. 65
- [146] P. Roach, D. Farrar, and C. Perry, “Interpretation of protein adsorption: surface-induced conformational changes,” *Journal of the American Chemical Society*, vol. 127, no. 22, pp. 8168–8173, 2005. 65
- [147] G. Baneyx, L. Baugh, and V. Vogel, “Coexisting conformations of fibronectin in cell culture imaged using fluorescence resonance energy transfer,” *Proceedings of the National Academy of Sciences of the United States of America*, vol. 98, no. 25, pp. 14464–14468, 2001. 65
- [148] W. Strober, “Trypan blue exclusion test of cell viability.” *Current Protocols in Immunology*, vol. Appendix 3B, pp. A.3B.1–A.3B.2, 1997. 67
- [149] B. Herman, Ed., *Fluorescence Microscopy*, 2nd ed., ser. Microscopy handbooks. BIOS Scientific in association with the Royal Microscopical Society, 1998, vol. 40. 69

- [150] W. Amos, “Instruments for fluorescence imaging,” *Protein Localization by Fluorescence Microscopy: a practical approach*, pp. 67–108, 2000. 69
- [151] G. Cox, *Optical Imaging Techniques in Cell Biology*. Boca Raton CRC/Taylor & Francis, 2007. 69, 75
- [152] G. Baneyx, L. Baugh, and V. Vogel, “Fibronectin extension and unfolding within cell matrix fibrils controlled by cytoskeletal tension,” *Proceedings of the National Academy of Sciences of the United States of America*, vol. 99, no. 8, pp. 5139–5143, 2002. 71
- [153] G. Baneyx and V. Vogel, “Self-assembly of fibronectin into fibrillar networks underneath dipalmitoyl phosphatidylcholine monolayers: role of lipid matrix and tensile forces,” *Proceedings of the National Academy of Sciences of the United States of America*, vol. 96, no. 22, pp. 12 518–12 523, 1999. 71
- [154] J. Pickering, L. Chow, S. Li, K. Rogers, E. Rocnik, R. Zhong, and B. Chan, “ $\alpha 5 \beta 1$  integrin expression and luminal edge fibronectin matrix assembly by smooth muscle cells after arterial injury,” *American Journal of Pathology*, vol. 156, no. 2, pp. 453–465, 2000. 71
- [155] V. Allan, *Protein Localization by Fluorescence Microscopy: a practical approach*, ser. The Practical Approach Series. Oxford New York: Oxford University Press Inc., 2000, ch. Basic immunofluorescence, pp. 1–26. 72
- [156] J. Pawley, Ed., *Handbook of Biological Confocal Microscopy*, 3rd ed. New York, NY: Springer, 2006. 75
- [157] W. Tsai, J. Grunkemeier, and T. Horbett, “Human plasma fibrinogen adsorption and platelet adhesion to polystyrene,” *Journal of Biomedical Materials Research Part A*, vol. 44, no. 2, pp. 130–139, 1999. 80, 81
- [158] E. Dejana, M. Lampugnani, M. Giorgi, M. Gaboli, and P. Marchisio, “Fibrinogen induces endothelial cell adhesion and spreading via the release of endogenous matrix proteins and the recruitment of more than one integrin receptor,” *Blood*, vol. 75, no. 7, p. 1509, 1990. 81
- [159] S. Sousa, M. Lamghari, P. Sampaio, P. Moradas-Ferreira, and M. Barbosa, “Osteoblast adhesion and morphology on TiO<sub>2</sub> depends on the competitive preadsorption of albumin and fibronectin,” *Journal of Biomedical Materials Research Part A*, vol. 84, no. 2, pp. 281–290, 2008. 88
- [160] P. DeGarmo, B. J.T., and R. Kohser, *Materials and Processes in Manufacturing*, 7th ed. New York, NY: Macmillan Pub. Co., 1988. 96



- [161] *BioScope II Controller Manual*, 1st ed., Veeco Instruments, Santa Barbara, CA, 2006. 101, 102
- [162] H. Butt, B. Cappella, and M. Kappl, “Force measurements with the atomic force microscope: Technique, interpretation and applications,” *Surface Science Reports*, vol. 59, no. 1-6, pp. 1–152, 2005. 101, 102
- [163] N. Bowden, S. Brittain, A. Evans, J. Hutchinson, and G. Whitesides, “Spontaneous formation of ordered structures in thin films of metals supported on an elastomeric polymer,” *Nature*, vol. 393, no. 6681, pp. 146–149, 1998. 105, 107, 110
- [164] D. Armani, C. Liu, and N. Aluru, “Re-configurable fluid circuits by PDMS elastomer micromachining,” in *Proc. IEEE Conference on Micro-Electro Mechanical Systems (17–21 January 1999)*, 1999, pp. 222–7. 114
- [165] F. Carrillo, S. Gupta, M. Balooch, S. Marshall, G. Marshall, L. Pruitt, and C. Puttlitz, “Nanoindentation of polydimethylsiloxane elastomers: Effect of crosslinking, work of adhesion, and fluid environment on elastic modulus,” *Journal of Materials Research*, vol. 20, no. 10, pp. 2820–2830, 2005. 114
- [166] D. Fuard, T. Tzvetkova-Chevolleau, S. Decossas, P. Tracqui, and P. Schiavone, “Optimization of poly-di-methyl-siloxane (PDMS) substrates for studying cellular adhesion and motility,” *Microelectronic Engineering*, vol. 85, no. 5-6, pp. 1289–1293, 2008. 114
- [167] K. Burton, J. Park, and D. Taylor, “Keratocytes generate traction forces in two phases,” *Molecular Biology of the Cell*, vol. 10, no. 11, pp. 3745–3769, 1999. 115
- [168] J. El-Ali, P. Sorger, and K. Jensen, “Cells on chips,” *Nature*, vol. 442, no. 7101, pp. 403–411, 2006. 128, 131
- [169] H. Jansen, H. Gardeniers, M. Boer, M. Elwenspoek, and J. Fluitman, “A survey on the reactive ion etching of silicon in microtechnology,” *Journal of Micromechanics and Microengineering*, vol. 6, no. 1, pp. 14–26, 1996. 137
- [170] S. Bhattacharya, A. Datta, J. Berg, and S. Gangopadhyay, “Studies on surface wettability of poly (dimethyl) siloxane (PDMS) and glass under oxygen-plasma treatment and correlation with bond strength,” *Journal of Microelectromechanical Systems*, vol. 14, no. 3, pp. 590–597, 2005. 148
- [171] A. Lewis and E. Boose, “Estimating volume flow rates through xylem conduits,” *American Journal of Botany*, vol. 82, no. 9, pp. 1112–1116, 1995. 149

## Curriculum Vitae

**Name:** Jessica Mary Dechene

**Place of birth:** Windsor, Ontario, Canada

**Year of birth:** 1981

**Post-secondary Education and Degrees:** 2005-2010 PhD  
Chemistry  
The University of Western Ontario  
London, Ontario, Canada

2000-2005 H.B.Sc (with distinction)  
Chemistry  
The University of Windsor  
Windsor, Ontario, Canada

**Research Experience** 2005-2010 Research Assistant  
The University of Western Ontario  
Supervisor: P. R. Norton

2004-2005 Research Assistant  
The University of Windsor  
Supervisor: S. H. Eichhorn

2003-2003 Research Assistant  
The University of Windsor  
Supervisor: J. Wang

2001-2003 Laboratory Assistant  
Great Lakes Institute for Environmental Research  
Supervisor: R. Letcher

**Refereed Journal Publications:**

- 
- [1] C. Seguin, J. M. McLachlan, P.R. Norton, F. Lagugne-Labarthet, "Surface modification of poly (dimethylsiloxane) for microfluidic assay applications," *Applied Surface Science*, vol. 256, no. 8, p. 2524, 2010.
- [2] S. Varma, J. McLachlan, A.M. Leclair, B.C. Galarreta, P.R. Norton, F. Lagugne-Labarthet, "Positionally controlled growth of cells using a cytophobic fluorinated polymer," *Analytical and Bioanalytical Chemistry*, vol. 396, no. 3, p. 1159.
- [3] M. Iqbal, J. McLachlan, W. Jia, N. Braidy, G. Botton, S. H. Eichhorn, "Ligand effects on the size and purity of PD nanoparticles," *Journal of Thermal Analysis and Calorimetry*, vol. 96, no.1, p. 15, 2009.
- [4] N. Patrito, J. M. McLachlan, S. N. Faria, J. Chan, P.R. Norton, "A novel metal-protected plasma treatment for the robust bonding of polydimethylsiloxane," *Lab on a Chip*, vol. 7, no. 12, p. 1813, 2007.
- [5] W. Jia, J. McLachlan, J. Xu, S.M. Tadayyan, P.R. Norton, S.H. Eichhorn, "Characterization of Au and Pd nanoparticles by high-temperature TGA-MS," *Canadian Journal of Chemistry*, vol. 84, no. 7, p. 998, 2006.